

**NUMERICAL SIMULATION OF PRESSURE
RESPONSE IN PARTIALLY COMPLETED
OIL WELLS**

by

**Jonathan Patrick Strauss
B. Sc. Hons. (Natal)**

Submitted in partial fulfilment of the requirements
of the degree of Master of Science
in the School of Mathematics, Statistics and Information Technology
University of Natal

Pietermaritzburg

2002

Abstract

This work is concerned with the application of finite difference simulation to modelling the pressure response in partially penetrating oil wells. This has relevance to the oil and hydrology industries where pressure behaviour is used to infer the nature of aquifer or reservoir properties, particularly permeability. In the case of partially penetrating wells, the pressure response carries information regarding the magnitude of permeability in the vertical direction, a parameter that can be difficult to measure by other means and one that has a direct influence on both the total volumes of oil that can be recovered and on the rate of recovery.

The derivation of the non-linear differential equations that form the basis for multi-phase fluid flow in porous media is reviewed and it is shown how they can be converted into a set of finite difference equations. Techniques used to solve these equations are explained, with particular emphasis on the approach followed by the commercial simulation package used in this study. This involves use of Newton's method to linearize the equations followed by application of a pre-conditioned successive minimization technique to solve the resulting linear equations.

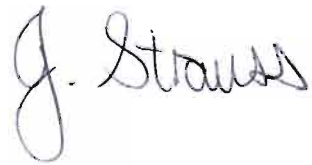
Finite difference simulation is applied to a hypothetical problem of solving pressure response in a partially penetrating well in an homogenous but anisotropic medium and the results compared with those from analytical solutions. Differences between the results are resolved, demonstrating that the required level of accuracy can be achieved through selective use of sufficiently small grid blocks and time-steps. Residual discrepancies with some of the analytical methods can be traced to differences in the boundary conditions used in their derivation.

The simulation method is applied to matching a complex real-life well test with vertical and lateral variation in properties (including fluid saturation). An accurate match can be achieved through judicious adjustment of the problem parameters with the proviso that the vertical permeability needs to be high. This suggests that the recovery mechanism in the oil field concerned can be expected to be highly efficient, something that has recently been confirmed by production results.

Preface

The work described in this dissertation was carried out on a part-time basis in the School of Mathematics, Statistics and Information Technology at the University of Natal, Pietermaritzburg, during the period from January 1993 to December 2002, under the supervision of Professor J. W. Hearne (Department of Mathematics and Applied Mathematics)

These studies represent original work by the author and have not been submitted in any other form to another university. Where use has been made of the work of others it has been duly acknowledged in the text.

A handwritten signature in black ink, reading "J. Strauss". The signature is written in a cursive style with a large, looped initial "J".

Acknowledgments

I would like to thank the national oil company of South Africa, PETROSA (previously known as Southern Oil Exploration Corporation or SOEKOR), for:

- Permission to use and reproduce data acquired on one of their oil fields,
- Financial support during the early phases of this work.

I gratefully acknowledge the support and guidance of my supervisor, Professor John Hearne.

Most of all, I would like to thank my wife Ann for her continual support and encouragement.

Contents

Chapter 1: Review	1
1.1 Introduction.....	1
1.2 Fluid Flow in Porous Media	5
1.3 Problems with Analytical Solutions	7
1.4 Resolution of Analytical Problems using Simulation.....	13
1.5 Unit Convention	14
1.6 Aims.....	15
Chapter 2: Derivation of Equations	17
2.1 Conservation of Mass	17
2.2 Darcy's law.....	19
2.3 Diffusivity Equations.....	19
2.4 Typical Boundary Conditions	22
2.5 Analytical Solutions of the Diffusivity Equation	24
2.6 Black-oil Fluid Model.....	25
2.7 Compositional model.....	27
2.8 Chapter Summary	28
Chapter 3: Numerical Scheme	29
3.1 Gridding	29
3.2 Finite Difference Equations.....	33
3.3 Calculation of Transmissibilities for a Radial Grid.....	38
3.4 Boundary Conditions and Well model	43
3.5 Solution of the Implicit Finite Difference Equations.....	45
3.6 Solution of the Non-linear Equations	46
3.7 Direct Solution of the Linear Equations for a One- Dimensional Grid	49
3.8 Iterative Solution of the Linear Equations using Orthomin.....	51
3.9 Nested Factorisation	55
3.10 Solution of Well Variables	61
3.11 Chapter Summary	62
Chapter 4: Application to a Hypothetical Problem.....	64
4.1 Definition of Hypothetical Problem	64
4.2 Modelling the Hypothetical Problem.....	66
4.3 Improvements to the Initial Model	70
4.4 Use of a Refined Grid	73

4.5	Use of a Nine-Point Scheme.....	85
4.6	Chapter Summary	92
Chapter 5: Application to a Real Life Problem		93
5.1	Background.....	93
5.2	Geology and Geophysics	93
5.3	Reservoir Engineering	97
5.4	Review of Well Test Using Analytical Techniques.....	101
5.5	Simulation Modelling of the Well Test	107
5.5	Chapter Summary	114
Chapter 6: Conclusions.....		116
References.....		119
Nomenclature.....		124
Glossary		130

Appendix 1: Eclipse Command File for Hypothetical Problem

Appendix 2: Listing of Computer Programs

Appendix 3: Eclipse Command File for Real-Life Problem

List of Figures

Figure 1.1:	Geometry of a Fully Penetrating Well	2
Figure 1.2a:	Schematic of a Partially Penetrating Well	3
Figure 1.2b:	Schematic of a Partially Completed Well.....	3
Figure 1.3:	Typical Pressure Response in a Partially Completed Well.....	9
Figure 1.4:	Partial Completion Geometry for Hantush Solution	11
Figure 2.1:	Geometry of Volume Element.....	18
Figure 3.1:	A Simple Cartesian Grid.....	30
Figure 3.2:	A Simple Radial Grid	30
Figure 3.3:	A Corner-Point Geometry Grid	31
Figure 3.4:	A PEBI Grid	32
Figure 3.4:	Distances for Harmonic Average.....	36
Figure 3.5:	Geometry for Vertical Transmissibility Calculation.....	39
Figure 3.6:	Geometry for Radial Transmissibility Calculation.....	41
Figure 3.7:	The Residual Vectors in Orthomin.....	52
Figure 3.8:	The Nested Tri-Diagonal Structure of the Jacobian for a 4 by 3 by 3 Grid	57
Figure 4.1:	Cross-Section Showing the Geometry of the Hypothetical Problem.....	65
Figure 4.2:	Comparison of Simulated Pressures with Two Analytical Solutions	68
Figure 4.3:	Schematic of Potential and Error in Flow Term Across a Grid Face.....	71
Figure 4.4:	Geometry of Adjacent Radial Blocks	72
Figure 4.5:	Comparison of Refined Grid Simulations with the Hantush Solution.....	74
Figure 4.6:	Pressure Potential Distribution for Refined Grid.....	75
Figure 4.7:	Early-Time Pressures from Simulations using Various Time Step Lengths	78
Figure 4.8:	Comparison of Inner Boundary Conditions.....	82
Figure 4.9:	Pressure Distribution in an Uniform Flux Well.....	83
Figure 4.10:	Comparison of Simulation with Yiidiz Solution.....	85
Figure 4.11:	Adjacent Grid Blocks for Derivative Estimation.....	86

Figure 5.1:	Depth to the Top of the Reservoir Interval	94
Figure 5.2:	Properties of the Reservoir Interval, Well A	96
Figure 5.3:	Sensitivity of Pressure Response of a Partially Penetrating Well to Vertical Permeability	99
Figure 5.4:	Pressure Response During DST#1A at Well A	103
Figure 5.5:	Pressure Response During Reservoir Evaluation Build-up at Well A.....	105
Figure 5.6:	Capillary Pressure Curves used for Simulation	108
Figure 5.7:	Relative Permeability Curves used for Simulation.....	109
Figure 5.8:	Pressure Match on Linear Time Plot	112
Figure 5.9:	Pressure Match on Horner Plot.....	112
Figure 5.10:	Analytical Partially Penetrating Model with Storage	114

List of Tables

Table 1.1:	Comparison of Different Unit Systems	16
Table 4.1:	Properties of the Hypothetical Model.....	66
Table 5.1:	Fluid and Rock Properties for Well A	102
Table 5.2:	Rates and Times for Flow Periods During DST#1A at Well A	102
Table 5.3:	Results of Horner Analysis for DST#1A at Well A	106
Table 5.4:	Zonation and Rock Properties for Well A	110

Chapter 1: Review

1.1 Introduction

Pressure measurements made in oil and gas wells provide useful information on the current and possible future performance of the individual well and the oil or gas field as a whole. For example, some of the possibilities are:

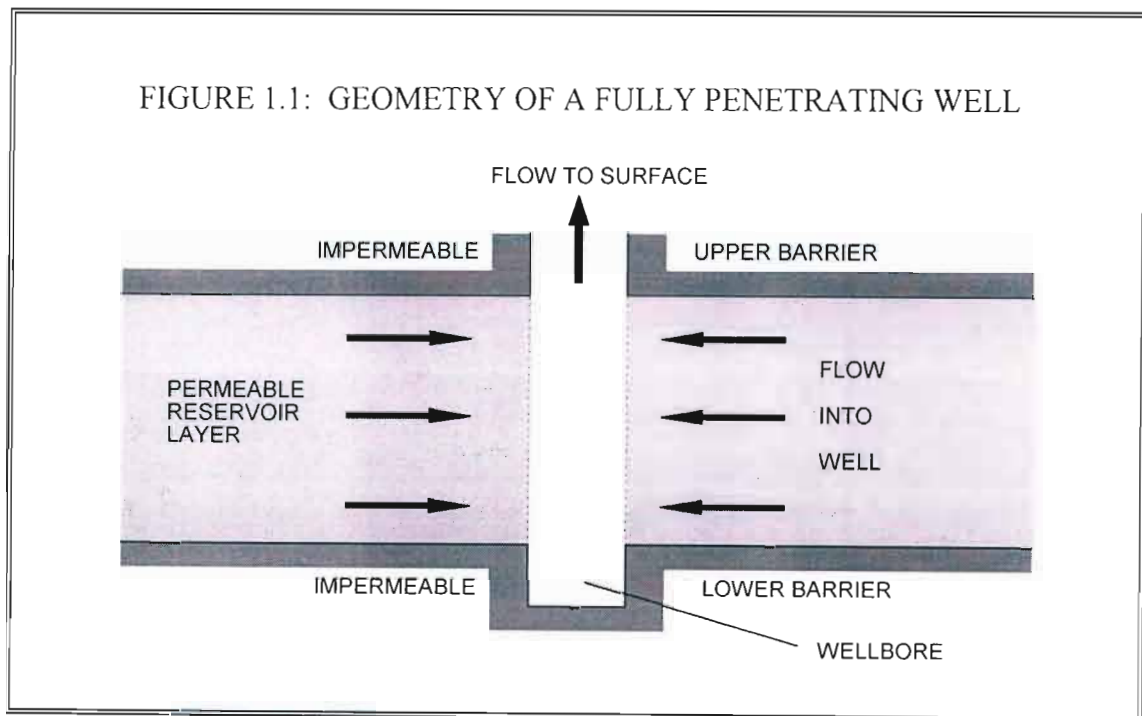
- the determination of average pressures for the hydrocarbon reservoir may indicate how quickly the field is being depleted by production, and hence how long the life of the field will be;
- the analysis of individual well performance may indicate that remedial work is needed to improve the productivity of a well;
- the degree to which different wells are in hydraulic communication may indicate that a change in the production policy is necessary to maximise the recovery of hydrocarbons.

Typically the data that are gathered about the properties of the hydrocarbon reservoir are fairly sparse, being limited to information gathered from the intersections of the reservoir by wells. Other data are often indirect: seismic reflections from the strata containing the reservoir, for example. Pressure measurements represent a direct measurement of the dynamic behaviour of the reservoir and are therefore very useful in providing information about the properties and characteristics of the reservoir. This in turn may reduce the uncertainties in forecasting the production from the reservoir, and hence reduce the risk in developing the oil or gas field.

The application of pressure measurements first occurred in the 1920's¹ in the United States, where initially the main objective was to record a static reservoir pressure. It was soon found that when a producing well was closed in order to allow the pressure to build up to that of the surrounding reservoir, the length of time taken for the pressure to stabilise was a function of the properties of rock.

It was not until 1937, when Muskat² developed an extrapolation theory relating the change in pressure with time to the properties of the reservoir, that a quantitative basis for evaluating dynamic pressures existed. Muskat's theory, while a big step forward, must be regarded as incomplete as it does not take into consideration the compressibility of the reservoir fluid.

In the early 1950s two different approaches were developed which include the effects of fluid compressibility. These are the method of Miller, Dyes and Hutchinson³ (MDH) and the method of Horner⁴ which together form the basis for a large part of modern well test analysis. In their simplest form these theories obtain a solution for the pressure behaviour by assuming that the reservoir consists of a radially infinite, homogeneous and isotropic, porous medium containing a fluid of constant viscosity with small and constant compressibility. They also assume that the entire reservoir interval has been intersected by the well and that flow takes place across the entire length of the intersection. This geometry is depicted in Figure 1.1. The methods show how the pressure measured in the production well responds to a change in production rate for this simple geometry.



In this thesis the pressure response in partially penetrating and partially completed wells is considered.

The geometry of partially penetrating wells differs from the simple radial geometry discussed above in that only a portion of the reservoir is intersected by the well (see Figure 1.2a). In other words, the fluid from the reservoir can only flow into the wellbore from the portion of the reservoir that the well intersects. Partially completed wells are wells that intersect the entire reservoir interval but are sealed off from the reservoir over part of the intersection (see Figure 1.2b). For most practical purposes partially penetrating wells can be regarded as being a subset of partially completed

wells where the partial completion occurs at the top of the reservoir. The consequence of both these geometries is that, for a given flow rate, there is a greater drop in pressure from the reservoir to the well than for the simple radial case. This additional pressure drop is due to the convergence of the flow lines near the well where the same volume of fluid is required to flow into a smaller well intersection.

FIGURE 1.2a: SCHEMATIC OF A PARTIALLY PENETRATING WELL

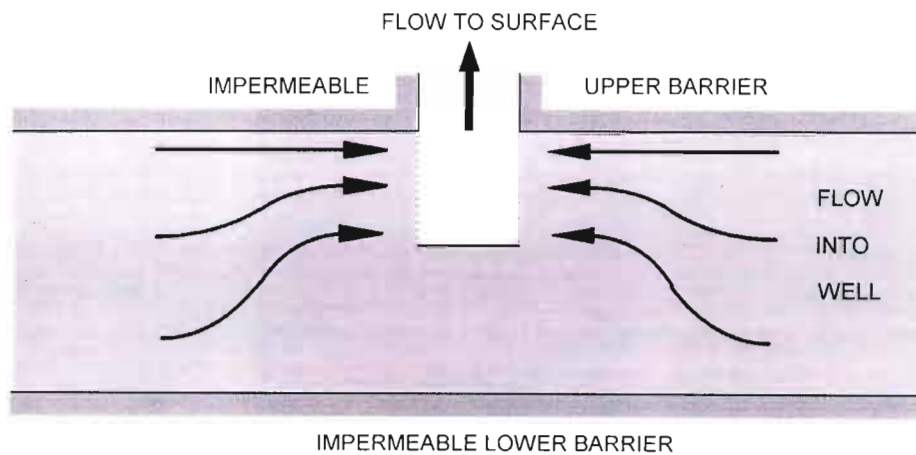
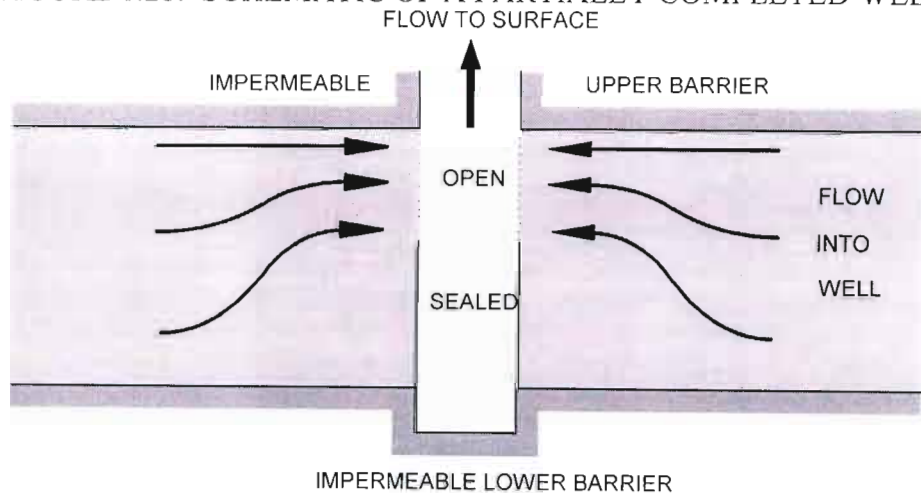


FIGURE 1.2b: SCHEMATIC OF A PARTIALLY COMPLETED WELL



Various authors⁵⁻¹⁰ have derived analytical solutions for partially perforated geometries:

- Muskat⁵ calculated productivities for an anisotropic system under steady-state conditions for incompressible fluid.

- Nisle⁶ derived a solution for partially penetrating wells in an isotropic medium.
- Brons and Marting⁷ extended this work and calculated the impact of the partial penetration on productivity. They evaluated the solution numerically in order to produce tables of values that could be used to determine productivity impairment for wells with a range of penetration ratios.
- Hantush⁸ used a combination of Laplace and Fourier transforms to solve the transient anisotropic version of the problem.
- Odeh⁹ obtained a solution of the steady-state problem using a finite cosine transform.
- Gringarten and Ramey¹⁰ used Green's functions to solve the problem for the case where the well-bore has constant pressure along its length. That is, the fluid conductivity within the well itself is infinite in comparison to the conductivity in the reservoir. Their approach was to superimpose a number of discrete flux sections of different strengths in order to obtain a uniform pressure along the well.

Unfortunately most of these solutions are difficult to evaluate in that they involve infinite series or integrals that need to be calculated numerically.

An alternative approach followed by some authors¹¹⁻¹³ has been to use finite difference simulators to model the geometry of the problem, either to check the analytical solutions or to derive useful correlations. Finite difference simulation packages have become commonplace in the oil industry because of the need to forecast and match historical production from fields with heterogeneities that are difficult to account for in analytical models. Most engineers therefore have access to these numerical simulation packages.

The work in this thesis was prompted by a simulation study conducted at the Southern Oil Exploration Corporation (SOEKOR) on one of its partially completed wells¹⁴. In this study it was found that the analytical formulae describing the additional pressure drop due to partial completion broke down because the properties of the interval that was open to flow were not characteristic of the reservoir interval as a whole. Although the simulation model succeeded in explaining the observed pressure drop, some problems were encountered in matching the rate of change of pressure shortly after a change in production rate. These problems are believed to be related to errors introduced by the discretisation of the finite difference approach.

The aims of this thesis are two-fold: firstly, to investigate ways of minimising the errors inherent in the simulation of partly completed wells through the use of standard reservoir simulators that are commonplace throughout the oil-industry; secondly, to gain a better understanding of the reservoir characteristics at the specific well being analysed and consequent implications for future production.

Although specialised software exists that implements some of the numerical-analytical methods, the use of such software in this study has been limited to comparison purposes. The reasons for this are to try to make the techniques developed in this thesis as broadly applicable as possible and to allow the reservoirs with important heterogeneities or a mixture of fluid phases to be modelled.

An understanding of the errors is essential in determining the limits of applicability of the techniques developed. Reducing the errors has the potential to greatly improve the analysis of pressures measured in partially completed wells. Although the non-radial geometry of partially completed wells introduces complications into the pressure analysis, the pressures also carry additional information about the anisotropy of the reservoir. This information is of great importance in forecasting such reservoir behaviour as gas or water coning, and also has a bearing on the fraction of oil in the reservoir that is recovered by production.

1.2 Fluid Flow in Porous Media

In order to gain an understanding of the pressure behaviour in oil and gas wells it is necessary to first cover the fundamentals of the behaviour of fluid flowing through reservoir rock.

Any potential reservoir rock has pores or, in some cases, fractures which create a void space between the grains of rock. This space can be filled with water or a combination of water and hydrocarbon liquids and/or gases. The degree to which the pores are interconnected controls the ease with which the fluid can move from pore to pore and ultimately into the wellbore. Resistance of the fluid to flow will also be dependant on the viscosity of the fluid. Thus we can expect the flow behaviour to be a function of the properties of both the fluid and the rock.

A nineteenth century French engineer, Henry Darcy, was the first to publish an account¹⁵ of an experiment in which the flow of fluids through porous media was investigated. He found that the velocity of the flow of water through a vertical sand pack was directly proportional to the difference in the manometric height as evaluated above and below the sand pack. Others later extended his work to other fluids

(including compressible fluids) and to flow that is not vertical, leading to the formulation of Darcy's law

$$u = -\frac{k\gamma}{\mu} \frac{d\Phi}{dl}, \quad (1)$$

where u is the flow velocity, k is the fluid conductivity or permeability of the rock, μ is the viscosity of the fluid, $\gamma = \rho g$, ρ is the fluid density, g is the acceleration due to gravity, and Φ is the fluid potential.

In this equation and the other equations in this chapter, it has been assumed that a self-consistent set of units such as SI is being used. This avoids unnecessary constants other than those that arise naturally through the physics and geometry of the problem at hand. A more complete description of the different systems of units is given in section 1.5.

The fluid potential is in turn given by

$$\Phi = \int_{p''}^p \frac{dp}{\rho \gamma} - D, \quad (2)$$

where p is the fluid pressure, p'' is a reference pressure, and D is the depth within the porous medium. This definition of fluid potential is necessary to ensure the condition of no flow under hydrostatic conditions for a compressible fluid. Although Darcy's law was originally defined in a one-dimensional form (as given in Equation 1), it can be extended into three dimensions, where it is normally assumed that permeability is a diagonal property tensor of the form

$$k = \begin{bmatrix} k_x & 0 & 0 \\ 0 & k_y & 0 \\ 0 & 0 & k_z \end{bmatrix}. \quad (3)$$

Darcy's law then becomes

$$\underline{u} = -\frac{k\gamma}{\mu} \nabla\Phi \approx -\frac{k}{\mu} (\nabla p - \gamma \nabla D), \quad (4)$$

where \underline{u} is the flow velocity vector and ∇ is the differential vector operator ($\partial/\partial x, \partial/\partial y, \partial/\partial z$).

Although Darcy's law is empirically derived, King Hubbert¹⁶ has shown how the law can be derived from the well known Navier-Stokes equations.

As given in Equation 4, the law assumes that the flow is monophasic. When extended to multiphase flow it is normally assumed that the law applies separately to each fluid with the proviso that permeability is modified to take into account the reduction of available pore space due to the presence of another fluid. This is achieved through the multiplication of permeability by a factor between zero and one. This factor is known as relative permeability and is normally taken to be a function of fluid saturation and sometimes saturation history. Relative permeabilities vary from reservoir to reservoir and are therefore normally measured specifically for the reservoir of interest, using elaborate laboratory experiments.

1.3 Problems with Analytical Solutions

Many of the analytical solutions of pressure behaviour in reservoirs are based on the radial diffusivity equation,

$$\frac{\partial^2 p}{\partial r^2} + \frac{1}{r} \frac{\partial p}{\partial r} = \frac{\mu c \phi}{k} \frac{\partial p}{\partial t}, \quad (5)$$

where p is the pressure in the reservoir, r is the radial distance from the centre of the wellbore, μ is the fluid viscosity, c is the fluid compressibility, ϕ is the fractional porosity, k is the permeability, and t is time.

This equation is derived in Section 2.3. The assumptions implicit in the equation are that: a single fluid of small and constant compressibility is present; the reservoir rock is homogenous and isotropic; and gravitational terms are negligible (the pressure increases linearly with depth). If in addition one assumes that the entire reservoir interval is open to flow, that the volume occupied by well bore is insignificant, and that the lateral extent of the reservoir is infinite, then it is possible to derive the well known transient solution with a line-source,

$$\Delta p = -\frac{q\mu B_o}{4\pi kh} \text{Ei} \left[\frac{r^2 \mu c \phi}{4kt} \right], \quad (6)$$

where Δp is the change in pressure at time t and radial distance r , after a change in flow rate from zero to q (q positive for flow from the reservoir to the well), h is the thickness of the reservoir layer, B_o is the oil formation volume factor (a factor relating the surface rate to the downhole rate), and Ei is the well known exponential integral, $\text{Ei}(x) = \int_x^\infty \frac{e^{-u}}{u} du$. The pressure response for a sequence of rate changes can be obtained from this basic solution by using the principle of superposition.

Furthermore, if one uses the logarithmic approximation to the Eifunction and evaluates the equation at a radius equivalent to the wellbore radius, r_w , then one obtains

$$\Delta p \approx -\frac{q\mu B_o}{4\pi kh} \left(\ln(t) + \ln \left[\frac{4k}{\xi\mu c\phi r_w^2} \right] \right), \quad (7)$$

where $\xi = e^{0.5772\dots}$. 0.5772... is Euler's constant.

From Equation 7 it is evident that plotting the pressure drop against the logarithm of time will give a line of constant slope. Plots of this kind will be used in discussing the theoretical response of partially completed wells.

Under normal circumstances it is difficult to keep the rate constant and the pressures stable during a flow period. Thus the well is shut in after flowing for some time and the pressures are monitored as they recover. This is known as a flow/build-up test. If the length of the flow period is t and a time δt has elapsed since the well was shut in, then by the principle of superposition the pressure change is given by

$$\Delta p = -\frac{q\mu B_o}{4\pi kh} (\ln(t + \delta t) - \ln(\delta t)) = -\frac{q\mu B_o}{4\pi kh} \ln \left(\frac{t + \delta t}{\delta t} \right), \quad (8)$$

where the solution given in Equation 7 has been evaluated at time $t + \delta t$ and rate q , and summed with the solution at time δt and rate $-q$.

Equation 8 is the basis of the Horner⁴ method of well test analysis where pressure is plotted against the logarithm of $(t + \delta t)/\delta t$. On such a plot pressure should follow a linear trend with a slope proportional to $q\mu/kh$. Plots of this kind will be used when dealing with real life examples in Chapter 5.

In practice the assumptions that the formation is homogenous and isotropic are far from correct. Sedimentary rocks generally exhibit some form of layering and successive layers can have properties that differ by an order of magnitude. In spite of this, the Horner method is often successful when used to infer average properties. This is because the properties within a layer can be relatively constant. If all the layers have been intersected by the well and the direction of the well is orthogonal to the layers, then the permeability in the direction parallel to the well is relatively unimportant.

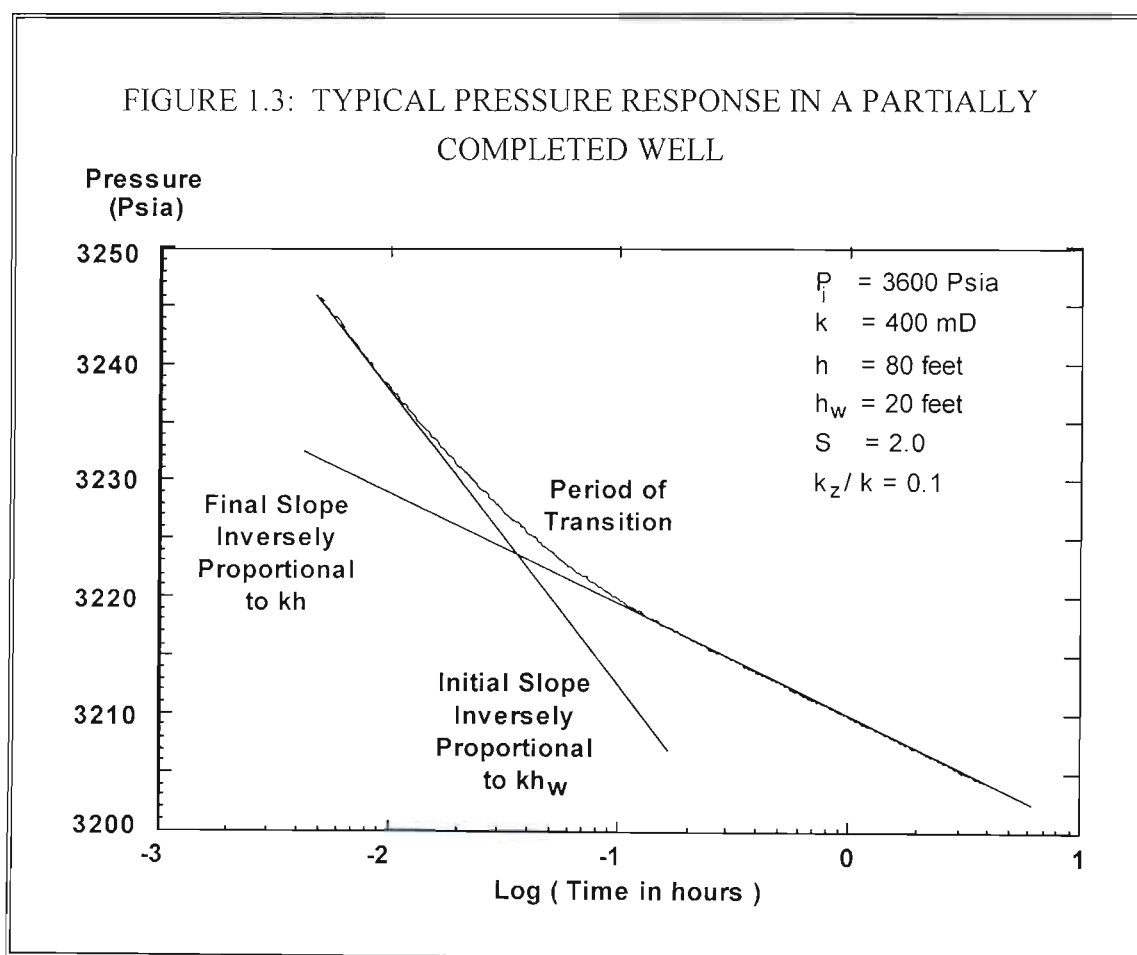
Another inhomogeneity that affects the validity of the transient line-source solution is the presence of a zone of altered permeability immediately about the wellbore. This

zone is either a consequence of damage to the formation that occurred during the drilling process, or the result of remedial work, such as acidizing that has improved the permeability around the wellbore. The manifestation of this zone is an additional (or reduced) pressure drop over and above that expected from Equation 7. Van Everdingen¹⁷ resolved this problem by introducing the concept of a skin effect which changes Equation 7 to

$$\Delta p = -\frac{q\mu B_o}{4\pi kh} \left(\ln(t) + \ln \left[\frac{4k}{\xi\mu c\phi r_w^2} \right] + 2S \right), \quad (9)$$

where S is a skin factor, normally determined empirically.

As noted previously, the effect of partial completion is to introduce a pressure drop additional to that expected in a fully completed well. This additional pressure drop is often also modelled as a skin allowing the use of Equation 9 in describing the pressure behaviour. Unfortunately this approach is only adequate in describing the well behaviour some time after a change in rate. The characteristic pressure response of a partially completed well after a change in rate is depicted in Figure 1.3.



Initially the well response is linear with respect to the logarithm of time, with a slope inversely proportional to the value of kh for the perforated interval. This is followed by a period of transition, the length of which is dependant on both the proportion of the reservoir that has been completed and the vertical permeability of the rock. Finally there is again a linear response, but this time the slope is proportional to the value of kh for the entire reservoir interval.

In practice, the early-time pressure behaviour is often masked by effects related to the compression or expansion of the volume of fluid within the wellbore itself. At late times the response can be complicated by the perturbations related to the presence of lateral boundaries some distance from the well.

Brons and Marting⁷ have produced tables and graphs that allow the skin factor resulting from partial completion to be estimated. To obtain these values they numerically evaluated an analytical solution of the partial completion problem derived by Nisle⁶. The most serious shortcoming in their work is the assumption of isotropy which is clearly inappropriate for most sedimentary rocks.

A set of correlations for the skin factor which takes into account the differences between vertical and horizontal permeability has been presented by Odeh⁹. These correlations were derived from an analytical solution of the steady state version of the problem.

Both the Brons and Marting approach and the Odeh approach suffer from the drawback that they assume constant flux along the length of the wellbore. In reality the effective permeability in the wellbore is often several orders of magnitude higher than that in the adjacent reservoir. A more realistic assumption under most circumstances is therefore that of a constant pressure potential within the wellbore. This is known as the infinite conductivity approach.

Both the Brons and Marting method and the Odeh method deal with steady state behaviour. These results can be applied by analogy to the late-time transient well behaviour. While such behaviour is applicable to production situations where major rate changes occur infrequently, excessive concentration on this portion of the pressure response ignores a major part of the information contained in transient well tests.

Hantush⁸ solved the transient (infinite reservoir) case for an anisotropic reservoir using Laplace and Fourier transforms. Evaluation of the Hantush solution requires the numerical calculation of the expression

$$\Delta p(r, z, t) = \frac{q\mu B_o}{4\pi k_H h} \left\{ \text{Ei} \left(\frac{\mu\phi cr^2}{4kt} \right) + \frac{2h}{\pi h_w} \sum_{n=1}^{\infty} \frac{1}{n} P(n\pi) W \left(\frac{\mu\phi cr^2}{4kt}, n\pi r_D \right) \right\}, \quad (10)$$

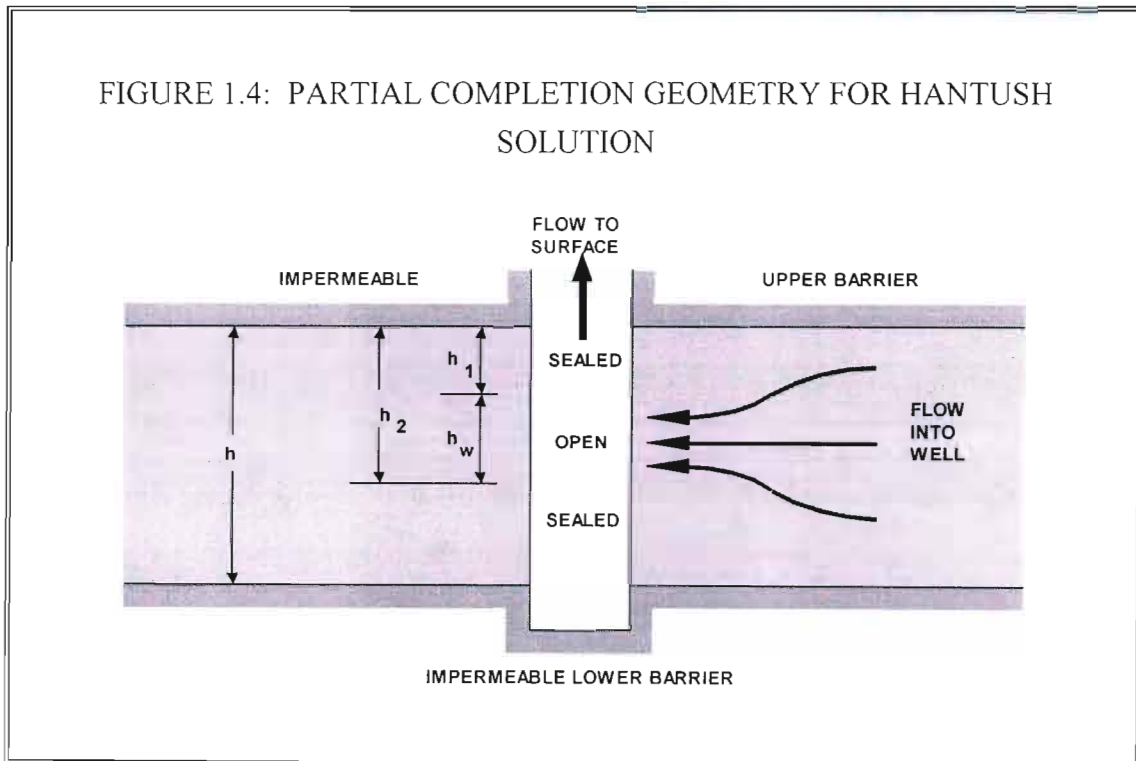
where

$$P(n\pi) = \left[\sin(n\pi h_{2D}) - \sin(n\pi h_{1D}) \right] \cos(n\pi z_D), \quad (11)$$

$$W(u, \beta) = \int_u^{\infty} \frac{1}{y} \exp \left(-y - \frac{\beta^2}{4y} \right) dy, \quad (12)$$

$$r_D = (r/h) \sqrt{k_V/k_H}. \quad (13)$$

r is the radial distance measured from the centre of the wellbore, z is the vertical position measured from the top of the reservoir, k_V and k_H are the vertical and horizontal permeability respectively, and h , h_w , h_1 , and h_2 are lengths defining the completion geometry as shown in Figure 1.4. Note that the notation h_{1D} implies that the dimensionless length should be used, i.e. $h_{1D} = h_1/h$ etc.



Equation 10 converges relatively slowly and this limits its use to non-interactive applications. In this thesis the Hantush solution is compared with finite difference simulations as well as the analytical solution from a commercial well-test analysis

package. The Hantush solution is based on the constant flux assumption previously described in the Brons and Marting and the Odeh approaches.

An infinite conductivity solution for anisotropic reservoirs has been derived by Gringarten and Ramey¹⁰, who superimposed a number of discrete flux segments of different strengths so that the pressure at the centre of each flux segment was constant. Their method relies on the use of Green's functions. A comparison made between constant flux and infinite conductivity solutions showed that the two are equivalent provided that the constant flux solution is evaluated at the correct vertical position in the wellbore.

More recently, Odeh and Babu¹⁸ have developed a solution that obtains a solution for a horizontal well by using the method of integrating point Green's functions. Their method can be applied to partially completed wells by a simple rotation of the coordinate system. This solution is used in the Intera well-test analysis package WELTEST.

Another recent method is that of Ozkan and Raghavan¹⁹, who derive solutions for a variety of problems in the Laplace-transform domain. The Laplace-transform inversion is performed numerically.

The concerns regarding the level of approximation relating to non-radial flow, anisotropy and well boundary conditions are adequately dealt with by the more recent analytical solutions. Problems still remain when trying to deal with inhomogeneity, continuously or frequently varying flow rates, or multiple phases. In theory, varying rates can be dealt with using the principle of superposition, but in practice the numerical evaluation of the analytical solutions is too slow to allow more than a few rate changes to be modelled comfortably. Specialised software is also necessary for some of the more complicated solutions and the software imposes its own constraints. The analytical models are sufficient for simpler wells but more complicated problems require the use of numerical simulation. A set of correlations has recently been presented by Ding and Reynolds²⁰ to allow the partial completion skin to be calculated for multi-layer reservoirs, which is the most common form of heterogeneity encountered. These correlations are of course only useful in describing the late transient or steady state well behaviour.

1.4 Resolution of Analytical Problems using Simulation

There are various numerical simulation techniques that could be used to model the problem. These include finite difference methods, finite element methods and various hybrid schemes.

Finite element methods have been used in reservoir simulation but are often not as computationally efficient as finite difference methods. Techniques have been developed to deal with multi-phasic flow and time varying problems using finite elements but most implementations are restricted to one or two spatial dimensions. Commercial reservoir simulation packages are therefore almost exclusively based on finite differences.

Finite difference simulators have the flexibility to model all the required effects and have the added advantage that they are commonplace in the oil industry. Most of these reservoir simulators have a large number of controlling options which allow the well to be controlled according to surface rates, surface pressures, or bottomhole pressures.

Finite difference simulators do however introduce their own set of problems. Most of these relate to the fact that a physical process, continuous in time and space, has been modelled in terms of discrete time steps and grid blocks. These errors can be reduced by decreasing the length of the time steps and the size of the grid blocks, though computer time and space availability limit the extent to which this can be pursued. The best results are achieved by selectively reducing the size of blocks where changes are most rapid. An example of this is given in this thesis for the partial completion problem. Orientation of the simulation grid can also affect results, in that there may be a preference for flow parallel to the axes of the grid as opposed to flow diagonally across grid blocks. Other problems can be the stability of the solution and lack of convergence. The simulator used in this thesis is Eclipse, a propriety reservoir simulator from Intera. Eclipse uses a fully-implicit technique which is known to provide stable and reliable solutions for difficult problems.

This thesis will concentrate on the single phase version of the partial completion problem though the solution technique is capable of handling multiphase flow. Extension of the Eclipse program input to deal with multiple phases is straightforward. In reality it is a common occurrence to have a well that is perforated in an oil zone with either an overlying gas cap or an underlying aquifer. It is important that these situations can be modelled. The gas cap (or aquifer) is often modelled analytically as an upper (or lower) constant pressure boundary, as in

Strelstova-Adams^{21,22} for example. Simulation work by Al-Khalifa²³ has shown that to consider these situations as special cases of partially completed wells may be more appropriate. The difference in viscosity between the oil and water, or the gas and oil, immediately makes the problem inhomogeneous, thereby requiring the use of simulation to achieve a solution.

1.5 Unit Convention

In this thesis two sets of units are used. For the theoretical equations the SI system of units is used. This has the advantage that these units are self consistent (absolute) and do not involve unnecessary constants that are a function of the chosen unit system. The only constants entering the equations are a function of the geometry and physics of the problem being considered. For the practical examples a hybrid system of units known as "field" units has been used. These units consist of a mixture of imperial units that have traditionally been used in the British and American oil industries and are often of a more convenient size for the problems being considered. The use of field units is still commonplace throughout the oil industry.

A third set of units known as Darcy units is also often used in the literature. This is a set of hybrid units which, like the systems of absolute units, is designed to avoid unnecessary constants but has units of a more convenient size. Unfortunately Darcy units are only partly successful in that conversion constants are only avoided if the gravity terms in Darcy's law are ignored.

Darcy's law expressed in each of the systems of units is given below:

$$\underline{u} = -\frac{k}{\mu}(\nabla p - \rho g \nabla D) \quad \text{Absolute units}$$

$$\underline{u} = -1.127 \times 10^{-3} \frac{k}{\mu}(\nabla p - 0.4335 \omega \nabla D) \quad \text{Field units (for liquids)}$$

$$\underline{u} = -\frac{k}{\mu}(\nabla p - 9.869 \times 10^{-7} \rho g \nabla D) \quad \text{Darcy units}$$

The equation for field units has been expressed in terms of ω , the specific gravity of the fluid.

To avoid confusion a table of the units used in the various systems has been modified from that given by Earlougher²⁴ and Dake²⁵ and reproduced in Table 1.1 below. The field units of stock tank barrels and stock tank barrels per day for volume and flow rate are intended for liquids. Equivalent units for gases would be standard cubic feet

(**scf**) and thousand standard cubic feet per day (**Mscf/d**). The terms "stock tank" and "standard" indicate that the volumes are measured at surface at standard conditions of 14.7 psia and 60°F. Note that the unit "psia" implies an absolute pressure, i.e. relative to a complete vacuum, whereas the unit "psig" implies a pressure relative to a atmospheric pressure. When describing a pressure change the unit simply becomes "psi". Volumes expressed in SI units are often given at normal conditions of 0°C and 101.5 Kpa.

1.6 Aims

In summary, the aims of this thesis are the following:

1. To review the literature relating to the pressure response in partially penetrating wells
2. To gain insight into the solution techniques applied by the finite-difference simulation package used in this thesis
3. To investigate ways of minimising the errors inherent in the simulation of partly completed wells when using finite-difference simulation
4. To gain a better understanding of the reservoir characteristics at the specific well being analysed and consequent implications for future production

The intention is that the techniques established to minimise the errors should be widely applicable without the use of specialized software. Most practising reservoir engineers would have access to finite difference reservoir simulation packages that could be used to model the problems considered here.

In the next chapter the partial differential equations that govern fluid flow in porous media will be derived. These equations form the basis of both analytical and simulation methods. In subsequent chapters these equations will be converted to finite difference form and the approach used to solve the equations will be discussed. Application of finite difference simulation to an abstract and easily analytically modelled problem will allow the magnitude of the errors associated with simulation to be assessed. Steps will be taken to reduce, and as far as possible, eliminate the errors. The lessons learned from the abstract problem will then be applied to modelling a real-life problem, that of a partially penetrating well with lateral and vertical variation in properties (including saturation).

Table 1.1: Comparison of Different Unit Systems

Parameter	Symbol	Dimensions	SI Units	Darcy Units	Field Units
Length	l	L	metre m	centimetre cm	feet ft
Mass	m	M	kilogram kg	gram gm	pound lb
Time	t	T	second s	second s	hour hr
Velocity	u	L/T	metres per second m.s⁻¹	centimetres per second cm.s⁻¹	feet per second ft.s⁻¹
Volume	v	L ³	cubic metres m³	cubic centimetres cc	stock tank barrels stb
Flow rate	q	L ³ /T	cubic metres per second m³.s⁻¹	cubic centimetres per second cc.s⁻¹	stock tank barrels per day stb/d
Pressure	p	M/LT ²	Pascal Pa	atmosphere atm	pounds per square inch psia
Density	ρ	M/L ³	kilograms per cubic metre kg.m⁻³	grams per cubic centimetre gm.cc⁻¹	pounds per cubic foot lb/cu.ft
Viscosity	μ	M/LT	Pascal-seconds Pa.s	centipoise cp	centipoise cp
Permeability	k	L ²	square metres m²	Darcy D	milliDarcy mD

Chapter 2: Derivation of Equations

In this chapter the equations that govern fluid flow through porous media will be derived. These equations are a result of the combination of the principle of conservation of mass with Darcy's law. Multiphase flow of oil, gas, and water is accommodated by the extension of Darcy's law to several phases. A simplified equation is derived which is applicable to single phase flow of a fluid with small and constant compressibility. Boundary conditions typical of many reservoir problems are discussed. Some analytical solutions of this simplified equation when subject to the boundary conditions are considered. The Black-oil model is used to simplify the full equations in such a way that the fluid flow can be described in terms of the mass flow of three independent components. This completes the description of the reservoir in terms of a set of equations. Chapter 3 describes how these equations are solved numerically.

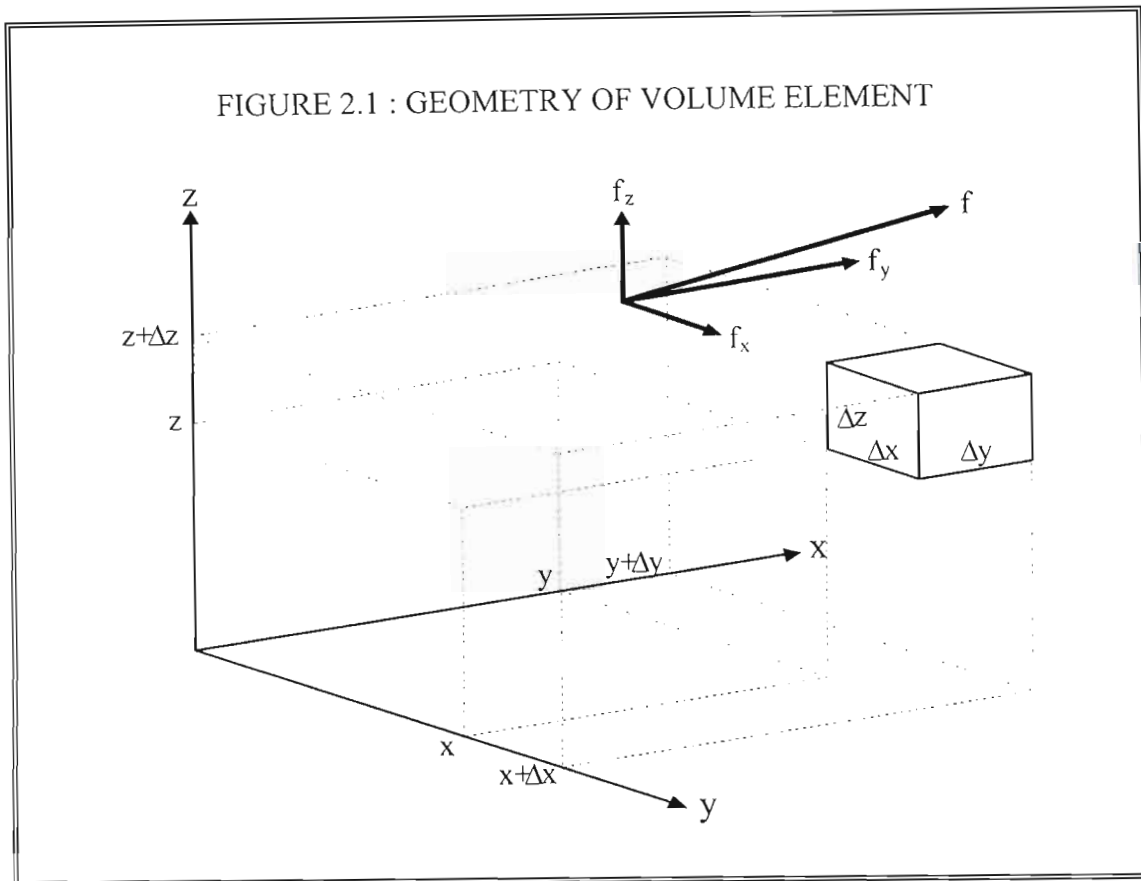
2.1 Conservation of Mass

Consider the volume element $\Delta V = \Delta x \Delta y \Delta z$ within the reservoir as depicted in Figure 2.1. This volume element is assumed to have faces orthogonal to the principle axes at positions x , $x + \Delta x$, y , $y + \Delta y$, z , and $z + \Delta z$ respectively. By conservation of mass the net inflow of fluids, I , must equal the accumulation of mass, A , within the volume element. If the mass flow rate vector, \underline{f} , is broken up into flow components parallel to the axes, then I represents the sum of the contributions from all the components. For the component f_x the net inflow is the difference between the flow across the face at x and the flow across the opposite face at $x + \Delta x$. Over a time period Δt the net inflow due to f_x is given by $[f_x(x) - f_x(x + \Delta x)]\Delta y \Delta z \Delta t$ where $\Delta y \Delta z$ is the area of the faces. Similarly for the components f_y and f_z giving a total inflow of

$$I = \Delta t \left\{ \begin{array}{l} [f_x(x) - f_x(x + \Delta x)]\Delta y \Delta z \\ + [f_y(y) - f_y(y + \Delta y)]\Delta x \Delta z \\ + [f_z(z) - f_z(z + \Delta z)]\Delta x \Delta y \end{array} \right\}. \quad (14)$$

The accumulation of mass within the volume element must be equal to the change in the product of pore volume and fluid density. Over a time period Δt the accumulation is given by

$$A = \left[\frac{\partial}{\partial t} (\rho \phi \Delta V) \right] \Delta t. \quad (15)$$



Equating A and I and dividing by $\Delta V \Delta t$ gives

$$\frac{\partial}{\partial t}(\rho\phi) = \frac{f_x(x) - f_x(x + \Delta x)}{\Delta x} + \frac{f_y(y) - f_y(y + \Delta y)}{\Delta y} + \frac{f_z(z) - f_z(z + \Delta z)}{\Delta z}. \quad (16)$$

Taking the limit as $\Delta x, \Delta y, \Delta z \rightarrow 0$ gives

$$\frac{\partial}{\partial t}(\rho\phi) = -\nabla \cdot \underline{f}. \quad (17)$$

Replacing \underline{f} with $\rho \underline{u}$ gives

$$\frac{\partial}{\partial t}(\rho\phi) = -\nabla \cdot \rho \underline{u}, \quad (18)$$

which is the mass conservation equation for a single phase. If multiple phases and components are present, then the equation needs to be modified to account for the mass fraction of each component in each phase and for the fraction of the pore space occupied by each phase. Each component must independently satisfy the equation

$$\frac{\partial}{\partial t} \left(\sum_p \rho_p y_{p,c} S_p \phi \right) = -\nabla \cdot \left(\sum_p \rho_p y_{p,c} \underline{u} \right), \quad (19)$$

where the notation $y_{p,c}$ represents the mass-fraction of component c in phase p , and S_p is the fraction of the pore space occupied by phase p .

2.2 Darcy's law

Darcy's law (Equation 4) can be used to relate \underline{u} to the fluid pressure potential, Φ . Making these changes to Equation 18 gives

$$\frac{\partial}{\partial t} (\rho \phi) = \nabla \cdot \left(\frac{\rho k \gamma}{\mu} \nabla \Phi \right). \quad (20)$$

This is the general mass-flow equation. Note that ρ , ϕ , μ , and Φ can all be functions of pressure which makes the equation non-linear.

When several phases are present, Darcy's law needs to be modified to account for the reduction of available pore space for each phase to flow through. This is traditionally done through the inclusion of a factor between 0 and 1. This factor is known as relative permeability and is a function of the phase saturation. The multi-phase form of Darcy's law is

$$\underline{u}_p = -\frac{k_{rp} k \gamma_p}{\mu_p} \nabla \Phi_p, \quad (21)$$

where k_{rp} is the relative permeability for phase p . Substituting Equation 21 into Equation 19 gives

$$\frac{\partial}{\partial t} \left(\sum_p \rho_p y_{p,c} S_p \phi \right) = -\nabla \cdot \left(\sum_p \rho_p y_{p,c} \frac{k_{rp} k \gamma_p}{\mu_p} \nabla \Phi_p \right), \quad (22)$$

which is the full mass-flow equation for multi-phase flow.

2.3 Diffusivity Equations

Since the mass flow equation is non-linear it is difficult to solve analytically. In order to provide a basis for simpler solutions it is necessary to first linearize the equation. The simplest method of linearizing the equation is to assume that the reservoir fluid has a small constant compressibility. This is an appropriate assumption for most liquid flow. There are other methods of linearizing the equation but they will not be dealt with here. Although this thesis is primarily concerned with the finite difference

formulation of the general equation, a simplified equation is useful when discussing purely geometrical effects.

The defining expression for isothermal fluid compressibility, c_f , is

$$c_f = -\frac{1}{V} \frac{\partial V}{\partial p} \Big|_T = \frac{1}{\rho} \frac{\partial \rho}{\partial p} \Big|_T. \quad (23)$$

If c_f is constant over the range of interest then Equation 23 can be integrated giving

$$c_f (p - p^o) = \ln \left(\frac{\rho}{\rho^o} \right), \quad (24)$$

where ρ^o is the density at the reference pressure of p^o . Rearranging Equation 24 and using a Taylor expansion for the exponential function gives

$$\begin{aligned} \rho &= \rho^o \exp[c_f (p - p^o)] \\ &= \rho^o \left[1 + c_f (p - p^o) + \frac{1}{2!} c_f^2 (p - p^o)^2 + \dots \right] \\ &\approx \rho^o [1 + c_f (p - p^o)]. \end{aligned} \quad (25)$$

For small compressibilities, which is often the case for liquid flow, terms involving c^2 or higher orders can be ignored. Similarly, the compressibility associated with the pore space, c_r , is usually small and the porosity can therefore be adequately represented by the equation

$$\phi \approx \phi^o [1 + c_r (p - p^o)]. \quad (26)$$

Replacing ϕ and ρ in the left hand side of Equation 20 with the expressions given in Equations 25 and 26 gives

$$\begin{aligned} \frac{\partial}{\partial t} (\phi \rho) &= \phi^o \rho^o \frac{\partial}{\partial t} [1 + c_f (p - p^o)] [1 + c_r (p - p^o)] \\ &= \phi^o \rho^o (c_r + c_f) \frac{\partial p}{\partial t}, \end{aligned} \quad (27)$$

where the product rule for differentiation has been used and terms involving $c_r c_f$ have been ignored. The right hand side of Equation 20 is given by

$$\nabla \cdot \frac{\rho k \gamma}{\mu} \nabla \Phi = \nabla \frac{\rho k \gamma}{\mu} \cdot \nabla \Phi + \frac{\rho k \gamma}{\mu} \nabla^2 \Phi. \quad (28)$$

Expanding the first term on the right-hand side of Equation 28 using the relationship $\gamma = \rho g$ and Equation 25 gives

$$\nabla \frac{\rho k \gamma}{\mu} \cdot \nabla \Phi = \frac{gk}{\mu} \nabla \rho^2 \cdot \nabla \Phi = \frac{2\rho gk}{\mu} c_f \nabla p \cdot \nabla \Phi, \quad (29)$$

where it has been assumed that k and μ are constant. If it is assumed that the pressure gradients, and hence the potential gradients, are small then this term can be neglected as it contains a product of pressure and potential gradients multiplied by the small fluid compressibility. Substituting Equation 27 and the remaining term from Equation 28 into Equation 20 gives

$$\frac{\rho k \gamma}{\mu} \nabla^2 \Phi = \phi^o \rho^o (c_r + c_f) \frac{\partial p}{\partial t}. \quad (30)$$

Dividing both sides by $\rho k \gamma / \mu$ and using the relationship $\frac{\partial \Phi}{\partial t} = \frac{1}{\gamma} \frac{\partial p}{\partial t}$ gives

$$\nabla^2 \Phi = \frac{\rho^o}{\rho} \frac{\mu \phi^o (c_r + c_f)}{k} \frac{\partial \Phi}{\partial t}. \quad (31)$$

But $\rho^o / \rho \approx 1$ because the compressibility is assumed to be small, and Equation 31 becomes

$$\nabla^2 \Phi = \frac{\mu \phi^o (c_r + c_f)}{k} \frac{\partial \Phi}{\partial t}, \quad (32)$$

which is known as the diffusivity equation and is a second order linear differential equation.

In practice, the linearization procedure is highly successful when applied to problems involving relatively incompressible fluids such as water or oil, like those considered in this thesis. As a consequence, virtually all the analytical solutions for pressure behaviour in reservoir systems are based directly on solutions of the diffusivity equation rather than the underlying mass flow equation. Further discussion of the validity of the linearization procedure is beyond the scope of this thesis and analytical solutions of the diffusivity equation will be regarded as representing the true solution that reservoir simulation needs to match. Note that reservoir simulation solves the full mass flow equation numerically and gives virtually identical pressure responses to the

analytical solutions of the diffusivity equation for simple geometries, with any differences being traceable to errors introduced by the simulation itself.

For oil reservoirs there is generally water accompanying the oil in the pore space. This is because the pore space was originally occupied by water alone and some is trapped by surface tension forces during the displacement by oil. If the water is immobile then Equation 32 for single phase flow can be used with the proviso that the compressibility is modified to take into account the fraction of the pore that is occupied by water. That is, the compressibility is given by $c = c_r + c_o S_o + c_w S_w$.

The cylindrical symmetry of the well suggests that it may be useful to express the spatial derivatives in Equation 32 in the cylindrical co-ordinates (r, θ, z) , where the well intersects the reservoir in the z -direction, r represents the radial direction measured outward from the centre of the well, and θ is the tangential direction. Thus $\partial\Phi/\partial\theta$ can be assumed to be zero if the reservoir properties are taken to be symmetrical about the well giving:

$$\frac{\partial^2\Phi}{\partial r^2} + \frac{1}{r} \frac{\partial\Phi}{\partial r} + \frac{\partial^2\Phi}{\partial z^2} = \frac{\mu\phi c}{k} \frac{\partial\Phi}{\partial t}. \quad (33)$$

Equation 5, which is the basis of the solution for the fully penetrating well, can be derived from Equation 33 by ignoring gravitational effects (i.e. assuming that $\partial\Phi/\partial z$ is constant and that gradients of Φ are equivalent to gradients of p).

2.4 Typical Boundary Conditions

Boundary conditions can be broken up into those that specify rate and those that specify pressure (or potential) at a particular region in the reservoir. While it is possible to have mixed boundary conditions, this will not be considered in this thesis.

Flow boundary conditions can implemented using the definition of Darcy's law, Equation 4, by setting the spatial derivatives according to the equation

$$\frac{\partial}{\partial l} \Phi = -\frac{\mu}{k\gamma} u, \quad (34)$$

where l is a direction perpendicular to the boundary and u is required flow velocity in this direction. A special case of the flow boundary conditions is the no-flow boundary where a complete barrier to flow is modelled where the appropriate derivative is set to zero. In the case of the partial penetration problem, the top and bottom of the reservoir interval represent no-flow boundaries resulting in the condition

$$\frac{\partial}{\partial z} \Phi = 0, \text{ for } z = 0 \text{ and } z = h, \quad (35)$$

where the origin of the co-ordinate system has been taken to be at the centre of the well where it intersects with the top of the reservoir interval. The well itself is required to produce at constant rate and also provides a flow boundary condition. If the total required rate from the well is q then the radial velocity, and hence the radial potential gradient, at the well is defined in terms of the equation

$$q = -2\pi r_w \int_{h_1}^{h_2} u dz = \frac{2\pi r_w k \gamma}{\mu} \int_{h_1}^{h_2} \frac{\partial \Phi}{\partial r} dz, \quad (36)$$

where the well geometry is shown in Figure 1.4. The constant flux assumption is that u is constant along the well and the required constraint becomes

$$\left(\frac{\partial \Phi}{\partial r} \right)_{r=r_w, h_1 \leq z \leq h_2} = \frac{q \mu}{2\pi r_w k h_w \gamma}. \quad (37)$$

On the other hand, if the infinite conductivity assumption is used then the potential is constant along the well bore,

$$\left(\frac{\partial \Phi}{\partial z} \right)_{r=r_w, h_1 \leq z \leq h_2} = 0, \quad (38)$$

and

$$\left(\int_{h_1}^{h_2} \frac{\partial \Phi}{\partial r} dz \right)_{r=r_w} = \frac{q \mu}{2\pi r_w k \gamma}. \quad (39)$$

Equations 37, 38, and 39 are difficult to deal with analytically and so are often taken to apply only in the limit as $r_w \rightarrow 0$. Solutions using this assumption are known as line source solutions.

Initially, before the flow begins, the reservoir is taken to be in hydrostatic equilibrium. That is

$$\Phi = \Phi_i, \text{ at } t = 0, \text{ for all } r. \quad (40)$$

To satisfy the requirement for transience the potential at any lateral boundary must be unaffected by the disturbance at the well. To achieve this a constant potential can be defined at an infinite distance from the well. For example,

$$\Phi = \Phi_i, \text{ at } r = \infty, \text{ for all } t. \quad (41)$$

The use of these boundary conditions (Equations 35, 37, 40 and 41) in conjunction with the diffusivity equation (Equation 33) is sufficient to fully describe the single phase isotropic version of the problem for liquid flow. The anisotropic problem requires slight modification to Equation 33 in that permeability needs to be treated as a property tensor rather than as a scalar. Some additional formulae are needed for the multi-phase problem and these are dealt with in Section 2.6.

2.5 Analytical Solutions of the Diffusivity Equation

The petroleum engineering literature is full of papers describing various solutions of the diffusivity equation for specific boundary conditions and using different approaches for solution. It is not intended to give anything other than a brief description here.

Probably the most fundamental solution for the purpose of well test analysis is that of a fully penetrating well in an infinite radially symmetric system subject to a boundary condition of a single change in rate at the well bore with the rate held constant thereafter. This is known as the constant terminal rate solution. A simplified solution can be obtained using the line source inner boundary condition as mentioned in the previous section. This leads to a simple two-dimensional problem that can be solved using a simple transformation of variables giving an equation involving the exponential integral with time and radius as variables (Equation 6). Using the logarithmic approximation to the exponential integral and evaluating the function at the well bore radius gives an equation where the pressure is a logarithmic function of time (Equation 7).

A large part of well test analysis therefore consists of plotting pressure in terms of logarithmic functions of time in order to assess the degree of adherence to ideal behaviour. Variations from this behaviour can be interpreted in terms of deviations from ideal geometry or in terms of changes in reservoir properties. In Chapter 5 analysis techniques based on the line source solution will be discussed further and will be used to infer the magnitude of permeability in the well being modelled.

Much of the advantage in using the diffusivity equation as the basis for analytical techniques is that it is linear and therefore more complex solutions can be built up using superposition in time and space. In the case of real well tests the rate is normally variable involving both flowing periods and periods when the well is closed requiring superposition in time in order to model the pressure response. In other cases

complex geometries can be built up through the superposition of flux elements. Many of the partially penetrating well solutions mentioned in Section 1.1 are of this nature.

The application of Laplace transforms to the diffusivity equation for particular boundary conditions often results in problems that are easier to solve. In many cases the solution is left in Laplace space as an analytical inversion is difficult to obtain. In Chapter 4 two such solutions for partially penetrating wells will be evaluated using a numerical inversion of the Laplace space solution.

2.6 Black-oil Fluid Model

The complex behaviour of hydrocarbon fluids under changing conditions of pressure, volume, and temperature (PVT) make it difficult to model multi-phase problems adequately.

Most of the fluid behaviour in the reservoir can be regarded as occurring under isothermal conditions. This is because the reservoir is relatively thin in comparison to rock above and below it. The surrounding rock acts as a heat reservoir that can, for all practical purposes, be regarded as infinite. However, when the reservoir fluid is brought to the surface it undergoes changes in pressure and temperature. The major source of difficulty is that as conditions change gas can be liberated from the liquid phase and liquid can condense from the gas phase.

An approximation that is often used in the oil industry is to assume that the reservoir hydrocarbons are made up of only two components, namely one that is liquid at surface conditions (stock tank oil or condensate) and one that is gaseous at surface conditions (dry gas). Both the reservoir liquid phase and the reservoir gas phase are made up of both components. At reservoir conditions some of the surface gas dissolves in the reservoir liquid and vaporised surface liquid is present in the gas phase. This approximation is known as the black oil model and can adequately describe PVT behaviour of hydrocarbons for many reservoir engineering problems.

Four parameters are needed for a complete description of the hydrocarbons. These have been expressed in terms of field units below:

- B_o , the oil formation volume factor. This is the volume that liquid occupies in the reservoir relative to the volume of surface liquids that would be generated on taking the reservoir liquid to surface. B_o has units of reservoir barrels per stock tank barrel (rb/stb). Note that B_o is generally larger than one because of the extra gas dissolved in the oil at reservoir conditions.

- B_g , the gas formation volume factor. This is the volume that gas occupies in the reservoir relative to the volume of surface gas that would be generated on taking the reservoir gas to surface. B_g is normally given in terms of reservoir barrels per standard cubic feet (rb/scf).
- R_x , the solution (or dissolved) gas-oil ratio. This is the ratio of surface gas to surface liquid that results when the reservoir liquid phase is brought to surface conditions. R_x has units of standard cubic feet per stock tank barrel (scf/stb).
- R_v , the vaporised oil fraction. This is the ratio of surface gas to surface liquid that results when the reservoir gas phase is brought to surface conditions. R_v has units of stock tank barrel per standard cubic feet (stb/scf).

A third component is necessary to describe the flow of reservoir brine or injected water. It is generally assumed that there is no solubility between the hydrocarbons and the water phase. Only one additional parameter is therefore necessary and this is the water formation volume factor B_w .

The multi-phase flow equation (Equation 22) can now be defined for each component. The product $\rho_p y_{p,c}$ can be replaced with the product of surface density and equivalent surface volume. For example, for the component stock tank oil (sto) and reservoir oil phase (ro), $\rho_{ro} y_{ro,sto}$ is replaced by ρ_{sto} / B_o . Since the density at surface conditions is a constant for each component and it appears on both sides of the equation it can be eliminated, giving:

$$\frac{\partial}{\partial t} \left[\left(\frac{S_o}{B_o} + \frac{R_v S_g}{B_g} \right) \phi \right] = -\nabla \cdot k \left[\frac{k_{ro} \gamma_o}{B_o \mu_o} \nabla \Phi_o + \frac{R_v k_{rg} \gamma_g}{B_g \mu_g} \nabla \Phi_g \right]; \quad (42)$$

$$\frac{\partial}{\partial t} \left[\left(\frac{S_g}{B_g} + \frac{R_x S_o}{B_o} \right) \phi \right] = -\nabla \cdot k \left[\frac{k_{rg} \gamma_g}{B_g \mu_g} \nabla \Phi_g + \frac{R_x k_{ro} \gamma_o}{B_o \mu_o} \nabla \Phi_o \right]; \quad (43)$$

$$\frac{\partial}{\partial t} \left[\frac{S_w}{B_w} \phi \right] = -\nabla \cdot k \left[\frac{k_{rw} \gamma_w}{B_w \mu_w} \nabla \Phi_w \right], \quad (44)$$

which are the oil, gas, and water equations respectively. These equations can also be expressed in terms of pressures using the approximate relationship

$$\gamma \nabla \Phi \approx \nabla p - \gamma \nabla D. \quad (45)$$

When more than one fluid occupies the pore space of the reservoir rock, surface tension effects dictate that the pressures in the two phases are different. This pressure

difference is known as the capillary pressure. Generally one of the phases has a greater affinity for the surface of the rock than the other and therefore occupies the smaller pores. This phase is known as the wetting phase. As the capillary pressure increases the other (non-wetting) phase can enter smaller and smaller pores, displacing the wetting phase. Thus, like relative permeability, capillary pressure is a function of saturation and the pore geometry of the rock. It is therefore normally measured in the laboratory on rock samples taken from the reservoir of interest. Capillary pressure relationships allow the pressures and hence potentials of the gas and water phases to be related to the oil phase pressure through the equations

$$p_w = p_o - p_{c,ow}(S_w) \quad (46)$$

and

$$p_g = p_o + p_{c,og}(S_g). \quad (47)$$

A final equation that completes the description is

$$S_o = 1 - S_w - S_g, \quad (48)$$

which is simply a statement of the fact that the pore space is completely occupied by the three phases. Equations 42 to 48 can be solved for all the phase saturations and pressures. The state of the system at any point in the reservoir is completely described by the variables p_o , S_w , and S_g since the other variables can be established using Equations 46 to 48.

2.7 Compositional model

Some reservoir engineering problems deal with fluids whose PVT behaviour is too complicated to be described using the black oil model. An example of such a fluid is one that is close to its critical point. A small change in pressure for such a fluid can dramatically change the ratio of liquid to vapour in the reservoir and also the properties of each phase.

For these more difficult problems it is possible to model the fluid behaviour in terms of the interaction of its molecular components. Typically this is achieved through the use of an equation of state such as the Peng-Robinson equation of state. This allows the molar fraction of each component in the liquid and vapour to be estimated, which in turn allows the mass fractions to be substituted into the flow equation (Equation 22). Computationally, compositional models are very expensive as they require the numerical solution of the equation of state at every grid block for every trial pressure.

In practice it is not possible to deal with more than a few components and it is therefore necessary to group together molecules with similar properties. In order to have validity it is necessary to match the behaviour of the compositional model to experiments performed on the reservoir fluid in the laboratory.

Compositional models will not be considered further in this thesis.

2.8 Chapter Summary

In this chapter the non-linear differential equations governing multi-phase fluid flow in porous media were derived. Combining Darcy's Law with conservation of mass led to the formulation of the mass-flow equation, which was extended to multi-phase systems using the concepts of relative permeability and capillary pressure. Pressure dependent properties were accommodated through the use of a simplified fluid PVT representation, the black-oil model. In the special case of single phase flow of a slightly compressible fluid, it is possible to make approximations that convert the mass-flow equation to a second order linear equation known as the diffusivity equation. This forms a basis for the analytical solutions that the simulation will be compared to.

In the next chapter the numerical methods used to solve the multi-phase mass flow equation will be reviewed. The differential equations will be approximated by a set of finite difference equations that can more readily be solved numerically and that can accommodate spatially varying properties such as those to be used in the real-life problem.

Chapter 3: Numerical Scheme

Analytical techniques attempt to solve the equations developed in Chapter 2 by finding a function that satisfies the equations for a continuous interval in time and space. While it is possible to solve these equations analytically for particular simplified cases, general solutions are not possible. One of the factors that makes real life problems difficult is the occurrence of heterogeneous properties. As has been discussed in Chapter 1, heterogeneous and strongly anisotropic properties are the rule rather than the exception when dealing with the sedimentary rocks that oil is commonly found in.

This chapter discusses a numerical scheme that allows approximate solutions to be obtained. This scheme, unlike the analytical techniques, evaluates the state of the system at discrete points in time and space. For each of the chosen points in space the future state of the point is determined from the current state of all the other points. The equations given in Chapter 2 are modified to obtain new equations in terms of these discrete points, the number of equations being related to the number of points chosen. These equations are then solved simultaneously for each of the required time values. It is possible to choose points that are sufficiently close together to obtain the accuracy required for practical purposes, the major limitations being the speed and memory capabilities of the computer used to solve the discrete equations.

3.1 Gridding

The process of choosing the spatial points (grid points) at which the discrete equations will be evaluated is known as gridding. Typically, the reservoir is represented as a series of discrete volume elements (grid blocks) with a single such element associated with each grid point. Each property, although possibly varying within a grid block, is represented by a single value at the grid point. An important consideration in terms of minimising the errors associated with this simplification is the choice of the most appropriate position of either the grid point within the grid block or alternatively the grid block boundaries (faces) between grid points.

Various gridding systems are supported by reservoir simulation. The most common forms of grid are the Cartesian grid and the radial grid. In the Cartesian grid, the grid points are arranged in lines parallel to the Cartesian axes (x , y) giving rise to rectangular grid blocks. Note that the spacing between successive lines of grid points need not be constant. Three dimensional grids may consist of several layers. Adjacent grid blocks may be displaced in the z -direction to accommodate changes in the depth of a layer. An example of a Cartesian grid is shown in Figure 3.1.

FIGURE 3.1: A SIMPLE CARTESIAN GRID

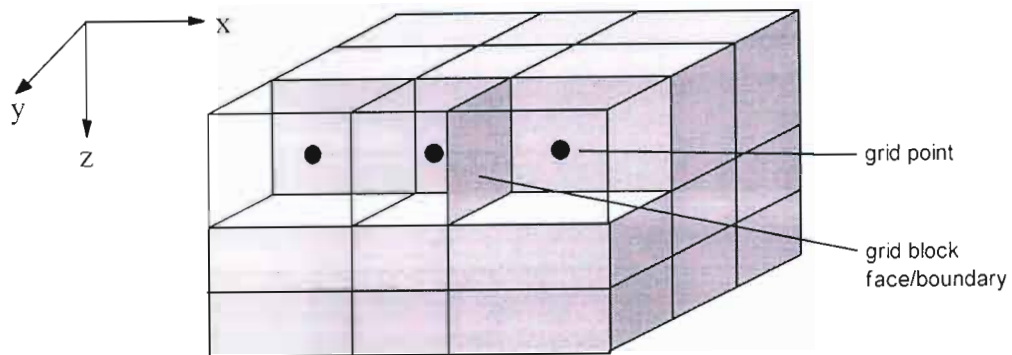
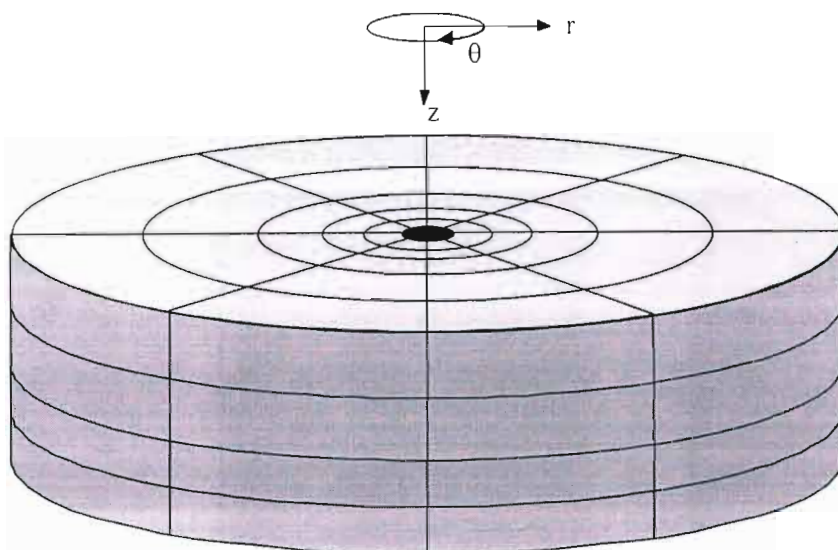


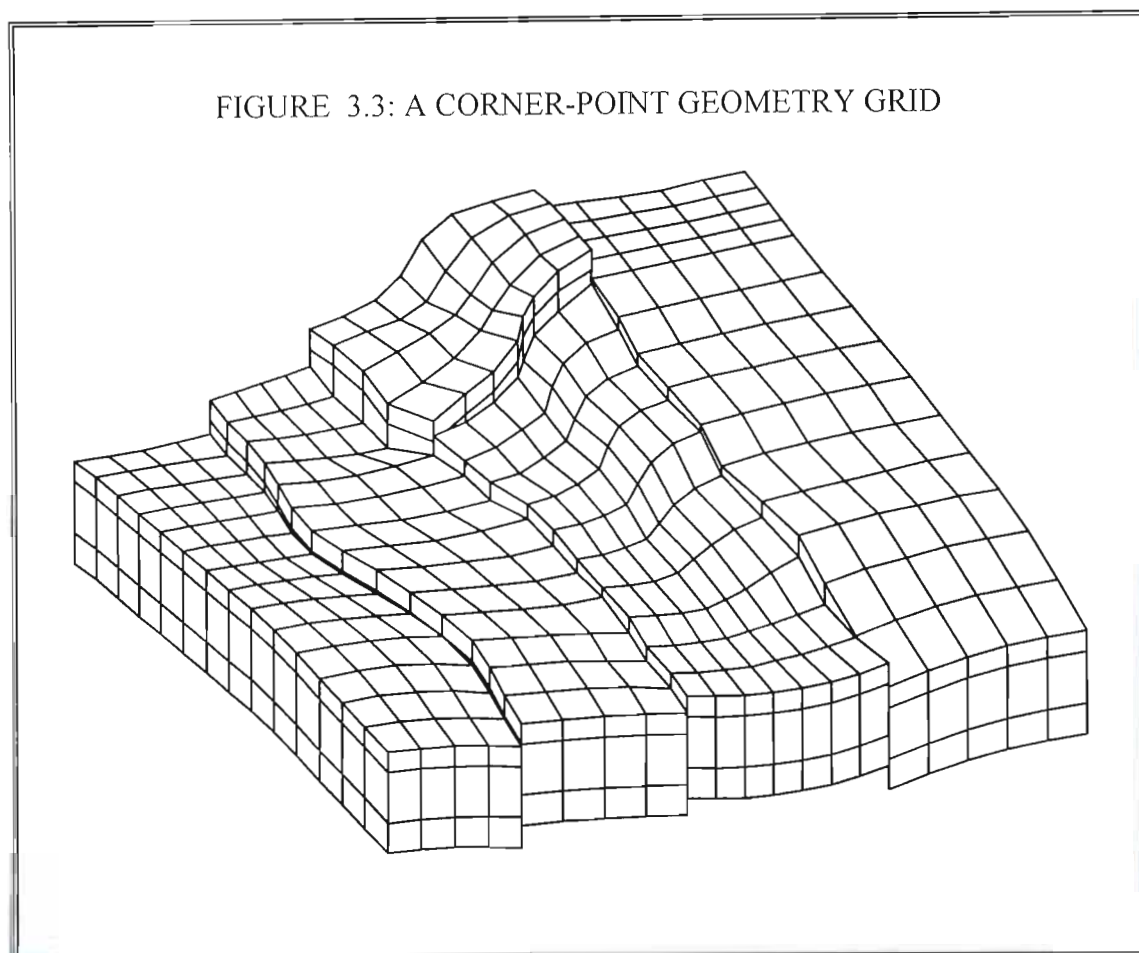
FIGURE 3.2: A SIMPLE RADIAL GRID



Radial grids have grid points arranged along lines corresponding to a cylindrical coordinate system (r, θ, z) resulting in grid blocks that are segments of cylindrical shells about the line $r=0$. Because of their geometry, radial grids lend themselves naturally to single well problems. The theta direction can be ignored when there is reason to believe that there is cylindrical symmetry about the well bore, giving a two-dimensional set of grid-points spaced along the r and z axes. Cylindrical symmetry is

often a reasonable assumption when the well is vertical and the sedimentary layers of the rock horizontal. An example of a radial grid is shown in Figure 3.2.

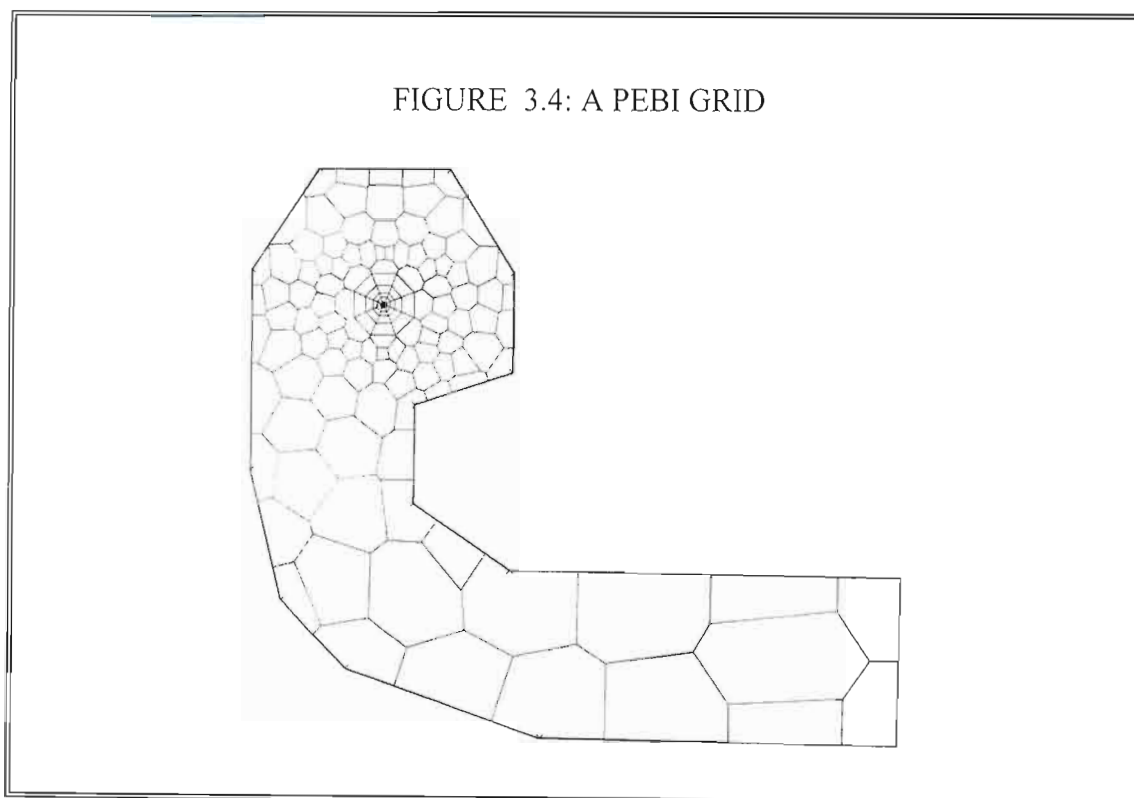
Real reservoirs are often structurally too complex to be accurately represented by a rigid Cartesian grid. This has led to the use of gridding schemes with more geometrical flexibility. One such scheme is the corner point geometry grid where the individual blocks are no longer strictly rectangular. In this scheme the grid block corners lie on lines that are not perfectly straight but are slightly distorted in order to follow natural features in the reservoir.



A common reason for wanting to use corner point geometry is that the reservoir is geologically faulted, i.e. layers that were originally adjacent have been displaced so that they are no longer adjacent. The fault plane, or surface along which the displacement has taken place, can be curved and may intersect the reservoir at an angle. In this instance the corners of the grid blocks would be shifted so that they lie on the fault plane. An example of a corner point geometry used to model a complex reservoir is given in Figure 3.3. Unfortunately the added convenience comes at the cost of reduced accuracy if a conventional numerical scheme is used to solve the flow

equations for such a grid. Abdou et al²⁶ have found significant differences between simulation results obtained with a normal Cartesian grid and those obtained using a corner point grid when simulating a highly faulted reservoir in the Middle-East. Typically, the error in the solution is a function of the extent to which the grid blocks differ from a perfect rectangular prism.

More recently, methods with even greater geometric flexibility and without the reduced accuracy of the corner point grid have been developed. One such method is the use of Voronoi, or perpendicular bisection (PEBI), grids which has been pioneered by Heinemann²⁷ for use in reservoir simulation. These grids have the property that the faces of the grid blocks perpendicularly bisect the lines joining adjacent grid-points. An example showing the block boundaries for a two-dimensional PEBI grid is given in Figure 3.4.



Three dimensional PEBI grids using irregular polyhedral grid blocks can be constructed but are complex to visualise. Usually a PEBI grid is defined in a horizontal plane and then projected vertically onto a number of layers giving grid blocks that are polygonal prisms. The grid construction is further complicated in three dimensions when strong anisotropy exists between vertical and horizontal properties. Amando et al²⁸ have demonstrated how arbitrary PEBI grid blocks can be constructed for this case. There are few commercial reservoir simulators that currently offer PEBI

grids. One of these is a well testing package from Intera which allows the user to set up complex reservoir shapes and then simulate the pressure response that results.

3.2 Finite Difference Equations

The black-oil fluid flow formulae given in Equations 42 to 44 in Section 2.6 can be summarised as:

$$\frac{\partial}{\partial t} M = -\nabla \cdot F, \quad (49)$$

where M and F are vectors with one element per component and are defined by

$$M = \begin{bmatrix} \frac{S_o}{B_o} + \frac{R_v S_g}{B_g} \\ \frac{S_g}{B_g} + \frac{R_s S_o}{B_o} \\ \frac{S_w}{B_w} \end{bmatrix} \phi, \quad (50)$$

which represents the mass accumulation terms and

$$F = k \begin{bmatrix} \frac{k_{ro} \gamma_o}{B_o \mu_o} \nabla \Phi_o + \frac{R_v k_{rg} \gamma_g}{B_g \mu_g} \nabla \Phi_g \\ \frac{k_{rg} \gamma_g}{B_g \mu_g} \nabla \Phi_g + \frac{R_s k_{ro} \gamma_o}{B_o \mu_o} \nabla \Phi_o \\ \frac{k_{rw} \gamma_w}{B_w \mu_w} \nabla \Phi_w \end{bmatrix}, \quad (51)$$

which represents the flow terms.

A backward difference approximation for the time derivative can be obtained by using a Taylor series to expand the mass term at a new time, $M(t + \Delta t)$, about the current mass term, $M(t)$, giving

$$M(t + \Delta t) = M(t) + \Delta t \frac{\partial M}{\partial t} + \frac{\Delta t^2}{2} \frac{\partial^2 M}{\partial t^2} + \dots \quad (52)$$

Re-arranging Equation 52 gives

$$\frac{\partial M}{\partial t} = \frac{M(t + \Delta t) - M(t)}{\Delta t} + \varepsilon_t, \quad (53)$$

where ε_t is the time discretisation error which can be ignored for sufficiently small time increments.

Discretisation of the spatial derivatives is a little more complex. Aziz and Settari²⁹ discuss three discretisation methods: the Taylor series method (similar to that used for the time discretisation above); the integral method; the variational method. The variational method is the basis of the finite element approach and will not be discussed further. From a physical point of view the integral method is the easiest to understand and will be discussed here. The Taylor series is discussed further in Section 4.5 where it is used to derive an alternative nine-point discretisation scheme.

As part of the gridding process the reservoir model has been broken up into a number of grid blocks. Equation 49 applies to every point in the reservoir and can be integrated over the volume of a grid block giving:

$$\int_V \frac{M(t + \Delta t) - M(t)}{\Delta t} dV = - \int_V \nabla \cdot F dV, \quad (54)$$

where the time discretisation has been incorporated into the equation. Green's divergence theorem can be used to convert the volume integral of the flow terms into a surface integral:

$$- \int_V \nabla \cdot F dV = - \int_A F \cdot \bar{n} dA \quad (55)$$

where the integral is over all the surfaces of the grid block and \bar{n} is the outward unit vector normal to the surface. The surface integral can be split into a sum of the surface integrals for each face of the grid block so that :

$$\int_V \frac{M(t + \Delta t) - M(t)}{\Delta t} dV = - \sum_m \int_{A_m} F \cdot \bar{n} dA \quad (56)$$

The integrals are now evaluated by taking the average value of the integrand and multiplying by either the grid block volume or the face area as appropriate. For example, the mass terms therefore simply become

$$\int_V \frac{M(t + \Delta t) - M(t)}{\Delta t} dV \approx \left[\frac{M(t + \Delta t) - M(t)}{\Delta t} \right] V, \quad (57)$$

where M is evaluated at the grid point of the block in question.

The gradients inherent in the flow terms are converted into finite differences involving the value of the appropriate variables at adjacent grid points. In the simplest case the finite differences for a given face are formed only from the values of the two grid points of the blocks that share the face. For example, the flow terms for the stock tank oil component across a single face are approximated by

$$\begin{aligned}
 - \int_{A_m} F \cdot \bar{n} \, dA &= -A_m k \left(\frac{k_{ro} \gamma_o}{B_o \mu_o} \nabla \Phi_o + \frac{R_v k_{rg} \gamma_g}{B_g \mu_g} \nabla \Phi_g \right) \cdot \bar{n} \\
 &= \frac{A_m k_x}{\Delta x} \left(\frac{k_{ro} \gamma_o}{B_o \mu_o} \Delta \Phi_o + \frac{R_v k_{rg} \gamma_g}{B_g \mu_g} \Delta \Phi_g \right), \quad (58)
 \end{aligned}$$

where it has been assumed that \bar{n} is parallel to the line joining the grid points and furthermore that the grid is oriented to coincide with the principal axes of the permeability tensor. The average component of the permeability parallel to \bar{n} has been labelled k_x . A_m is the area of the common face and Δx is the distance between the grid points of the adjacent cells. In a practical sense in reservoir simulation and for ease of use it is often more convenient to work in terms of pressure differences. For this reason the potential differences are often expressed in terms of a pressure potential, Ψ , that directly incorporates the fluid density gradient factor, γ . The relationship between the two types of potential is $\Delta \Psi = \lambda \Delta \Phi$. The pressure potential differences are then given by:

$$\Delta \Psi_o = p_{o,n} - p_{o,i} - \gamma_o (D_n - D_i); \quad (59)$$

$$\Delta \Psi_g = p_{o,n} - p_{o,i} - \gamma_g (D_n - D_i) - p_{cog,n} + p_{cog,i}, \quad (60)$$

where D is the depth of the grid point and the subscripts, n and i , refer to the neighbouring and current blocks respectively. Similar finite difference equations can be defined for the other two components, water and gas. The water component requires the definition of the water potential difference

$$\Delta \Psi_w = p_{o,n} - p_{o,i} - \gamma_w (D_n - D_i) - p_{cow,n} + p_{cow,i}. \quad (61)$$

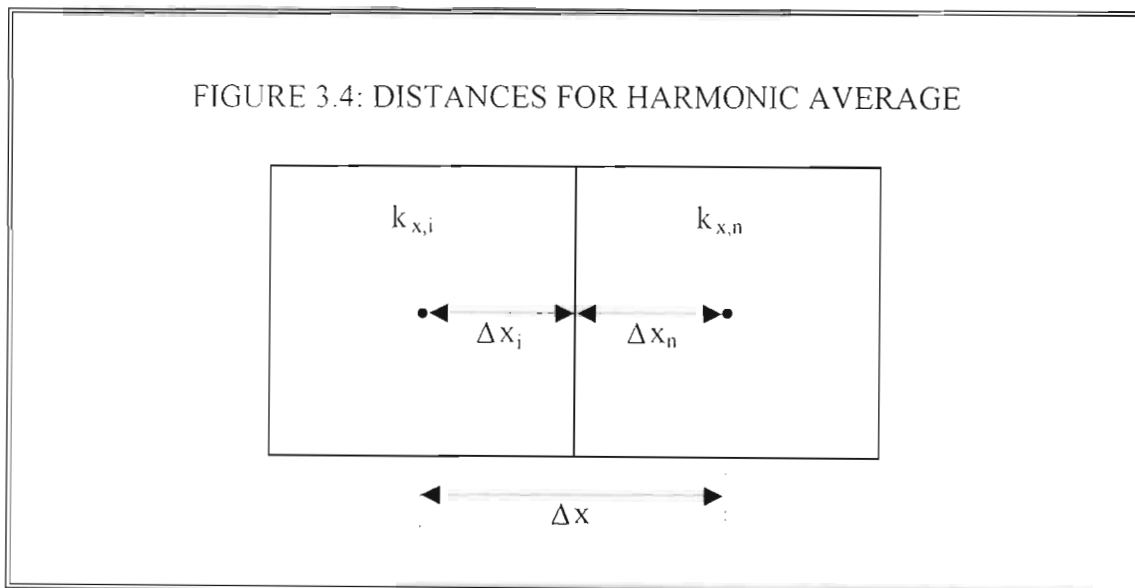
Note that potential differences are based on Equation 45, and have been expressed in terms of the oil pressure using the capillary pressure relationships given in Equations 46 and 47.

The average permeability component across the face, k_x , is normally calculated by assuming that permeability is constant within each block and changes sharply at the face of the grid block. The subscript x denotes the component of permeability in the

x-direction, parallel to \bar{n} . By assuming that steady state linear flow occurs between the grid blocks one can show that the harmonic average

$$k_x = \frac{\Delta x}{\frac{\Delta x_n}{k_{x,n}} + \frac{\Delta x_i}{k_{x,i}}}, \quad (62)$$

is appropriate. In this formula the subscripts n and i indicate properties of the neighbouring block and the initial block respectively. Δx is the distance between the adjacent grid points, Δx_n and Δx_i are the distances from the appropriate grid point to the common block boundary, as depicted in Figure 3.4. Typically the factor, $T = A_m k_v / \Delta x$, is grouped together as one item and is known as the transmissibility. Note that there is no unique way of calculating the transmissibility. Aziz and Settari²⁹ derive several equations that may be relevant for particular cases. In particular, the assumption of linear flow may not be the most efficient in situations where one is dealing with near well-bore effects such as the partially completed well considered in this thesis. The calculation of transmissibilities for a radial grid, given in Section 3.3, takes this into account.



Transmissibility is a constant throughout time for a particular pair of blocks and applies equally to all the phases. The factors: $k_{ro} / B_o \mu_o$; $k_{rg} / B_g \mu_g$; $k_{rw} / B_w \mu_w$, on the other hand are fluid specific and are termed the fluid mobilities. They are functions of the pressure and saturation of the block and therefore vary with time.

From a numerical point of view it would seem that these mobilities should be evaluated using some sort of mid-point weighting scheme that uses the properties of

the fluid in both blocks. Aziz and Settari²⁹ have shown that a mid-point weighting scheme can converge to a physically incorrect solution while an upstream weighting scheme gives the correct solution. Generally, therefore, the mobilities and associated R_x and R_y are evaluated in the block that the flow is coming from. Formally, if λ denotes the fluid mobility then

$$\lambda = \begin{cases} \lambda_i, & \text{if } \Psi_i > \Psi_n \\ \lambda_n, & \text{if } \Psi_n \geq \Psi_i \end{cases} \quad (63)$$

There is one outstanding issue that needs to be settled before the definition of the finite difference equations is complete and that is the definition of the time variable for the flow terms. For the mass terms it is quite clear at which time value the variables are to be evaluated, but for the flow terms it is not clear if they should be evaluated at the beginning, end, or middle of the time step. The simplest is clearly to evaluate the flow terms at the beginning of the time step when all the values are known from the previous time step. This is known as the explicit method. The drawback of the method is that it is potentially unstable. Aziz³⁰ states that the limits placed on time step size by stability requirements in the explicit method are totally impractical for typical compressibilities of reservoir fluids.

The method used by Eclipse³¹ is the fully implicit method which is totally stable. In this method the values of all the variables affecting the flow terms are evaluated at the end of the time step. This of course immediately implies a need to simultaneously solve the entire set of difference equations for all the unknowns - the pressure and saturations at each and every grid block.

Aziz and Settari²⁹ deal at length with the problems of stability and consistency for reservoir models. Stability relates to whether errors in the estimated solution grow from time step to time step, and consistency relates to whether the errors tend to zero as the time step and block size tend to zero. These issues, though important, will not be dealt with further in this thesis. Suffice it to say that the Eclipse model satisfies these constraints provided care is taken not to define highly irregular grids.

In summary, we now have a set of non-linear equations with one equation per grid block per fluid component. These equations have the form:

$$R(X) = \frac{M(t + \Delta t) - M(t)}{\Delta t} V - F(t + \Delta t) = \bar{0}, \quad (64)$$

where $\bar{0}$ is the null vector, M , F , and V are vectors with one element per grid block. Furthermore, each element of M is itself a vector with one element per fluid

component as defined by Equation 50. X is the state vector containing the values of oil pressure, water saturation and gas saturation at the end of the current time step for every grid block. Solution of the equations at each time step hinges on trying to find a X such that $R(X) = \bar{0}$. Elements of F are formed from the sum of the flows from the neighbouring blocks and each element is also a vector with one element per fluid component. That is, for the i -th block:

$$F_i = \sum_n F_{ni}, \quad (65)$$

where the subscript n refers to the neighbouring block and

$$F_{ni} = T_{ni} \begin{bmatrix} \lambda_o & 0 & R_v \lambda_g \\ 0 & \lambda_w & 0 \\ R_s \lambda_o & 0 & \lambda_g \end{bmatrix} \begin{bmatrix} \Delta\Psi_o \\ \Delta\Psi_w \\ \Delta\Psi_g \end{bmatrix} \quad (66)$$

where λ represents the fluid mobility and the pressure potential difference, $\Delta\Psi$, is as defined by Equations 59 to 61.

In a three-dimensional radial or Cartesian grid, the flow element for each block is a function of the properties of seven blocks: the grid block being considered and the six adjacent grid blocks that share faces with it. In a two dimensional grid the flow element involves the properties of five blocks. These spatial discretisation schemes are therefore known as the seven and five point methods respectively. For example, a single element of R for the interior block with grid co-ordinates (i, j, k) is given by:

$$R_{(i,j,k)} = \frac{\Delta M_{(i,j,k)} V_{(i,j,k)}}{\Delta t} - F_{(i,j,k)(i-1,j,k)} - F_{(i,j,k)(i+1,j,k)} - F_{(i,j,k)(i,j-1,k)} - F_{(i,j,k)(i,j+1,k)} - F_{(i,j,k)(i,j,k-1)} - F_{(i,j,k)(i,j,k+1)}, \quad (67)$$

where ΔM is a function of the properties at the block located at (i, j, k) only and each of the F terms is a function of the properties at this block and a neighbouring block. There are other discretisation methods which also involve the properties of the diagonally adjacent blocks giving a nine point scheme in two dimensions and a twenty-seven point scheme in three dimensions.

3.3 Calculation of Transmissibilities for a Radial Grid

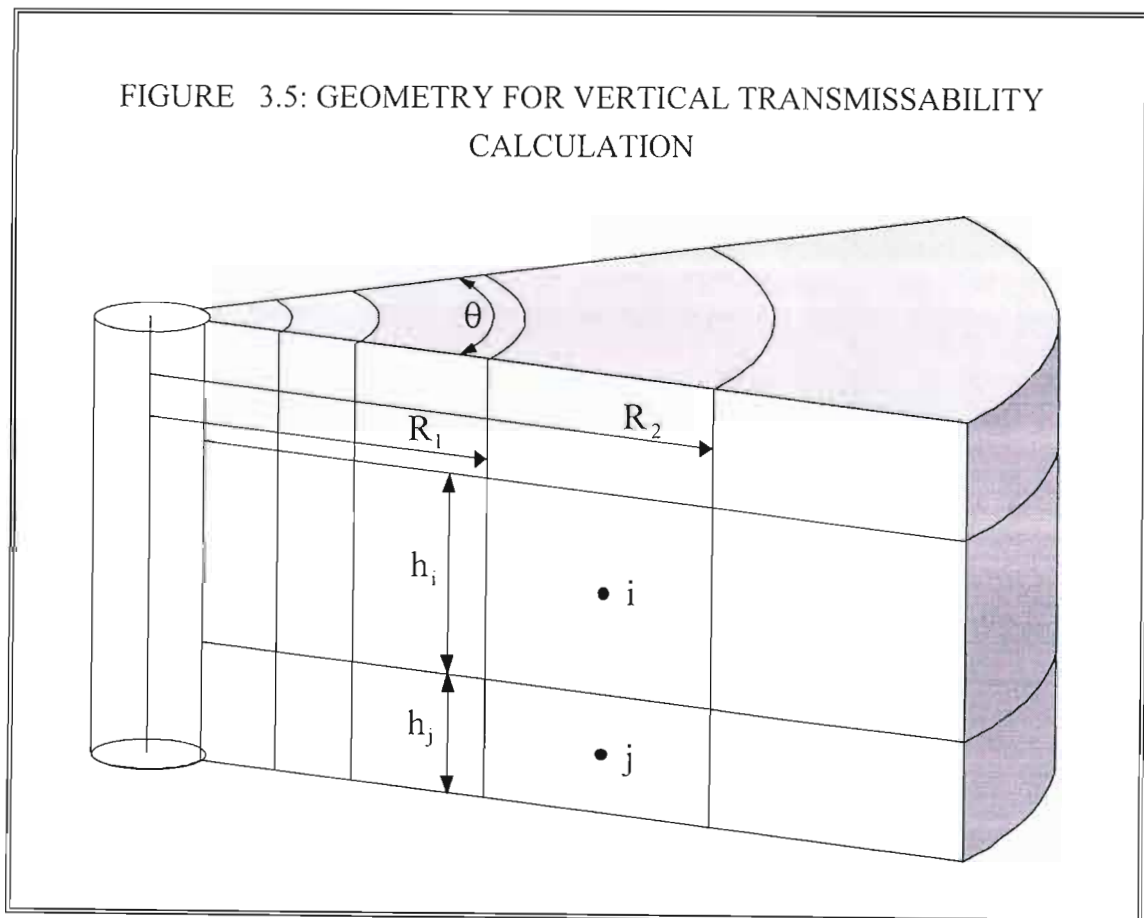
Radial grids are often used for near well-bore problems where pressure as a function of radius is strongly non-linear. For these grids, therefore, it is better to calculate transmissibilities using the assumption that pressure varies linearly according to the logarithm of radial distance from the well-bore. As will be shown this gives a

transmissibility that exactly relates the flow to pressure drop for steady-state radial flow. In the vertical direction it is normally assumed that pressure varies linearly.

The basis of both calculations is the definition of transmissibility, T , as providing a constant of proportionality between rate and potential difference:

$$q = T\lambda_f \Delta\Psi, \quad (67)$$

where q is the rate of flow between the blocks, $\lambda_f = k_{rf} / B_f \mu_f$ is the mobility of the fluid in question, and $\Delta\Psi$ is the difference in pressure potential at the two grid points. For purposes of calculating the transmissibility, it can be assumed that the mobility is constant.



To calculate the transmissibility in the vertical direction, the steady state relationship between pressure potential and rate within a grid block of constant properties is used. From Darcy's Law (Equation 1), the potential difference between the centre of the block and the face of the vertically adjacent block can be shown to be given by:

$$\Delta\Psi = \frac{q B_j \mu_j}{k_{r,j} k A} \Delta l = \frac{hq}{\lambda_j k_z \theta (R_2^2 - R_1^2)}, \quad (68)$$

where Δl is the distance over which the potential difference is measured, A is the area over which the flow is measured, k is the component of permeability in the direction of flow, and where the grid block is a cylindrical slice (Figure 3.5) of angle θ , vertical thickness h , inner radius R_1 , outer radius R_2 , and k_z is the component of the permeability tensor in the vertical direction.

The overall potential difference from the centre of block i to the centre of block j is then the sum of the potential differences within each block:

$$\Delta\Psi = \frac{q}{\lambda_j (R_2^2 - R_1^2)} \left[\frac{h_i}{k_{z,i} \theta_i} + \frac{h_j}{k_{z,j} \theta_j} \right], \quad (69)$$

where the rate is constant because of the steady state assumption. Comparison with Equation 67 shows that the vertical transmissibility, T_z , between blocks i and j is given by:

$$T_z = \frac{(R_2^2 - R_1^2)}{\frac{h_i}{k_{z,i} \theta_i} + \frac{h_j}{k_{z,j} \theta_j}}. \quad (70)$$

The transmissibility in the radial direction presents more of a problem. For purely radial, steady state flow from the radius r_2 to the radius r_1 in a cylindrical slice of angle θ and vertical thickness h , the relationship between rate and potential difference is given by²⁵:

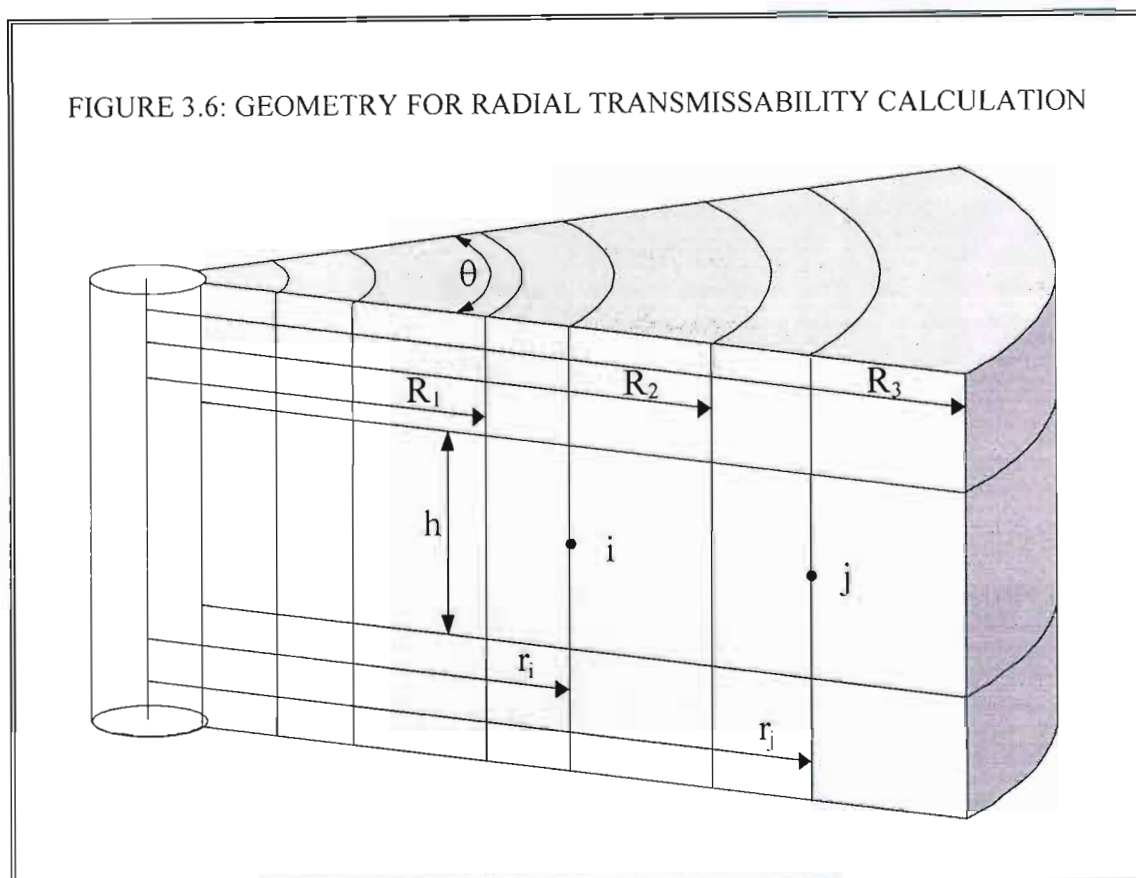
$$q = \frac{k_r \theta h}{\ln(r_2/r_1)} \lambda_j \Delta\Psi, \quad (71)$$

where θ is measured in radians and k_r is the permeability in the radial direction.

Let R_1 be the innermost radius of block i , R_2 be the outermost radius of block i and innermost radius of block j , and R_3 be the outermost radius of block j . If one assumes that k_r , θ , and h , are constant within each block and change sharply at the block boundary then Equation 71 can be used to evaluate the potential drop between grid point and block boundary for each block, giving:

$$\Delta\Psi = (\Delta\Psi_i + \Delta\Psi_j) = \frac{q}{\lambda_j} \left[\frac{\ln(R_2/r_i)}{k_{r,i} \theta_i h_i} + \frac{\ln(r_j/R_2)}{k_{r,j} \theta_j h_j} \right], \quad (72)$$

where r_i is the radius of the grid point for block i , r_j is the radius of the grid point for block j . The geometry of the blocks is depicted in Figure 3.6.



Comparing Equation 72 with Equation 67 shows that

$$T_r = \frac{1}{\frac{1}{T_i} + \frac{1}{T_j}} = \frac{1}{\frac{\ln(R_2/r_i)}{k_{r,i}\theta_i h_i} + \frac{\ln(r_i/R_2)}{k_{r,j}\theta_j h_j}} \quad (73)$$

There are a number of possible assumptions for the position of the grid point:

(a) Grid Point at the Geometric Mean of Inner and Outer Radii

Typically a radial grid will have grid blocks that have a geometric spacing in the radial direction. This minimises the truncation errors in the discretisation of the flow terms because there is an equal pressure drop across each cell for steady state radial flow. It therefore seems reasonable to assume that the grid point is at the geometric mean of the inner and outer radii will put the grid point at a position where its pressure potential is midway between that at the two boundaries. Thus the radius of the grid

point for block i is $r_i = \sqrt{R_1 R_2}$ and that for block j is $r_j = \sqrt{R_2 R_3}$. Substituting for r_i and r_j in Equation 73 gives

$$T_r = \frac{1}{\frac{\ln(R_2 / \sqrt{R_1 R_2})}{k_{r,i} \theta_i h_i} + \frac{\ln(\sqrt{R_2 R_3} / R_2)}{k_{r,j} \theta_j h_j}} \quad (74)$$

Simplifying leads to

$$T_r = \frac{2}{\frac{\ln(R_2 / R_1)}{k_{r,i} \theta_i h_i} + \frac{\ln(R_3 / R_2)}{k_{r,j} \theta_j h_j}} \quad (75)$$

This equation assumes that the grid point is at the pressure centre of the grid block. Note that this is not the same as the centre of mass of the grid block. This may cause problems with the mass accumulation terms in the finite difference equations if the mass in the block is strongly related to the pressure.

(b) Grid Point at the Centre of Mass

If one assumes that the grid point is at the centre of mass of the grid block then the radii of the grid points become $r_i = \sqrt{(R_1^2 + R_2^2)/2}$ and $r_j = \sqrt{(R_2^2 + R_3^2)/2}$ for blocks i and j respectively. Substituting these new radii in Equation 73 gives:

$$T_r = \frac{1}{\frac{\ln\left(R_2 / \sqrt{(R_1^2 + R_2^2)/2}\right)}{k_{r,i} \theta_i h_i} + \frac{\ln\left(\sqrt{(R_2^2 + R_3^2)/2}\right)}{k_{r,j} \theta_j h_j}} \quad (76)$$

Simplifying leads to:

$$T_r = \frac{2}{\frac{\ln\left[R_2^2 / (R_1^2 + R_2^2)\right] + \ln 2}{k_{r,i} \theta_i h_i} + \frac{\ln\left[(R_2^2 + R_3^2) / R_2^2\right] - \ln 2}{k_{r,j} \theta_j h_j}} \quad (77)$$

This still does not completely solve the problem since we really need the radius at which the pressure is equal to the volume weighted average pressure. This is also known as the pressure equivalent radius.

(c) Grid Point at the Pressure Equivalent Radius

To calculate the pressure equivalent radius it is first necessary to calculate the volume weighted average pressure, \bar{p} , for the block concerned. For steady state radial flow in block i the pressure as a function of radius is given by

$$p(r) = p(R_1) + c \ln(r / R_1), \quad (78)$$

where $c = q / \lambda_j k_{r,i} \theta_i h_i$ is a constant for the block. \bar{p} is obtained by integrating the pressure over the volume of the block and dividing by total block volume.

$$\bar{p} = \frac{1}{V} \int p dV = \frac{1}{\pi(R_2^2 - R_1^2)} \int_{R_1}^{R_2} p(r) 2\pi r dr. \quad (79)$$

Evaluating the integral and simplifying:

$$\bar{p} = p(R_1) - c \ln R_1 - \frac{c}{2} + c \left(\frac{R_2^2 \ln R_2 - R_1^2 \ln R_1}{R_2^2 - R_1^2} \right). \quad (80)$$

The pressure equivalent radius, r_i , is the radius such that $p(r_i) = \bar{p}$. Equating Equations 78 and 80 and solving for r_i gives

$$r_i = \exp \left(\frac{R_2^2 \ln R_2 - R_1^2 \ln R_1}{R_2^2 - R_1^2} - \frac{1}{2} \right). \quad (81)$$

The equation for r_j can be obtained by substituting R_2 for R_1 , and R_3 for R_2 , so that

$$r_j = \exp \left(\frac{R_3^2 \ln R_3 - R_2^2 \ln R_2}{R_3^2 - R_2^2} - \frac{1}{2} \right). \quad (82)$$

Substituting these radii in Equation 73 and simplifying gives:

$$T_r = \frac{1}{\frac{R_1^2 \ln(R_1 / R_2) / (R_2^2 - R_1^2) + \frac{1}{2} R_3^2 \ln(R_3 / R_2) (R_3^2 - R_2^2) - \frac{1}{2}}}{\frac{k_{r,i} \theta_i h_i}{k_{r,j} \theta_j h_j}}, \quad (83)$$

which is the formula used by Eclipse.

3.4 Boundary Conditions and Well model

The finite difference equations derived so far have not incorporated the required boundary conditions discussed in Section 2.4. The no-flow boundaries are easily dealt

with by simply setting the transmissibility of the appropriate face to zero. Where this face corresponds to the edge of the grid this is the default situation anyway. This is the method used by Eclipse. Aziz and Settari²⁹ have pointed out that this is a poor approximation and that ideally the grid point, as opposed to the grid face, should lie at the boundary. It is possible to achieve this using Eclipse by defining grid blocks that extend beyond the boundary with the grid point lying on the boundary. The pore volume and transmissibilities of the block parallel to the boundary are then reduced to compensate for the portion of the block that lies outside the boundary.

The remaining boundary conditions are associated with the well and its interface to the reservoir. Ultimately the problem that is being considered by this thesis is to be able to solve for the well bottom hole pressure, p_{bh} , that results from a particular sequence of fixed production rates. It is necessary, therefore, to relate the p_{bh} to the well rate, q , and the pressure of grid blocks adjacent to the well. The flow rate of an individual cell into the well bore is given by:

$$q_i = -T_{wi}(p_{oi} - H_i - p_{bh}) \begin{bmatrix} \lambda_o + R_v \lambda_g \\ \lambda_w \\ \lambda_g + R_s \lambda_o \end{bmatrix}, \quad (84)$$

where T_{wi} represents the transmissibility between the well-bore and the grid point of block i , H_i is a hydrostatic head correction for the difference in depth between the datum plane for p_{bh} and the grid block, and the mobilities, λ , are evaluated in block i . In a radial grid the q_i represent additional flow terms associated with the inner boundary of the innermost cells of the radial grid. To maintain consistency with the rest of the grid q_i is taken as positive for flow from the well into the grid block. The description is completed by the constraint:

$$\sum_i q_i = q. \quad (85)$$

The well transmissibilities are calculated by assuming steady state radial flow between the well-bore radius and the pressure equivalent radius of the connecting grid block. For the rate convention of this section the steady state equation is²⁵:

$$q_i = -\frac{\lambda_i k_i \theta_i h_i}{\ln(r_i / r_w) + S} (p_{oi} - p_{bh}), \quad (87)$$

where S is the skin factor. Substituting Equation 81 for the pressure equivalent radius and simplifying gives:

$$q_i = - \frac{\lambda_i k_i \theta_i h_i}{\frac{R_2^2}{R_2^2 - r_w^2} \ln\left(\frac{R_2}{r_w}\right) - \frac{1}{2} + S} (p_{oi} - p_{bh}), \quad (89)$$

where R_2 is the outer radius of the connecting grid block. Comparison with Equation 84 shows that:

$$T_{wi} = \frac{k_i \theta_i h_i}{\frac{R_2^2}{R_2^2 - r_w^2} \ln\left(\frac{R_2}{r_w}\right) - \frac{1}{2} + S}. \quad (90)$$

As a result of including the well the finite difference equations need to be expanded to:

$$R(X) = \frac{M(t + \Delta t) - M(t)}{\Delta t} V - F(t + \Delta t) - Q(t + \Delta t) = \bar{0}, \quad (91)$$

where Q represents the mass sink due to the well. In addition, the state vector X has been expanded by adding a single new element, w , that describes the state of the well. The three state variables for w are the flowing fractions for water and for gas, and the bottom hole flowing pressure. In other words, the well itself is treated as an additional grid block with the well bottom hole pressure acting as the equivalent of grid block pressure and the flowing fractions acting as the equivalent of the grid block saturations. Transmissibilities between the well and other grid blocks have already been defined through Equation 90. In this way the solution of the well variables becomes strongly coupled to the solution of the rest of the grid blocks.

3.5 Solution of the Implicit Finite Difference Equations

An outline of the procedure used to solve the finite difference equations is as follows:

First the non-linear equations of Equation 91 are linearized using a Newton-Raphson method. The resulting linear equations that are created at each Newton iteration are solved to a high level of precision using an iterative procedure known as Orthomin.

Orthomin was developed by Vinsome³² to solve sparse banded sets of simultaneous linear equations. It makes use of an easily inverted approximation of the equations to be solved to calculate the changes to be made for the next iteration. At each iteration the residual error in current estimate is evaluated using the original equations. The easily inverted approximation is known as a preconditioning matrix. Eclipse uses Nested Factorisation, a method developed by Appleyard and Cheshire³³, to perform the preconditioning. Cheshire³⁴ claims that Orthomin preconditioned by Nested

Factorisation remains the most powerful technique in common use in reservoir simulation for the solution of large difficult problems. Cheshire's account of how Eclipse solves the finite-difference equations forms the underlying basis of what is given here, though this account has been expanded, restructured, and reworded to clarify some issues.

3.6 Solution of the Non-linear Equations

Newton's method is derived using the Taylor expansion:

$$R(X^{n+1}) \approx R(X^n) + \frac{\partial R(X^n)}{\partial X} (X^{n+1} - X^n), \quad (92)$$

where X^n is the current best estimate for X and X^{n+1} is the best estimate at the next iteration. We are trying to find X such that $R(X) = \bar{0}$. Setting the left hand side of Equation 92 to zero and rearranging gives:

$$\frac{\partial R(X^n)}{\partial X} (X^{n+1} - X^n) = -R(X^n). \quad (93)$$

This gives a system of linear equations to be solved at each Newton iteration. The equations are linear because the differential is treated as a constant within each iteration. The Jacobian $\partial R / \partial X$ is a matrix with elements of the form $\partial R_i / \partial X_j$.

That is, every element of R is differentiated by every element of X . Since each element of X and R is itself a 3-component vector, each element of $\partial R / \partial X$ is a matrix of the form:

$$\frac{\partial R_i}{\partial X_j} = \begin{bmatrix} \frac{\partial R_{oi}}{\partial p_{oj}} & \frac{\partial R_{oi}}{\partial s_{wj}} & \frac{\partial R_{oi}}{\partial s_{gj}} \\ \frac{\partial R_{wi}}{\partial p_{oj}} & \frac{\partial R_{wi}}{\partial s_{wj}} & \frac{\partial R_{wi}}{\partial s_{gj}} \\ \frac{\partial R_{gi}}{\partial p_{oj}} & \frac{\partial R_{gi}}{\partial s_{wj}} & \frac{\partial R_{gi}}{\partial s_{gj}} \end{bmatrix}. \quad (94)$$

Equation 93 is commonly expressed in the form:

$$Ax = b \quad (95)$$

where the residual, b is given by

$$b = -R = -\frac{\Delta M}{\Delta t} + F + Q \quad (96)$$

and the Jacobian, A , can be expanded as

$$A = \frac{\partial R}{\partial X} = \frac{1}{\Delta t} \frac{\partial M}{\partial X} - \frac{\partial F}{\partial X} - \frac{\partial Q}{\partial X}. \quad (97)$$

Before considering the structure of A , an ordering system that relates the co-ordinate of a cell in the grid to its position in the vector needs to be defined. The simplest system for a 3-dimensional Cartesian or radial grid is to cycle through all the cells in line before moving to the next line. When all the lines in a plane have been completed then the cycling proceeds on the next plane, continuing until all the planes have been completed. Thus, the position of the cell with grid co-ordinates i, j, k is given by $i + (j - 1) \times m + (k - 1) \times n \times m$ where m is the number of cells in a single line of the grid and n is the number of lines in a plane.

The mass terms, M , for a given block are a function only of the state variable at that block and therefore contribute only to the diagonal of A . Likewise the mass sink terms, Q , are a function only of the state variable at the block itself and the well variable and therefore also contribute only to the diagonal.

The flow terms, F , on the other hand are a function of the state variable at the block itself and the state variables at each of the adjacent blocks as indicated by Equation 67. Therefore $\partial F / \partial X$ is zero for all non-adjacent blocks. As a result, the flow terms contribute only to the diagonal and to several off centre diagonal bands. The innermost bands correspond to cells that are neighbours within a given line and thus are the bands that are immediately adjacent to the diagonal. The next set of bands correspond to cells that are in adjacent lines with the same position in a line. These bands are offset from the diagonal by the number of cells in a line. The outermost set of bands arises through cells that lie in adjacent planes but have the same position in the plane. These outermost bands are offset from the diagonal by the number of cells in a plane. Note that there may be gaps in the bands that correspond to the edge of the grid. That is, a cell that lies at the edge of the grid does not have neighbouring cells in certain directions and the flow terms, and hence derivatives, corresponding to these directions are therefore zero.

As an example, A for a grid with 4 cells in a line, 2 lines in a plane, and 3 planes has the structure:

$$A = d + u_1 + l_1 + u_2 + l_2 + u_3 + l_3 \quad (98)$$

Eclipse is also specified in terms of a saturation, in this case as a fraction of the field pore volume.

A high level algorithm for the Newton iterations is as follows:

1. Compute initial residual, $R(X^0) = -b$, using state vector from previous time step as an initial guess for the solution.
2. While the material balance error and maximum saturation weighted residual are too large:
 - 2.1. Calculate the Jacobian, $A = \frac{\partial R(X^n)}{\partial X}$
 - 2.2. Solve the linear equations, $Ax = b$, for x
 - 2.3. Update the state vector, $X^{n+1} = X^n - x$
 - 2.4. Calculate the new residual, $R(X^{n+1}) = -b$

3.7 Direct Solution of the Linear Equations for a One-Dimensional Grid

The direct solution of the linear equations arising at each Newton iteration for typical problems is not practical from a computational point of view. The complex, three-dimensional, and frequently three-phase, problems often specified by reservoir engineers would simply take too long to solve. Iterative techniques are therefore normally used in solving the linear equations. Useful insight into the iterative techniques can however be gained by considering the direct solution of one of the simplest cases, namely that arising from a linear grid.

For a linear grid, the Jacobian has a tri-diagonal structure. For example, for a grid with 4 cells :

$$A = d + u + l = \begin{bmatrix} d_1 & u_1 & & \\ l_1 & d_2 & u_2 & \\ & l_2 & d_3 & u_3 \\ & & l_3 & d_4 \end{bmatrix}, \quad (99)$$

where u and l are respectively the upper and lower diagonal side bands. This can be factorised into the product of lower triangular, diagonal, and upper triangular matrices:

$$\begin{aligned}
A &= (\sigma + l)\sigma^{-1}(\sigma + u) \\
&= (\sigma + l)(I + \sigma^{-1}u)
\end{aligned}
\tag{100}$$

where σ is a diagonal matrix. Note that σ^{-1} is easily calculated since it is a diagonal matrix. Expanding Equation 100 and equating to Equation 99 gives:

$$\sigma = d - l\sigma^{-1}u. \tag{101}$$

The calculation of σ can now be made sequentially since the calculation of the first element of σ only involves d . The calculation of the second element of σ involves d and the first element of σ , and so on. That is:

$$\begin{aligned}
\sigma_1 &= d_1 \\
\sigma_2 &= d_2 - l_1\sigma_1^{-1}u_1 \\
\sigma_3 &= d_3 - l_2\sigma_2^{-1}u_2 \\
\sigma_4 &= d_4 - l_3\sigma_3^{-1}u_3
\end{aligned}
\tag{102}$$

The solution of $Ax = b$ involves two passes. In the first pass the equation $(\sigma + l)y = b$ is solved for y . In the second pass the equation $(I + \sigma^{-1}u)x = y$ is solved for x . For the first, forward, pass $(\sigma + l)y = b$ therefore $y = \sigma^{-1}(b - ly)$ and the solution is again sequential:

$$\begin{aligned}
y_1 &= \sigma_1^{-1}b_1; \\
y_2 &= \sigma_2^{-1}(b_2 - l_1y_1); \\
y_3 &= \sigma_3^{-1}(b_3 - l_2y_2); \\
y_4 &= \sigma_4^{-1}(b_4 - l_3y_3).
\end{aligned}
\tag{103}$$

For the second, backward, pass $(I + \sigma^{-1}u)x = y$ therefore $x = y - \sigma^{-1}ux$ and the sequential solution is:

$$\begin{aligned}
x_4 &= y_4; \\
x_3 &= y_3 - \sigma_3^{-1}u_3x_4; \\
x_2 &= y_2 - \sigma_2^{-1}u_2x_3; \\
x_1 &= y_1 - \sigma_1^{-1}u_1x_2.
\end{aligned}
\tag{104}$$

This technique is in fact equivalent to solving the tri-diagonal equation using Gaussian elimination as can easily be seen if one works through the equations. In the petroleum engineering literature it is frequently referred to as the Thomas algorithm. The method has been presented here to aid in the understanding of the nested factorisation method of inverting an approximation of the Jacobian.

3.8 Iterative Solution of the Linear Equations using Orthomin

Most simulators use iterative methods to solve the linear equations. Eclipse uses a technique known as Orthomin. This technique relies on the ability to calculate an easily inverted approximation, B , to the Jacobian, A . B^{-1} is then used to calculate a vector that represents the direction to move in that will bring one closer to the required solution. The solution is updated by moving along the vector by an amount that optimises the residual. This in turn involves a pre-multiplication by A in order to calculate the new residual. A special feature of the method is that the change to be made to the residual at each iteration is forced to be orthogonal to all previous changes. This speeds convergence by minimising the number of iterations required to reach a solution.

Orthomin is computationally very efficient, requiring one multiplication by the pre-conditioning matrix B^{-1} and one multiplication by A at each iteration. The enforced orthogonalisation does however require the storage of all previous changes to the solution and the residual which can use a considerable amount of computer memory.

The objective is to solve Equation 95 for x which can be re-phrased as reducing the residual, $r_n = b - Ax_n$, to zero where x_n is an estimate of the required solution. Note that if A could be inverted, an exact solution could be obtained by calculating $\Delta x_n = x - x_n = A^{-1}r_n$ and adding this to the current estimate. In practice however, inverting a matrix such as A is a non-trivial task. The change to be made to the solution is therefore calculated using the approximation B^{-1} .

At the first time step the initial estimate, x_0 , gives rise to the initial residual,

$$r_0 = b - Ax_0. \quad (105)$$

A new search direction for the solution, Δx_0 , is given by

$$\Delta x_0 = B^{-1}r_0. \quad (106)$$

But since B^{-1} is only an approximation for A^{-1} the solution is updated by moving a distance along the solution search direction that minimises the square of the new residual, r_1 . Thus:

$$x_1 = x_0 + \alpha_0 \Delta x_0, \quad (107)$$

and

$$\begin{aligned}
 r_1 &= b - Ax_1 \\
 &= b - Ax_0 - \alpha_0 A \Delta x_0 \\
 &= r_0 - \alpha_0 \Delta r_0,
 \end{aligned} \tag{108}$$

where the residual search direction, Δr_0 , is given by $\Delta r_0 = A \Delta x_0 = AB^{-1}r_0$ and α_0 is a scalar. To find the optimum value of α_0 , r_1^2 is differentiated with respect to α_0 and set to zero.

$$r_1^2 = r_0^2 - 2\alpha_0 r_0 \cdot \Delta r_0 + \alpha_0^2 \Delta r_0^2 \tag{109}$$

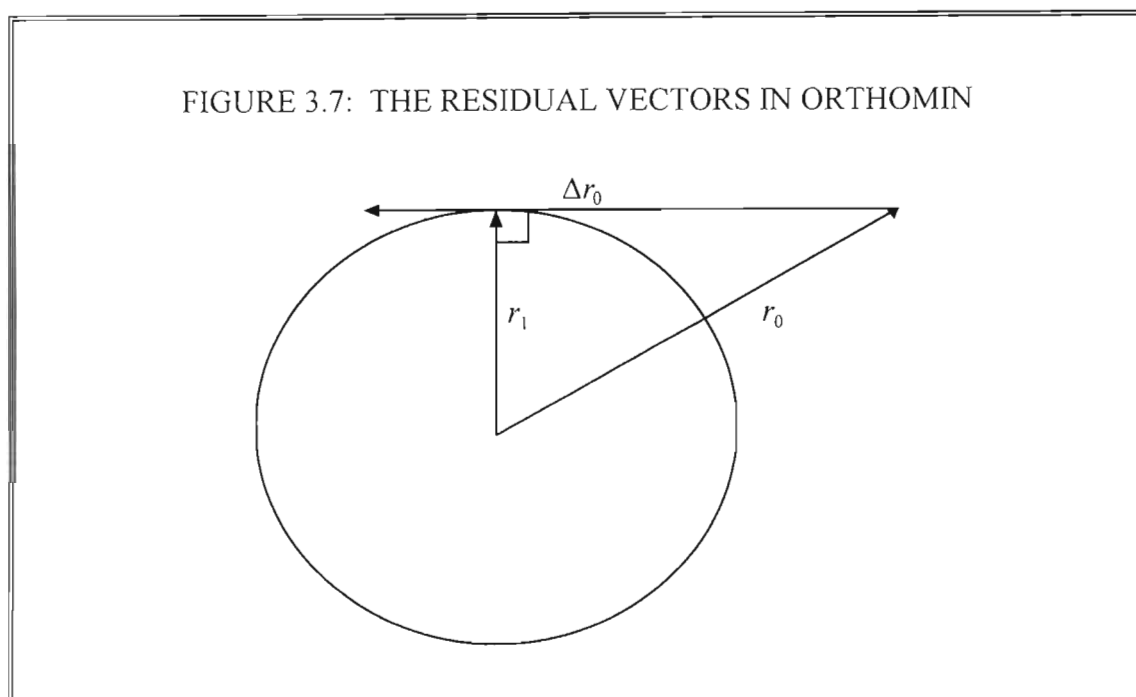
therefore

$$\frac{\partial r_1^2}{\partial \alpha_0} = -2r_0 \cdot \Delta r_0 + 2\alpha_0 \Delta r_0^2 = 0 \tag{110}$$

giving:

$$\alpha_0 = \frac{r_0 \cdot \Delta r_0}{\Delta r_0^2}. \tag{111}$$

Note that this choice of α_0 implies that the new residual is orthogonal to the previous search direction because $r_1 \cdot \Delta r_0 = 0$. The residual vectors are depicted in Figure 3.7.



It is important that no part of Δr_0 enters the residual at any subsequent iteration since the absolute minimum in the square of the residual has already been found for this

search direction. This is achieved by forcing the residual search direction to be orthogonal to all previous residual search directions. For the second iteration the extra degree of freedom needed is provided by adding a component of the previous search directions. The new search directions then become:

$$\Delta x_1 = B^{-1}r_1 + \beta_{10}\Delta x_0; \quad (112)$$

$$\Delta r_1 = AB^{-1}r_1 + \beta_{10}\Delta r_0, \quad (113)$$

where β_{10} is chosen so that

$$\Delta r_1 \cdot \Delta r_0 = 0. \quad (114)$$

Substituting Equation 113 in Equation 114 gives:

$$\beta_{10} = -\frac{(AB^{-1}r_1) \cdot \Delta r_0}{\Delta r_0^2}. \quad (115)$$

As before, the solution and residual are updated using the search directions:

$$\begin{aligned} x_2 &= x_1 + \alpha_1 \Delta x_1 \\ r_2 &= r_1 - \alpha_1 \Delta r_1 \end{aligned} \quad (116)$$

where α_1 is calculated to minimise r_2^2 . Differentiating r_2^2 with respect to α_1 and equating to zero gives:

$$\alpha_1 = \frac{r_1 \cdot \Delta r_1}{\Delta r_1^2} \quad (117)$$

so that $r_2 \cdot \Delta r_0 = 0$ and $r_2 \cdot \Delta r_1 = 0$, which implies that the current residual is orthogonal to both of the previous residual search directions.

At the next iteration the new search directions must be orthogonal to both sets of previous search directions therefore a component of x_1 is added, giving:

$$\Delta x_2 = B^{-1}r_2 + \beta_{21}\Delta x_1 + \beta_{20}\Delta x_0; \quad (118)$$

$$\Delta r_2 = AB^{-1}r_2 + \beta_{21}\Delta r_1 + \beta_{20}\Delta r_0, \quad (119)$$

where β_{21} and β_{20} are chosen so that :

$$\Delta r_2 \cdot \Delta r_1 = 0; \quad (120)$$

$$\Delta r_2 \cdot \Delta r_0 = 0. \quad (121)$$

Substituting Equation 119 into 120 gives:

$$\beta_{21} = -\frac{(AB^{-1}r_2)\Delta r_1}{\Delta r_1^2} \quad (122)$$

because the term involving β_{20} is multiplied by the dot-product of the orthogonal vectors Δr_0 and Δr_1 . Similarly, if Equation 119 is substituted into 121:

$$\beta_{20} = -\frac{(AB^{-1}r_2)\Delta r_0}{\Delta r_0^2}. \quad (123)$$

For the n-th iteration it becomes necessary to calculate n-1 coefficients and the search directions become:

$$\Delta x_n = B^{-1}r_n + \sum_{m=0}^{n-1} \beta_{nm} \Delta x_m; \quad (124)$$

$$\Delta r_n = AB^{-1}r_n + \sum_{m=0}^{n-1} \beta_{nm} \Delta r_m, \quad (125)$$

where

$$\beta_{nm} = -\frac{(AB^{-1}r_n)\Delta r_m}{\Delta r_m^2}. \quad (126)$$

Eclipse makes some slight modifications to the basic Orthomin procedure.

The first is that the residuals being minimised are saturation normalised as previously discussed for the non-linear iterations. Thus the procedure minimises \bar{r}_n^2 giving an optimum step size, α_n , of:

$$\alpha_n = \frac{\bar{r}_n \cdot \Delta \bar{r}_n}{\Delta \bar{r}_n^2}, \quad (127)$$

where \bar{r} signifies a residual that has been saturation normalised for each cell by multiplying by the time-step and fluid volume factor and dividing by the cell pore volume. That is, for cell i and component c , the saturation normalised residual is given by:

$$(\bar{r})_{i,c} = \frac{\Delta t B_c}{V_i} (r)_{i,c}, \quad (128)$$

where Δt is the time-step, B_c is the fluid volume factor for the component, and V_i is the pore volume of the block. Convergence is determined by checking whether the

maximum saturation normalised residual for all the cells is within the specified bounds. It is not necessary to test for material-balance in the linear iterations because the pre-conditioning matrix used by Eclipse preserves material balance at each linear iteration.

A second modification is that the initial approximation is calculated as

$$x_0 = B^{-1}b. \quad (129)$$

If the approximation B^{-1} does not introduce any material balance error then this ensures that material balance is preserved throughout the entire procedure.

A high level algorithm for the Orthomin procedure is as follows:

1. Calculate the initial estimate $x_0 = B^{-1}b$.
2. Calculate the initial residual $r_0 = b - Ax_0$.
3. While the maximum saturation residual is greater than the user specified limit:
 - 3.1. Compute new search directions,

$$\Delta x_n = B^{-1}r_n + \sum_{m=0}^{n-1} \beta_{nm} \Delta x_m,$$

$$\Delta r_n = AB^{-1}r_n + \sum_{m=0}^{n-1} \beta_{nm} \Delta r_m,$$

$$\beta_{nm} = -\frac{(AB^{-1}r_n) \Delta r_m}{\Delta r_m^2}.$$
 - 3.2. Determine the optimum step size,

$$\alpha_n = \frac{\bar{r}_n \cdot \Delta \bar{r}_n}{\Delta \bar{r}_n^2}.$$
 - 3.3. Update the solution and residual,

$$x_{n+1} = x_n + \alpha_n \Delta x_n,$$

$$r_{n+1} = r_n - \alpha_n \Delta r_n.$$
 - 3.4. Store previous search directions and increment n.

3.9 Nested Factorisation

Nested Factorisation is the pre-conditioning method used by Eclipse. The aim is to determine a matrix B that is a good approximation to A and to solve $B^{-1}r_n$ each time a new search direction is needed by the linear solver. One of the important considerations for a good approximation is that it should not introduce any material balance error. It will be demonstrated that this is the case if the sum of the elements in each column of A equals the sum of the elements of the equivalent column of B .

Let y be an approximate solution obtained through solving the equation:

$$By = b, \quad (130)$$

then the residual is given by:

$$r = b - Ay = (B - A)y. \quad (131)$$

This residual is a vector that represents the material balance error introduced into each cell by substituting B for A . To obtain the overall material balance error for the grid as a whole we sum the residual over all the blocks in the reservoir. Therefore the overall material balance error is zero if:

$$\sum_i r_i = \sum_{ij} (B - A)_{ij} y_j = 0. \quad (132)$$

One way of satisfying Equation 132 is if each coefficient of y_j is zero. That is,

$$\sum_i (B - A)_{ij} = 0 \quad (133)$$

which is equivalent to

$$\sum_i B_{ij} = \sum_i A_{ij} \quad (134)$$

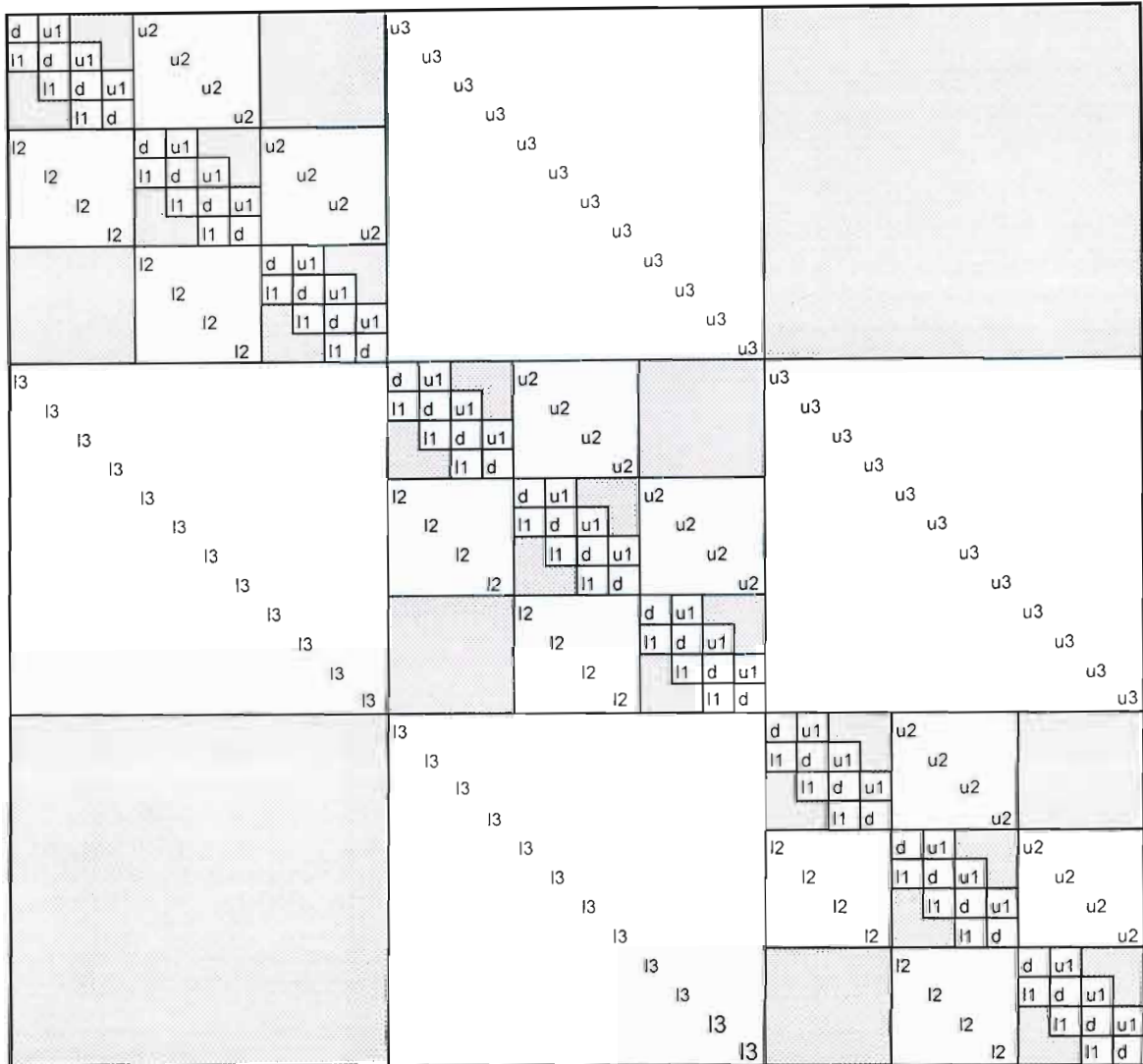
or

$$\text{Colsum}(B) = \text{Colsum}(A), \quad (135)$$

where $\text{Colsum}(B)$ is a diagonal matrix with each element on the diagonal equal to the sum of the elements in the equivalent column of B . Nested factorisation uses this constraint to eliminate the overall material balance error in the linear equations by adding terms to B to make its column sum equal to that of A .

The structure of the Jacobian can be thought of as a nested tri-diagonal matrix. An illustration of this is given in Figure 3.8 for the Jacobian that results from a 4 by 3 by 3 grid. At the outermost level there are two side bands, u_3 and l_3 , that represent interactions between planes of the grid, and a block diagonal made up of square matrices. Each of these square matrices represents the equations for one plane and is itself a nested tri-diagonal. The side-bands for this level, u_2 and l_2 , represent interactions between lines of cells in the grid and each square matrix in the block diagonal represents the equations within a line of cells. The innermost level is a simple tri-diagonal with side-bands, u_1 and l_1 , that result from interactions of cells within a line.

FIGURE 3.8: THE NESTED TRI-DIAGONAL STRUCTURE OF THE JACOBIAN FOR A 4 BY 3 BY 3 GRID



Nested factorisation exploits this nested structure by defining B in terms of the equations:

$$\begin{aligned}
 B &= (P + l_3)P^{-1}(P + u_3), \\
 P &= (T + l_2)T^{-1}(T + u_2), \\
 T &= (\sigma + l_1)\sigma^{-1}(\sigma + u_1),
 \end{aligned}
 \tag{136}$$

where σ is a diagonal matrix that is defined in such a way that material balance is preserved. This recursive definition appears to be a natural extension of the factorisation used in the Thomas algorithm. Expanding B gives:

$$B = \sigma + l_1 \sigma^{-1} u_1 + l_1 + u_1 + l_2 T^{-1} u_2 + l_2 + u_2 + l_3 P^{-1} u_3 + l_3 + u_3. \quad (137)$$

Comparing the structure of A in terms of side bands,

$$A = d + l_1 + u_1 + l_2 + u_2 + l_3 + u_3, \quad (138)$$

with Equation 137 shows that if σ is chosen so that

$$\sigma = d - l_1 \sigma^{-1} u_1 - \text{Colsum}(l_2 T^{-1} u_2) - \text{Colsum}(l_3 P^{-1} u_3) \quad (139)$$

then the column sums of the two matrices will be equal and no material balance error will be introduced by the approximation. At first sight it may seem as if Equation 139 is self referential but this is not the case because of the structure of the inverse matrices and effect of multiplying by the side bands l and u .

In general, the position of the elements of an arbitrary matrix C in the product matrix Cu are shifted to the left by a number of cells that is equivalent to the offset of the side band from the diagonal. This fills the first n columns with zeros where n is the offset. In addition each element of Cu has a factor that corresponds to the element of u in that same column. For example:

$$Cu = \begin{bmatrix} c_{11} & c_{12} & c_{13} & c_{14} & c_{15} & c_{16} \\ c_{21} & c_{22} & c_{23} & c_{24} & c_{25} & c_{26} \\ c_{31} & c_{32} & c_{33} & c_{34} & c_{35} & c_{36} \\ c_{41} & c_{42} & c_{43} & c_{44} & c_{45} & c_{46} \\ c_{51} & c_{52} & c_{53} & c_{54} & c_{55} & c_{56} \\ c_{61} & c_{62} & c_{63} & c_{64} & c_{65} & c_{66} \end{bmatrix} \begin{bmatrix} u_1 \\ u_2 \\ u_3 \end{bmatrix} = \begin{bmatrix} c_{11}u_1 & c_{12}u_2 & c_{13}u_3 \\ c_{21}u_1 & c_{22}u_2 & c_{23}u_3 \\ c_{31}u_1 & c_{32}u_2 & c_{33}u_3 \\ c_{41}u_1 & c_{42}u_2 & c_{43}u_3 \\ c_{51}u_1 & c_{52}u_2 & c_{53}u_3 \\ c_{61}u_1 & c_{62}u_2 & c_{63}u_3 \end{bmatrix} \quad (140)$$

Similarly, if C is pre-multiplied by l the effect is to shift the elements down by a number of rows that is equivalent to the offset of l . The elements of C that remain in

the product are multiplied by the element of l in the equivalent row. A combination of pre-multiplying by l and post-multiplying by u shifts the elements down and to the right by the offset. Each remaining element of C is multiplied by the element of l in the equivalent row and the element of u in the equivalent column.

In considering the structure of the inverse matrices it is important to consider the impact of the gaps in the side bands. These gaps are associated with the edges of the grid. Expanding the defining equation for T gives:

$$T = \sigma + l_1 + u_1 + l_1 \sigma^{-1} u_1. \quad (141)$$

Thus T is a tri-diagonal equation with gaps in the side-bands in the same position as the original matrix A . In this case the gaps separate lines in the grid with the result that the first portion of the inverse depends only the cells in the first line. Similarly the second portion of the inverse depends only on the cells in the second line and so on. The resulting inverse, T^{-1} , is therefore a block diagonal matrix with each block of non zero cells having the same number of rows and columns as there are cells in a line. Expanding the defining equation for P gives:

$$P = T + l_2 + u_2 + l_2 T^{-1} u_2. \quad (142)$$

Since T^{-1} is a block diagonal matrix, $l_2 T^{-1} u_2$ is also a block diagonal matrix, though with zeros as elements for the first block as a result of the shifting action of multiplying by the side-bands. The structure of P is therefore that of a block diagonal with side-bands, although in this case the gaps separate planes in the grid. The resulting inverse is therefore a block diagonal with the number of rows and columns per block equal to the number of cells in a plane.

Thus the calculation of σ can proceed sequentially. For the first cell, $\sigma = d$. For subsequent cells in the first line the shifting effect of the innermost side-bands, l_1 and u_1 , is such that once σ is known for a cell its contribution to σ for the next cell can be calculated. There is no contribution to σ from the term $Colsum(l_2 T^{-1} u_2)$ until σ for all the cells in the first line has been calculated. This is because the side-bands l_2 and u_2 shift the inverse by the number of cells in a line. For each subsequent line it is only necessary to know T^{-1} on the previous line to perform the calculation. Similarly, there is no contribution from $Colsum(l_3 P^{-1} u_3)$ until σ for all the lines on the first plane has been calculated. Once P is known for a plane its contribution to σ on the next plane can be calculated.

Each Newton iteration requires the definition of a new pre-conditioning matrix B and therefore the calculation of σ is performed once per Newton iteration. This is stored

and used to solve the equation $Bx = b$ at each iteration of Orthomin. At the highest level B can be re-written as:

$$B = (P + l_3)(I + P^{-1}u_3). \quad (143)$$

The solution therefore is performed in two phases. First $(P + l_3)y = b$ is solved for y and then $(I + P^{-1}u_3)x = y$ is solved for x . The first phase is performed by sweeping through the equations, one plane at a time, calculating:

$$y = P^{-1}(b - l_3y), \quad (144)$$

where the contribution of l_3y lags one plane behind thus allowing the equation to be solved. The second phase calculates:

$$x = y - P^{-1}u_3x, \quad (145)$$

starting on the last plane and moving backward. Note that u_3x makes no contribution to elements on the last plane. Once x is known on the last plane the contribution of u_3x to the previous plane can be calculated, and so on.

The calculation of $s = P^{-1}r$ within each plane follows a similar logic. Re-writing the defining equation for P gives:

$$P = (T + l_2)(I + T^{-1}u_2), \quad (146)$$

so that $(T + l_2)t = r$ is solved on the forward sweep and $(I + T^{-1}u_2)s = t$ is solved on the backward sweep. The calculation of

$$t = T^{-1}(r - l_2t) \quad (147)$$

is performed one line at a time starting from the first line on a plane and ending on the last line on the plane. On the backward sweep:

$$s = t - T^{-1}u_2s, \quad (148)$$

which is evaluated one line at a time starting with the last line on the plane and ending on the first line on the plane. Within a line the solution of the tri-diagonal, $g = T^{-1}f$, can proceed in the same fashion which, on this level, is identical to that used in the Thomas algorithm. Thus the forward calculation is:

$$h = \sigma^{-1}(f - l_1h), \quad (149)$$

and the backward calculation is:

$$g = h - \sigma^{-1} u_1 g. \quad (150)$$

The efficiency of the Nested Factorisation procedure depends on the ordering of the axes. Typically the direction associated with the innermost level of the solution is taken to be the z (vertical) direction because the transmissibilities are normally highest in this direction. Other considerations are the number of blocks in each direction and the predominant flow direction.

3.10 Solution of Well Variables

The solution technique described so far has concentrated on solving for the state variable at each of the grid blocks and has not considered the fact that the equations need to be expanded to include the well variable, w (See Section 3.4).

Eclipse uses a method known as the strongly coupled, fully implicit well model. This is described at length by Holmes³⁵. In general it is possible to have many wells in the simulation model with complex hierarchical control mechanisms which involve interactions between the wells. For the problem being considered in this thesis a much simpler model is sufficient. The discussion given here will therefore concentrate on how Holmes' method would be implemented for a single well under oil rate control.

The relationship between w and the state variables for the grid blocks connected to the well has been described in Section 3.4. At each Newton iteration the change, x , in the state variables is calculated using Equation 93. If w is directly incorporated into the state vector X then x and the residual need to be expanded by a single element and the Jacobian is expanded by a row and a column. The equations to be solved then become:

$$\begin{bmatrix} A & C \\ E & D \end{bmatrix} \begin{bmatrix} x \\ x_w \end{bmatrix} = - \begin{bmatrix} R \\ R_w \end{bmatrix}, \quad (151)$$

where A is the banded matrix $\partial R_i / \partial X_j$ that we have considered previously, C is a vector with elements of the form $\partial R_i / \partial w$, E is vector with elements of the form $\partial R_w / \partial X_j$, $D = \partial R_w / \partial w$, x_w is the change to be made to w , R and R_w are the residuals for the cells in the grid and the well respectively. Note that if the simulation model had several wells then C , D , and E would all be matrices.

Equation 151 can be partitioned into two equations, namely:

$$Ax + Cx_w = -R; \quad (152)$$

$$Ex + Dx_w = -R_w. \quad (153)$$

Re-writing Equation 153 gives:

$$x_w = -D^{-1}(R_w + Ex), \quad (154)$$

which can be used to eliminate x_w from Equation 152 so that:

$$(A - CD^{-1}E)x = CD^{-1}R_w - R. \quad (155)$$

This Equation can be solved by making a few simple modifications to Orthomin and Nested Factorisation. The first is to substitute $A - CD^{-1}E$ for A in the matrix multiplication step of Orthomin which is described by Equation 125 and hence also in the enforced orthogonalisation of Equation 126. Calculation of the preconditioning matrix B proceeds as before but with the inclusion of the term $\text{Colsum}(CD^{-1}E)$ in the diagonal matrix in order to preserve material balance. The modifications are completed by the extension of the residual to include the term $CD^{-1}R_w$.

Once the linear iterations of the Orthomin procedure are completed the change to be made to the grid block variables prior to the next Newton iteration is known. The change to be made to the well variable can then be determined from Equation 154.

3.11 Chapter Summary

In this chapter the methods by which the flow equation is converted to a set of finite difference equations and then solved numerically have been reviewed. The concept of breaking the problem up into a number of grid blocks and the use of different gridding systems are introduced. Flow from grid block to grid block is approximated using the differences in state variables at adjacent grid points. Discretisation in time is achieved through the introduction of the concept of time-steps with temporal derivatives being replaced by the differences in the values of the variables at the beginning and end of the time-step.

Appropriate relationships for transmissibility that give the correct flow from block to block are derived. In the case of a radial grid these involve the use of the assumptions that within a given time-step the flow in the vertical direction corresponds to steady-state linear flow whereas flow in the radial direction corresponds to purely radial (in the cylindrical sense) steady state flow. Use is made of a fully implicit method that

requires that the flow is assessed using the value of the variables at the end of the time-step. This necessitates the simultaneous solution of a set of non-linear finite difference equations that describe the flow into, and the mass accumulation within, every grid block.

The simultaneous equations are solved through iterative use of a Newton-Raphson method where the gradient of the residual is used to update the state variables at each iteration. Differentiation of the residual vector creates a matrix known as the Jacobian. The calculation of the update vector for the Newton method requires the solution of a set of linear equations involving the Jacobian. This is achieved through the use of a successive minimization scheme, Orthomin, that uses an easily inverted approximation of the Jacobian to update the solution at each iteration, a method known as pre-conditioning. The pre-conditioning technique used is known as Nested Factorisation and exploits the tri-diagonal nature of the Jacobian in performing an approximate inversion. In summary, the solution technique relies on two levels of solution, an outer level where the non-linear equations are solved using Newton's method generating a set of linear equations in the process, and an inner level where the linear equations are solved using Orthomin pre-conditioned by Nested Factorisation.

In the next chapter finite-difference simulation using the solution techniques reviewed in this chapter will be applied to solving a hypothetical problem, that of a partially penetrating well in an anisotropic medium. The understanding of: solution techniques; errors introduced by the discretisation process; the importance of choosing appropriate transmissibilities and grid block sizes; and the nature of the well boundary conditions, will play a role in optimising the simulation results for the hypothetical problem. Discussion of the calculation of grid block transmissibilities in the case of heterogeneous properties has relevance to the real-life problem discussed in the Chapter 5.

Chapter 4: Application to a Hypothetical Problem

This chapter applies the numerical model derived in Chapter 3 to solving the pressure response of a partially completed oil well to changes in oil rate. The method is applied to a hypothetical well with properties that allow the pressures to be modelled using an analytical solution. Comparison between the numerical and analytical solutions reveals errors. The source of these errors is discussed and various practical means of reducing the errors are investigated.

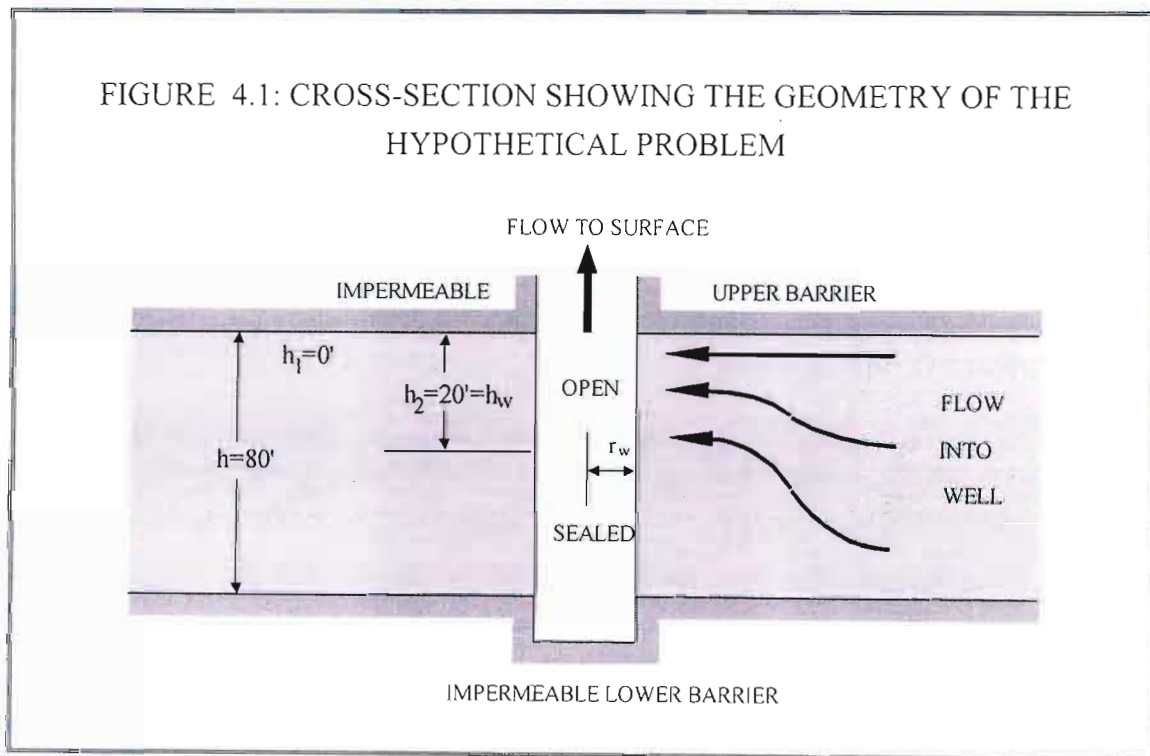
4.1 Definition of Hypothetical Problem

The problem to be solved is that of the pressure response of a partially completed oil well after being subjected to a change in rate. A rate change from zero to a fixed constant rate is the simplest case and is therefore that considered here. More complex rate constraints can be modelled by a superposition of solutions for this case. The flow rate that has been chosen is 5000 stb/d, which is similar to rates that have been achieved in wells in South African waters.

In order to allow the application of analytical solutions it has been assumed that the properties of the rock are homogenous. Permeability is anisotropic but radially symmetric with the horizontal component, k_h , having a magnitude of 500 mD. The ratio of vertical permeability, k_v , to k_h is 0.1. Only two phases are assumed to be present, namely oil and water with the water having an initial saturation of 0.1 of the pore volume. The relative permeabilities are defined so that the water is immobile while the relative permeability to oil is 1. In other words the oil can move freely through the rock with an effective permeability equal to absolute permeability without being hindered in any way by the presence of the water. This is simply a convenience to allow the analytical solutions, which are defined in terms of the effective permeabilities, to be easily compared to the simulation. The oil viscosity is 0.5 cP.

Although no mass transfer of water can take place in this model the water does have an influence on the result through its compressibility, c_w , of $3.0 \times 10^{-6} \text{ psi}^{-1}$. As a result the fraction of the pore space available to the oil will vary as a function of pressure. Similarly the total pore volume can also change as a result of rock compaction effects. This is accounted for through the use of a rock compressibility, c_r , in this case having a value of $2.0 \times 10^{-6} \text{ psi}^{-1}$. The initial pore volume is 0.2 of the total volume. The compressibility of the oil phase, c_o , at $20 \times 10^{-6} \text{ psi}^{-1}$ is far greater than that for either the water or the pore volume. The relationship between the surface and downhole flow rates is defined through the specification of the formation volume factor, B_o , which has a value of 1.5 rb/stb at the initial fluid pressure of 3500 psia.

The geometry of the problem is defined in Figure 4.1. A reservoir of 80 feet in thickness is intersected by a well with a radius, r_w , of 0.3615 feet. Only the first 20 feet of the intersection is perforated, the rest of the well is sealed off from the formation. The lateral extent of the reservoir is assumed to be infinite, though in practise it only needs to be far enough for the lateral boundaries to have a negligible influence on the pressure response.



The pressures are to be modelled for a flow period of 4 hours in duration. A rule of thumb for the furthest boundary that will have a measurable influence on the pressure response is given by the formula¹:

$$r_{inv} = 0.03 \sqrt{\frac{kt}{\phi \mu c}}, \quad (156)$$

where r_{inv} is the radius of investigation (or distance of the furthest boundary), t is the duration of the flow period, and c is the saturation weighted compressibility $c_r + S_w c_w + S_o c_o$. This distance is 1845 feet for the current problem.

A summary of the properties is given in Table 4.1.

Table 4.1: Properties of the Hypothetical Model

Rock Properties		
Porosity	ϕ	0.2
Horizontal Permeability	k_h	500 mD
Permeability Ratio	k_v/k_h	0.1
Rock Compressibility	c_r	2.0×10^{-6} psi
Fluid Properties		
Oil Viscosity	μ_o	0.5 cP
Oil Formation Volume Factor	B_o	1.5 rb/stb
Oil Compressibility	c_o	20.0×10^{-6} psi
Water Compressibility	c_w	3.0×10^{-6} psi
Water Saturation	S_w	0.1
Initial Fluid Pressure	p_i	3500 psia
Reservoir Geometry		
Reservoir Thickness	h	80 feet
Perforated Interval	h_w	20 feet
Distance to the Top Perforation	h_1	0 feet
Distance to the Bottom	h_2	20 feet
Perforation		
Wellbore Radius	r_w	0.3615 feet
Flow Specification		
Flow rate	q	5000 stb/d
Flow Duration	Δt	4 hours

4.2 Modelling the Hypothetical Problem

The hypothetical problem was modelled using the Eclipse program from Intera which implements the numerical scheme discussed in Chapter 3. A radial grid was defined with grid-block dimensions typical of a detailed coning study. In this grid the radial width of the innermost cell is 0.5 feet with each subsequent cell doubling in width. Choosing a geometric progression for the cell widths ensures an equal pressure drop across each cell for purely radial steady state flow. This in turn minimises the truncation errors that result in the discretisation process. The grid is made up of a total of 14 cells in the radial direction giving an outer radius of the grid of approximately 8200 feet. This is considerably further than the radius of investigation and therefore the model will behave as though it has infinite lateral extent. Vertically

the grid is split into 20 layers of 4 feet in thickness giving a total of 280 cells in the grid. The perforated interval is modelled by defining well connections between the wellbore and the innermost radial cells of the first 5 layers.

The rock and fluid properties are defined according to Table 4.1. The oil compressibility is not entered explicitly but is instead defined in terms of the rate of change of the formation volume factor for oil according to the formula: $\partial B_o / \partial p = -c_o B_o$. Relative permeability tables are provided which ensure that the relative permeability to oil is 1.0 for water saturations less than 0.5 of the pore volume. Similarly the relative permeability to water is zero over the same saturation range. Capillary pressure curves have no effect on the flowing behaviour of the model because they are only used in determining the water phase pressure and hence flow rate which is zero at all times. The curves are therefore defined in such a way as to ensure that the initial saturation is 0.1 of the pore volume throughout the grid, with little regard for how the capillary pressure changes as a function of saturation.

The time steps are defined in such a manner that the first time-step is very small (0.00004 Days \approx 0.001 Hours = 3.6 Seconds) and each subsequent time step increases by a constant factor thereafter. The rationale behind this choice lies in the desire to minimise the time discretisation (or truncation) error that is introduced in approximating the derivatives with respect to time. Examination of Equations 52 and 53 shows that the error is given by:

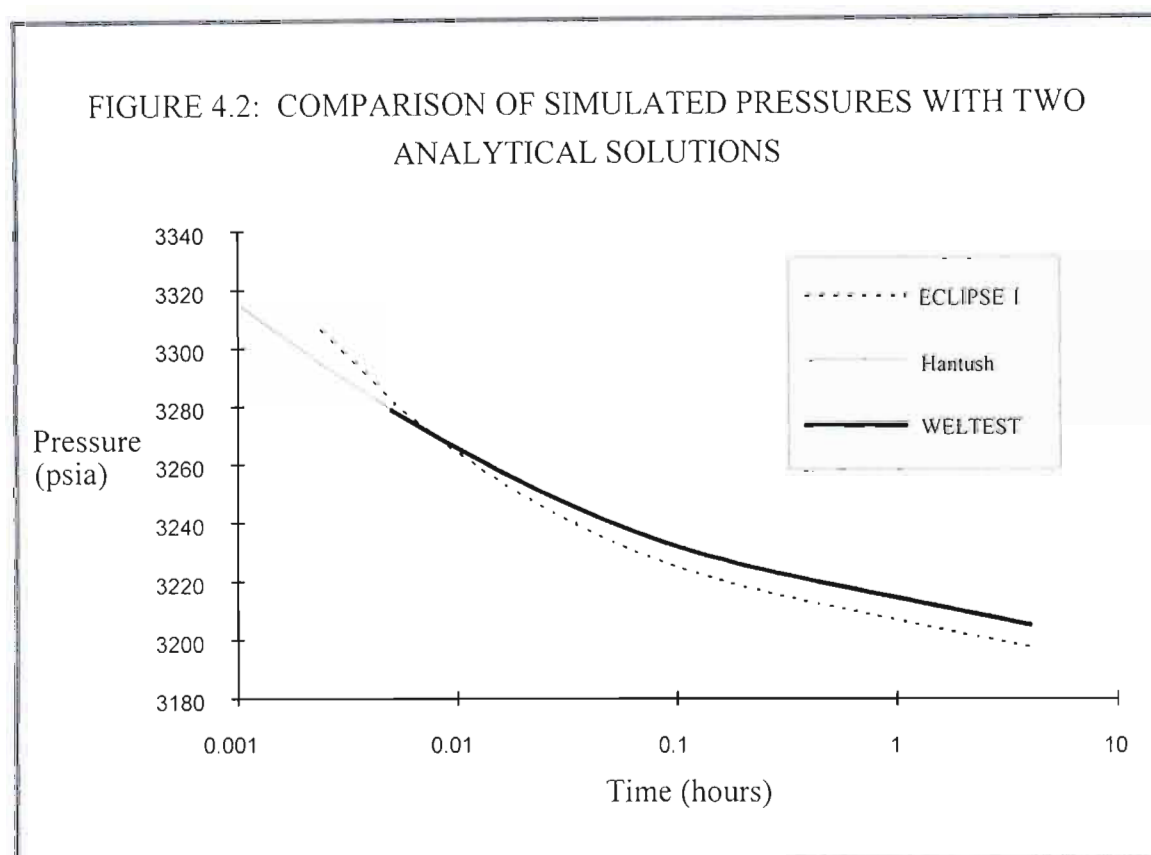
$$|\varepsilon_t| = \frac{\Delta t}{2} \frac{\partial^2 M}{\partial t^2} + \frac{\Delta t^2}{3!} \frac{\partial^3 M}{\partial t^3} + \frac{\Delta t^3}{4!} \frac{\partial^4 M}{\partial t^4} + \dots, \quad (157)$$

where the first term will dominate for small time-steps, Δt . Initially the changes are rapid and a small time-step is needed. As the flow proceeds the system becomes closer to steady state behaviour with changes that are almost constant from time-step to time-step. Thus the magnitude of $\partial^2 M / \partial t^2$ becomes smaller as time goes on and so the same degree of accuracy can be achieved with a much longer time-step.

A second reason for choosing increasing time-steps is a purely practical one. Most of the diagnostic plots display some function of pressure versus a logarithmic function of time. Allowing the time-step to increase gives a more even distribution of points on such a plot than a constant time-step would.

The control file containing the Eclipse commands for the simulation model has been included in Appendix 1.

The results of the simulation are displayed in Figure 4.2 where they are compared with two analytical models. It can be seen that the analytical models agree closely with each other, but that the Eclipse simulation has pressures that are too high soon after the flow begins and too low towards the end of the flow period. It is also clear that the rate of change of pressure with respect to time is too high at small time values for the Eclipse simulation. At large time values, when the slope is related to the permeability thickness product, kh , of the entire interval, the slopes agree.



The two analytical solutions used in Figure 4.2 are the method implemented in the WELTEST program from Intera and an implementation of the Hantush solution described by Equations 10 to 13, Chapter 1.

As mentioned in Chapter 1, the WELTEST program uses the horizontal well solution of Odeh and Babu¹⁸ to calculate the pressure response for partially completed wells.

A computer program was written to evaluate the Hantush solution. In this program, the exponential integral is evaluated using the well known series equivalent:

$$Ei(x) = -\gamma_e - \ln x - \sum_{n=1}^{\infty} \frac{(-x)^n}{n.n!}, \quad (158)$$

where $\gamma_c = 0.5772156$. The series is terminated when the terms become too small to have a significant influence on the result.

The integral, $W(u, \beta)$, in the Hantush method (Equation 12) is calculated by splitting the improper integral into a series of definite integrals and using a Simpson's rule procedure to evaluate each of the definite integrals.

An improper integral such as W can be defined in terms of limits as:

$$\int_L^\infty f(x) dx = \lim_{U \rightarrow \infty} \int_L^U f(x) dx. \quad (159)$$

This can in turn be used to rewrite the improper integral as a series,

$$\int_L^\infty f(x) dx = \int_L^{U_n} f(x) dx + \sum_{n=1}^{\infty} \int_{U_{n-1}}^{U_n} f(x) dx, \quad (160)$$

where U_n has been chosen to equal $10U_{n-1}$. The numerical sum is terminated when the term to be added becomes sufficiently small. Each definite integral in the series is evaluated using an adaptive form of Simpson's rule where the number of intervals used for the integration is doubled until the required accuracy is reached.

A listing of the computer program, which was written using Borland Turbo C++ 3.0, is given in Appendix 2

The Hantush solution is based on the assumption that the flux along the borehole is constant. As a result the pressure along the wellbore varies. The Eclipse simulation models the infinite conductivity solution, where pressure is constant along the wellbore. Gringarten and Ramey¹⁰ state that the results arising from the constant flux approximation are equivalent to those from the infinite conductivity solution provided the pressure is evaluated at the correct position along the length of the well. They provide a chart that relates the correct position to the dimensionless quantity

$$h_{wD} = \frac{h_w}{r_w} \sqrt{\frac{k_r}{k_z}}.$$

For the current problem the correct position, which was used in preparing Figure 4.2, is 72.4% of the length along the perforated interval.

The good agreement between the two analytical solutions is encouraging and they will be regarded as representing the true solution that the Eclipse simulation must try to duplicate.

4.3 Improvements to the Initial Model

The most likely source of the error in the Eclipse simulation is the truncation error introduced in the discretisation process. Sources of error such as round-off error are likely to be negligible, in part because high precision arithmetic is used by Eclipse and in part because the solution technique is iterative and therefore does not allow the error to accumulate. The truncation errors involved in terminating the Newton-Raphson and Orthomin iterations are directly controlled through the specification of the maximum permissible residual. Default values for these residuals are very low.

The discretisation error can be split into two parts, namely: that introduced by the discretisation in time and that resulting from the spatial discretisation. Time discretisation errors have been discussed in the previous section and could be reduced by shortening the time-steps. Such a change is, however, only likely to change the results soon after a rate change when the pressure distribution is far from that which would be obtained under steady state flow. The discrepancy in the late time pressures suggests that the bulk of the error is due to spatial discretisation error.

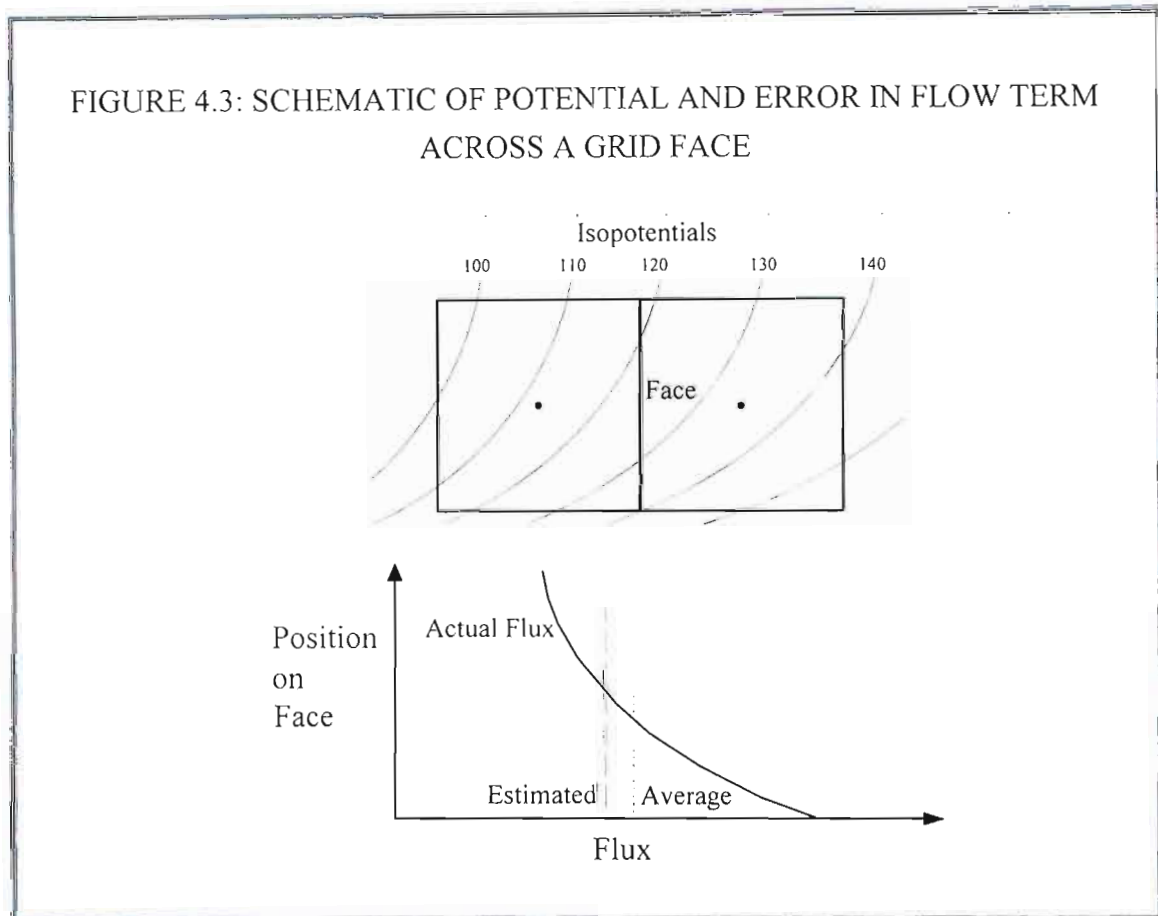
Evaluation of the spatial discretisation error is difficult when the integral method has been used to derive the finite difference equations that the simulation is based on. If a Taylor series method is used then the error is given by the higher order terms in the series that are not directly incorporated into the finite difference approximation of the spatial derivatives.

When the finite difference equations were derived it was assumed that the average flow across the face could be represented in terms of a pressure (or more correctly pressure potential) difference between the two grid-points that share the face as a block boundary. The transmissibility, which is a geometric coefficient of proportionality between flow rate and pressure difference, was defined so as to give an exact flow rate for steady state radial flow between the grid points.

The current problem, because of the flow convergence and the transient pressure behaviour, is neither steady state nor radial. This deviation from the assumed behaviour will therefore introduce discretisation errors. There are two aspects to these errors. The first relates to the estimation of the gradient of pressure potential at the block boundary between the two grid points and would be a source of error even for a purely radial, but transient, problem.

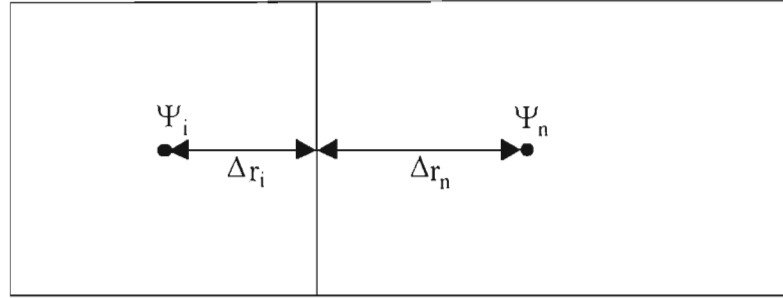
The second relates to the change of the potential gradient across the face of the block, which is a consequence of the non-radial nature of the problem being considered.

This problem will be greatest close to the end of the perforated section of the wellbore where the potential gradient may be sharply angled to the grid axes. Lines of isopotential are also expected to converge towards the base of the perforated section. The magnitude of this error is difficult to estimate but is represented schematically in Figure 4.3.



The first problem can be examined in more detail. At best, the approximation of the gradient of pressure in terms of a pressure difference at two points will be a first order one. That is, the dominant term in the error function will be proportional to the block size, probably multiplied by a second order derivative of pressure with respect to distance. This is demonstrated below by using a Taylor series discretisation to obtain the mid-point approximation for $\nabla\Psi$.

FIGURE 4.4: GEOMETRY OF ADJACENT RADIAL BLOCKS



Consider the two adjacent radial blocks depicted in Figure 4.4. One is trying to find a formula that relates $\partial\Psi/\partial r$ at the block boundary to the potential difference between the grid points, $\Delta\Psi = \Psi_n - \Psi_i$. For simplicity it will be assumed that the permeability in both blocks is constant. Using a Taylor series to expand the potentials at each of the grid-points gives:

$$\Psi_i = \Psi_b - \Delta r_i \left(\frac{\partial\Psi}{\partial r} \right)_b + \frac{\Delta r_i^2}{2} \left(\frac{\partial^2\Psi}{\partial r^2} \right)_b - \frac{\Delta r_i^3}{3!} \left(\frac{\partial^3\Psi}{\partial r^3} \right)_b + \dots \quad (161)$$

and

$$\Psi_n = \Psi_b + \Delta r_n \left(\frac{\partial\Psi}{\partial r} \right)_b + \frac{\Delta r_n^2}{2} \left(\frac{\partial^2\Psi}{\partial r^2} \right)_b + \frac{\Delta r_n^3}{3!} \left(\frac{\partial^3\Psi}{\partial r^3} \right)_b + \dots, \quad (162)$$

where Δr_i and Δr_n are the distances from the grid-points to the common boundary, and the subscript b implies that the quantity is to be evaluated at the grid block boundary.

Subtracting Equation 161 from 162 gives:

$$\left(\frac{\partial\Psi}{\partial r} \right)_b = \frac{\Psi_n - \Psi_i}{\Delta r_n + \Delta r_i} + R, \quad (163)$$

where the remainder, R , is

$$R = \frac{1}{2} (\Delta r_i - \Delta r_n) \left(\frac{\partial^2\Psi}{\partial r^2} \right)_b - \frac{1}{3!} \left(\frac{\Delta r_i^3 + \Delta r_n^3}{\Delta r_i + \Delta r_n} \right) \left(\frac{\partial^3\Psi}{\partial r^3} \right)_b + \dots \quad (164)$$

Thus the portion of the potential that does not obey steady-state radial flow will be subject to errors that are dominated by the first term.

It may seem as if it would have been better to define blocks with a constant increase in radius, that is $\Delta r_n = \Delta r_i$, since this would have eliminated the first term giving a higher order of approximation. This is not necessarily the case as the choice of transmissibilities made in Section 3.3c eliminates the remainder term completely for the portion of the potential that corresponds to radial steady-state flow. For the portion of the grid far from the well the radial assumption is a good one. Similarly the steady state flow assumption becomes a good one at late times. Thus the portion of the potential that does not obey these conditions is often small.

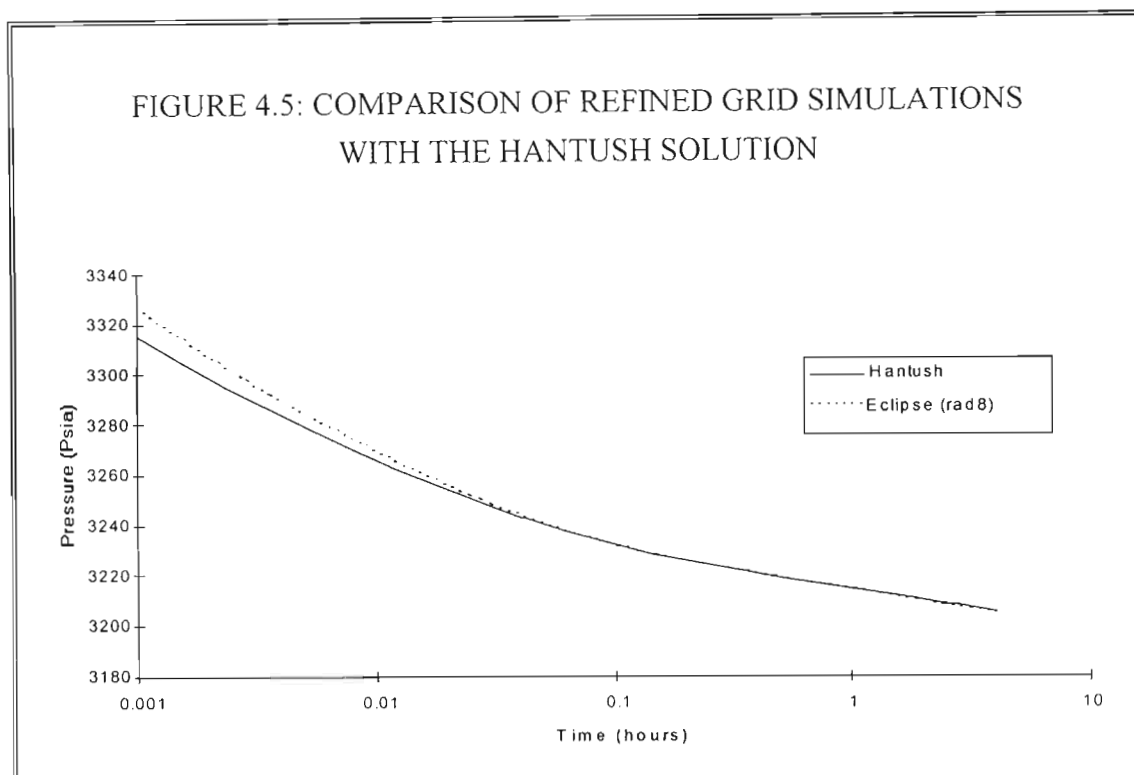
There are several possibilities that could be investigated as providing ways of reducing the errors. The most obvious of these is to reduce the block size, which should reduce both sources of error. Another might be to investigate alternative formulations for the transmissibilities, particularly in the problem areas close to the well and at the base of the perforations. The discretisation method could be extended to provide a better model for the potential gradients. One way of doing this would be to include additional grid points by using a nine point discretisation scheme.

4.4 Use of a Refined Grid

A number of experiments were performed to determine whether the discrepancy between the analytical models and the Eclipse simulation could be improved by defining smaller blocks. It was immediately apparent that there was an improvement, but the degree to which the block size had to be reduced in order to begin to approach the analytical solution was surprising. As a result the number of blocks in the grid soon became unmanageable.

A strategy of only decreasing the block size in the problem areas was followed in order to achieve a similar accuracy without using so many blocks. The grid was therefore refined close to the wellbore and also towards the base and immediately below the perforations. The radial width of the innermost block was ultimately reduced to 0.1 feet. Similarly the thickness of the layers at base of the perforations was also reduced to 0.1 feet.

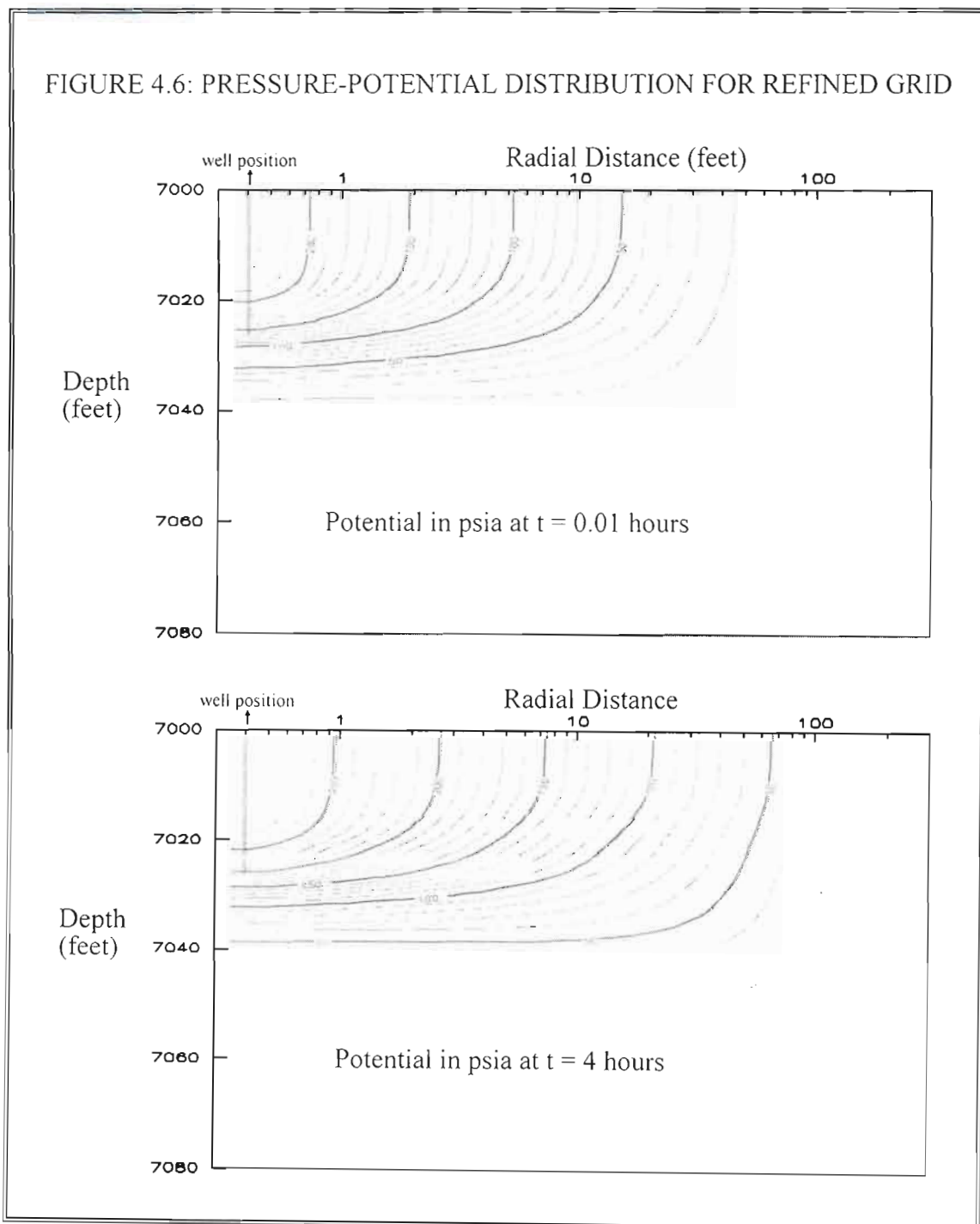
The result of the refined grid simulation is displayed in Figure 4.5. There is now good agreement in the late time portion of the data and the slope of the early time data is now closer to that of the analytical model.



A cross-section view of the distribution of pressure potential for the refined grid is given in Figure 4.6 for two different times. In creating these plots it has been assumed that the potential is initially zero and the potential difference has been displayed as a positive quantity. The convergence of the isopotential contours towards the base of the perforations is clearly visible, thus confirming the need to define fine layers in this area.

The sequence of development of the pressure field in a limited entry well is as follows. Initially the pressure disturbance is confined to an area immediately adjacent to the well interval that is open to flow. In the limiting case of zero vertical permeability the pressure disturbance would continue to be confined to this interval but would propagate radially outward with time. The pressure at the wellbore would decline linearly with respect to the logarithm of time and with a slope inversely proportional to the permeability thickness product of the open interval. If the vertical permeability is not zero then the pressure disturbance grows both radially and vertically. The wellbore pressure declines less rapidly than for zero vertical permeability owing to the increased volume of fluids accessible to the well. The pressure decline is concave upward when plotted against the logarithm of time and bears some similarity to that expected for hemispherical flow. As the pressure disturbance grows still further it reaches the lower no-flow boundary and this starts to have an impact on the wellbore pressures. Ultimately the shape of the pressure

contours in the inner region stabilise throughout the vertical section and the remaining growth of the pressure disturbance is purely radial as reflected by a linear decline of pressure with respect to the logarithm of time. The slope of the late time decline is inversely proportional to the permeability thickness product of the entire reservoir interval.



For our test case Figure 4.6 shows that at 0.01 hours the lower boundary has not had a significant influence on the wellbore pressure in that change in potential has not yet

reached this boundary. The radial influence is also limited to the region close to the wellbore. After flowing for 4 hours the shape of the contours in the inner portion of the grid has stabilised. The outermost contour now runs from the upper to the lower boundary implying that the full influence of the lower boundary should have been established. These observations are consistent with the pressure response plotted in Figure 4.5 where the transition to the final linear decline period only starts taking place at approximately 0.08 hours. At 4 hours the pressure is well onto the final period indicating that radial flow has been established over the entire reservoir interval.

During the expansion of the pressure disturbance the reservoir can be divided into three broad regions:

- A outer region where pressures have not yet been affected by the flow
- A inner region where the pressures have been reduced but the shape of the pressure contours has stabilised
- A transition region where rapid changes are taking place and the shape and spacing of the pressure contours has not stabilised

The inner region is one where flow approximates steady state behaviour very closely. Also noteworthy from the potential distribution is the fact that the radial spacing of the contours is almost constant in log space for the innermost portion of the grid. Under these circumstances the transmissibility calculation will be exact for the point at the centre of the grid block face. As a consequence one would expect spatial discretisation errors in this portion of the grid to be purely related to the contour convergence effect previously mentioned in Section 4.3. Pressure changes in the outer region are so small as to have no discernible effect on the wellbore pressure.

This leaves the transition region as the only portion of the grid where the steady state approximation is not honoured. The reason for the transition region can be demonstrated for a purely radial problem by differentiating the transient line-source solution (Equation 6) with respect to the radius, giving:

$$\frac{\partial \Psi}{\partial r} = \frac{q\mu B_o}{2\pi khr} e^{-\phi_{ucr}^2/4kt} \quad (165)$$

This can be compared with the potential gradient for radial steady-state flow that is given by:

$$\frac{\partial \Psi}{\partial r} = \frac{q\mu B_o}{2\pi khr} \quad (166)$$

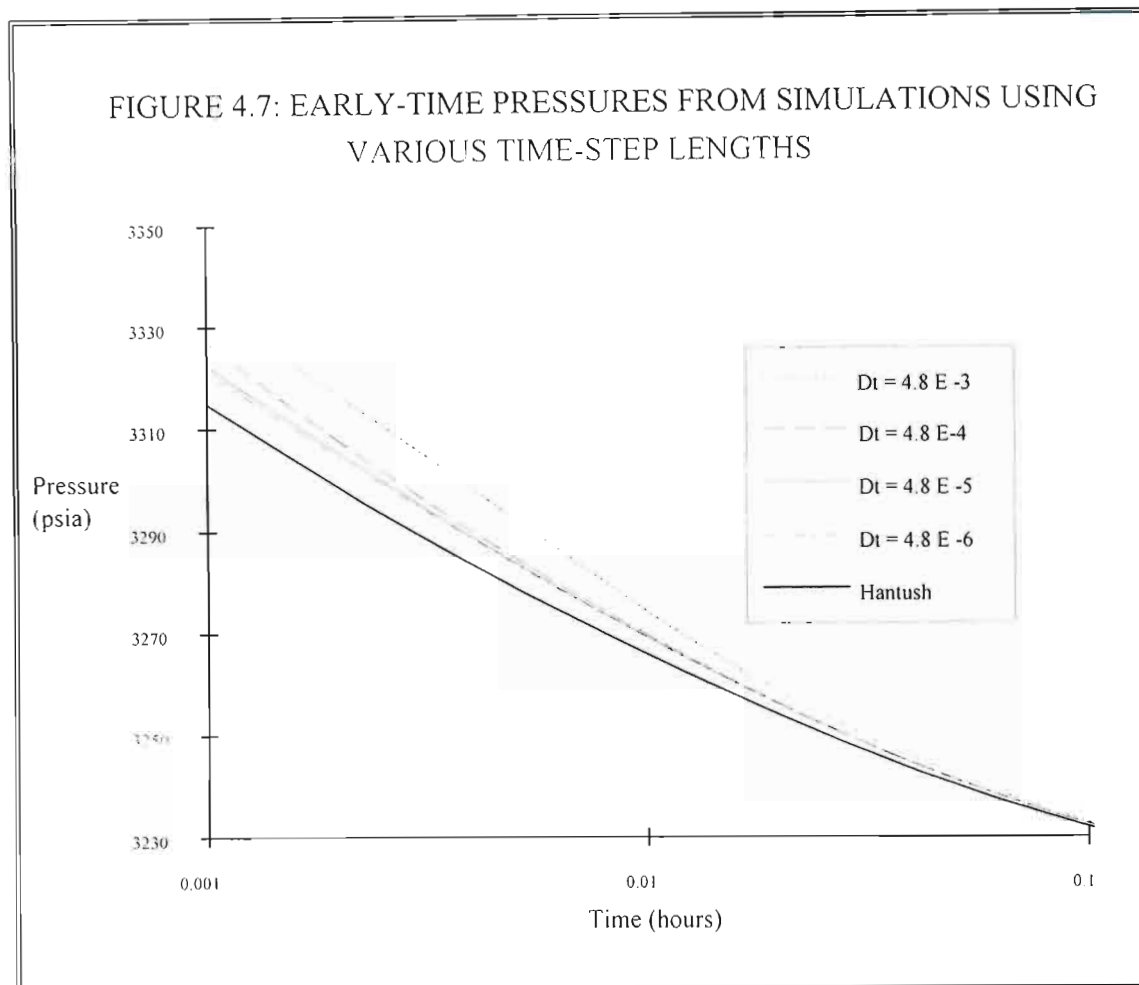
When the radius, r , is small the exponential factor in Equation 165 tends to unity and the transmissibility calculation is exact. As the time, t , increases, r can be larger while still preserving the same level of agreement between the equations. Thus the region displaying a constant potential gradient in log space will grow with time. Beyond this inner region the exponential factor starts to have a big impact on the potential gradient, defining the transition region. At still larger radii the potential gradient tends to zero and therefore the error in the flow terms also tends to zero.

It may therefore seem possible that one way of reducing the error in the simulation is to define smaller blocks in portion of the grid that corresponds to the region of transition at early times in the simulation. This does not necessarily comprise the innermost cells in the grid. Examining Figure 4.6 shows that the region of transition is from 20 to 70 feet from the wellbore for a time of 0.01 hours. At a time of 0.001 hours the transition will occur at a distance that is closer by a factor of $1/\sqrt{10} = 0.316\dots$ or 6.3 to 22 feet.

Several simulation runs were made to check the hypothesis that defining smaller blocks in the transition zone from 6 to 70 feet could reduce the early-time error. The results were only slightly different from those obtained using the original refined grid. This suggests that the bulk of the remaining spatial discretisation error is due to the fact that the potential gradient is not constant across the face of the block and not to the unsteady-state behaviour.

As a further check a purely radial, one-dimensional, simulation with a fully completed well was set up. The radial widths of the cells in this model were identical to those in the partial penetration simulation. Comparison of the results with the exact radial transient solution involving the Ei function (Equation 6) showed extremely close agreement confirming that the unsteady state behaviour is not the reason for the residual errors.

Further attempts to achieve a closer match to the Hantush solution concentrated on defining smaller cells in the problem areas or by optimising the grid spacing using the pressure potential plot of Figure 4.6 as a guide. Little improvement was achieved by either of these methods.



Up till now it has simply been assumed that the time steps are sufficiently small for the time discretisation errors to be small. In order to confirm this and determine an optimum time step size a number of simulations with different time step sizes were run using the refined grid. The results are given in Figure 4.7, where it can be seen that there is a big change in moving from a second time step of 0.005 days to 0.00005 days. Decreasing the length of the time-step still further makes very little difference.

One would expect the simulated result to converge on the analytical solution as the time step and the grid spacing is reduced. The residual discrepancy therefore casts some doubt on the validity of the analytical solution. This prompted an examination of the differences in the assumed boundary conditions for the two methods. Given that the discrepancy occurs soon after a rate change it is likely that the problem lies with the inner boundary condition, namely at the wellbore itself.

There are two major difference in the way the two methods treat the inner boundary. The first is that the Hantush solution assumes a line source for the well withdrawal (the well flow is assumed to originate at an infinitesimally thin line positioned at the

centre of the wellbore), whereas the simulation assumes a finite wellbore size. The second relates to the flux and potential distribution within the wellbore. The Hantush solution assumes that the flux distribution along the wellbore is constant whereas the simulation assumes potential is constant.

In the case of a fully penetrating well the differences between line source and finite wellbore solutions are well understood. Typically the differences are small enough to be ignored for most practical purposes and are confined to very early time. A commercially available well test analysis program was used to assess the impact of these assumptions for the same formation permeability as used in the test case. Differences between the solutions were barely noticeable even at 0.001 hours. It is conceivable that the differences could be amplified in the case of a partially penetrating well. It is however unlikely that they could account for more than a small portion of the observed discrepancy between simulation and the Hantush solution.

Flux and potential distributions along the wellbore were previously discussed in Section 4.2. The assumption of uniform flux used by the Hantush solution is simply a convenience to aid the superposition of flux elements used in deriving the solution. The uniform potential assumption used by the simulation is closer to the physical reality given the very high conductivity of the wellbore. Muskat³⁶ showed that infinite conductivity (uniform potential) and uniform flux solutions are equivalent for steady-state flow provided that the uniform flux solution is evaluated at a particular point along the wellbore. Gringarten and Ramey¹⁰ derived an infinite conductivity solution based on the superposition of flux elements of varying strength along the wellbore. They concluded that the infinite conductivity and uniform flux solutions are also equivalent for transient flow and provide a chart for calculating the position at which the uniform flux solution is to be evaluated. Most well test analysis packages use this result and indeed this was also the basis for the calculation of pressures using the Hantush solution as presented in this thesis.

Gringarten and Ramey's conclusion is somewhat misleading when subjected to closer examination. Their results are based on a stabilised flux distribution along the wellbore. In reality the flux distribution varies initially and only stabilises once the impact of the lower boundary is fully realised. Thus their result only applies the late time portion of the pressure response when the pressure declines linearly with respect to the logarithm of time. The misinterpretation of their results as being applicable to the entire time range is a consequence of the use of the word "transient" in their conclusions. To some engineers transience implies that the spatial gradients of pressure are still changing with time and is used to distinguish between this and

steady, or semi-steady, state behaviour (pressures changing at a constant rate). To other engineers the term implies a specific form of pressure behaviour associated with radial flow in a laterally infinite reservoir. This latter sense of the word is what Gringarten and Ramey are implying in their paper.

In many ways partially penetrating wells are very similar to horizontal wells (wells that are approximately parallel to the top and base of the reservoir interval) in their near well bore behaviour. As with partially penetrating wells the flux distribution for the infinite conductivity case will change with time and the pressure disturbance will grow from the tip of the well. It is therefore useful to consult the extensive literature available on pressure behaviour in horizontal wells to determine the views on use of different forms of the inner boundary condition.

Kuchuk et al³⁷ present an alternative approach to the uniform flux solution for horizontal wells where the pressure is averaged along the wellbore rather than evaluated at an equivalent pressure point. They show that this solution differs significantly from the conventional approach at early time. This would seem to imply that the equivalent pressure point shifts along the well with time. They claim that the pressure averaging should give an exact solution in the case of the wellbore radius tending to zero. Details of why this should be the case are, however, not presented within their paper but only within an internal service company document that is not readily available to the general public. Several arguments as to why pressure averaging is to be preferred are also given in their paper but none of these are conclusive.

Ozkan et al^{38,39} have constructed a model for horizontal well pressure behaviour that directly accounts for varying flux along the wellbore. Their method can accommodate a wide range of wellbore conductivities including infinite conductivity as a limiting case. The method breaks the wellbore into a number of discrete cylindrical strips whose analytical response is known. A finite element method is then used to solve for pressure losses in the wellbore and individual fluxes of the cylindrical strips.

In the case of a partially penetrating well the well length is typically considerably less than for a horizontal well implying that the infinite conductivity assumption is a good one. Ozkan's results show how the flux distribution for such a case varies with time. Initially, at the time of the rate change, the flux distribution is uniform along the well. Shortly after this the flux is concentrated at the tip of the well. The reason for this is that at the tip the volume in which the pressure change takes place grows hemispherically, whereas further along the well the volume grows cylindrically. Thus the reservoir volume affected by the rate change, and therefore the flux, grows most

quickly at the tip of the well. At later times the flux distribution becomes more uniform but retains a degree of concentration towards the tip of the well.

The flux behaviour in the infinite conductivity case will mirror what happens with the pressure distribution for a uniform flux case. At early time the pressure drop will be concentrated near the tip of the well becoming more evenly distributed later. The equivalent pressure point will therefore move along the well from near the tip at early time to a position close to that suggested by Gringarten and Ramey at later time. If a constant position is used for the equivalent pressure point then the uniform flux solution will underestimate the true pressure and the error will be greatest at early time. This is exactly what is observed for the difference between the simulated pressure and the uniform flux solution in the partial penetration case. The hypothesis is therefore that these differences are chiefly due to the difference in boundary conditions and the use of a constant equivalent pressure point.

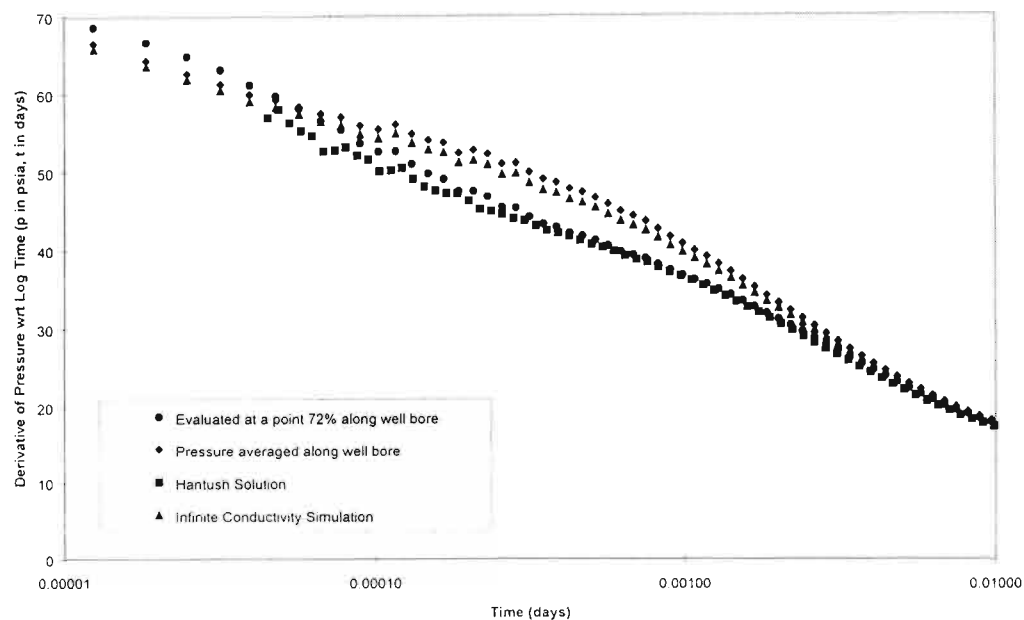
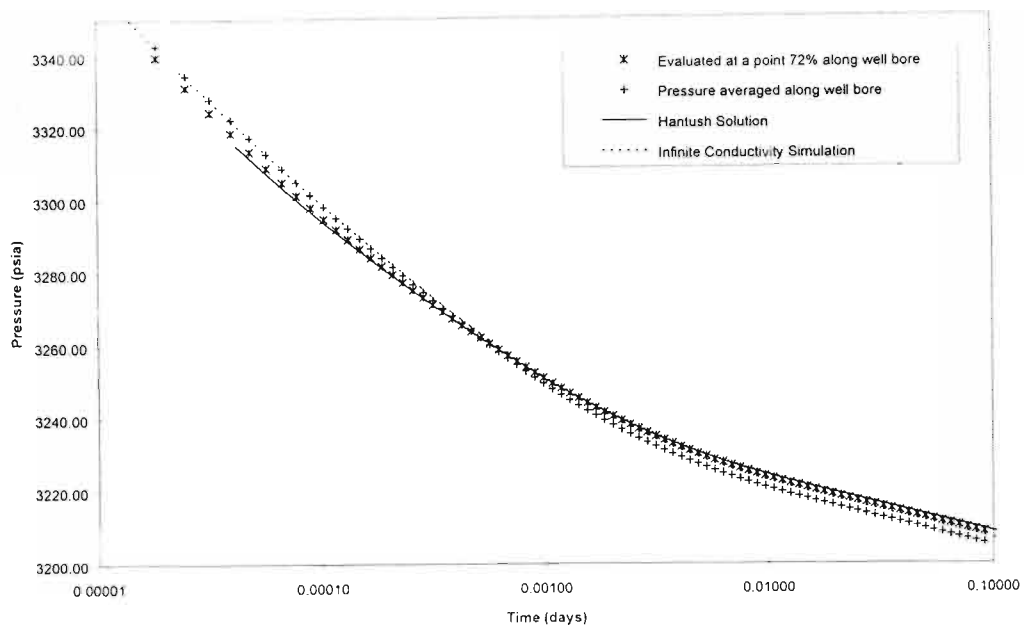
In order to test the hypothesis a uniform flux simulation with the same grid block geometry as previously used was run. This allows the following:

1. Comparison of pressures from numerical simulation with those from analytical solutions for the same boundary conditions
2. Comparison of pressure averaged along the wellbore in a uniform flux simulation with the infinite conductivity case
3. Measurement of pressure distribution along the wellbore and location of the equivalent pressure point

Results are displayed in Figure 4.8. The analytical (Hantush) solution agrees very closely with the uniform flux simulation evaluated at Gringarten and Ramey's equivalent pressure position. This suggests that the residual spatial and temporal discretisation errors are negligible. The same will apply to the infinite conductivity simulation as the two simulations have identical properties other than the inner boundary conditions.

The pressure averaged along the wellbore is in good agreement with the infinite conductivity simulation at early time but steadily diverges at later time. This suggests that approximations of the infinite conductivity solution that are based on pressure averaging are imperfect and should be used with caution. The consequence of the difference in late pressure would imply a slight difference in the apparent skin.

FIGURE 4.8: COMPARISON OF INNER BOUNDARY CONDITIONS



The mismatch between infinite conductivity simulation and the uniform flux methods could be more serious when analysing a real well test. If the early time behaviour were used to assess the vertical permeability then erroneous conclusions could be drawn through use of the uniform flux method. The potential error is proportional to the difference in slope on a pressure versus log time plot or to the magnitude of

pressure derivative with respect to the logarithm of time. In Figure 4.8 the difference in derivatives is approximately 10%, which is barely acceptable. Errors of preferably less than 5% and ideally of the order of 1% would be more acceptable.

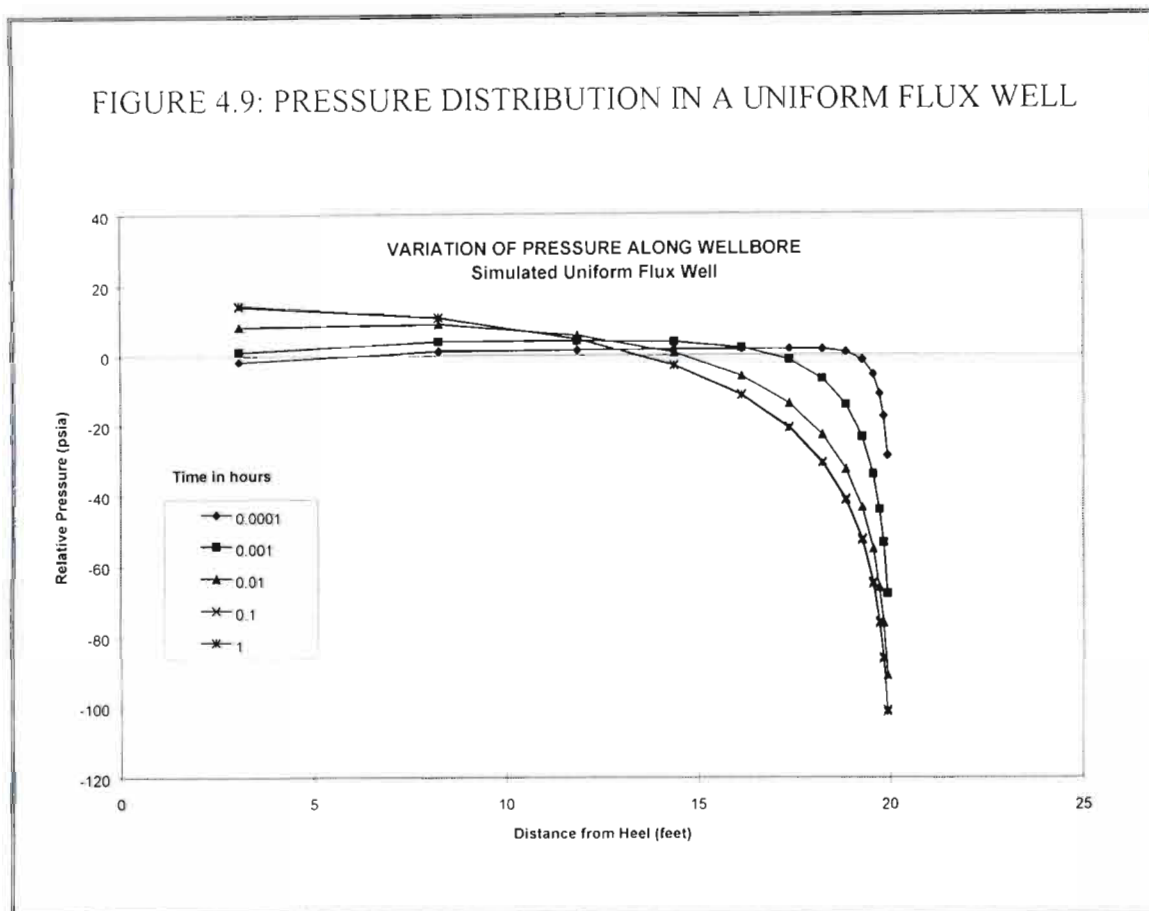


Figure 4.9 shows how the pressure distribution along the wellbore varies with time. In this plot the pressures are relative to the average well pressure at the given time. The plot confirms the earlier discussion of how pressure distribution will change with time. It is clear that the equivalent pressure point would need to move with time but stabilises at a position close to that suggested by Gringarten and Ramey.

A literature survey was conducted in order to find analytical solutions based on an infinite conductivity well boundary condition in order to provide a comparison with the infinite conductivity simulation. Yiidiz and Bassiouni⁴⁰ have derived such a solution as an infinite Fourier-Bessel series in Laplace space:

$$\tilde{P}_D(s) = \frac{1}{s^{3/2}} \frac{K_0(\sqrt{s})}{K_1(\sqrt{s})} + \frac{2}{h_{Dw}^2} \frac{1}{s} \sum_{m=1}^{\infty} \frac{1}{m^2 \pi^2 \lambda_m} \frac{K_0(\lambda_m)}{K_1(\lambda_m)} \gamma_m, \quad (167)$$

where

$$\lambda_m = \sqrt{s + \frac{k_z}{k_r} \left(m\pi \frac{r_w}{h} \right)^2}, \quad (168)$$

$$\gamma_m = [\sin m\pi(h_{Db} + h_{Dw}) - \sin m\pi h_{Db}]^2, \quad (169)$$

$$h_{Dw} = h_w / h, \quad (170)$$

$$h_{Db} = (h_1 + h_w) / h, \quad (171)$$

K_0 and K_1 are modified Bessel functions of the second kind with order zero and one respectively, $\tilde{p}_D(s)$ is the Laplace transform of the dimensionless pressure, $p_D(t_D)$, and s is the Laplace variable corresponding to the dimensionless time t_D . See Figure 4.1 for a reminder of the geometry of the problem.

Dimensionless pressure and time are defined by:

$$p_D = C_1 \frac{2\pi k_r h}{q\mu B_o} (p_i - p), \quad (172)$$

where C_1 is 1 for absolute unit systems and 1.127×10^{-3} for field units, and

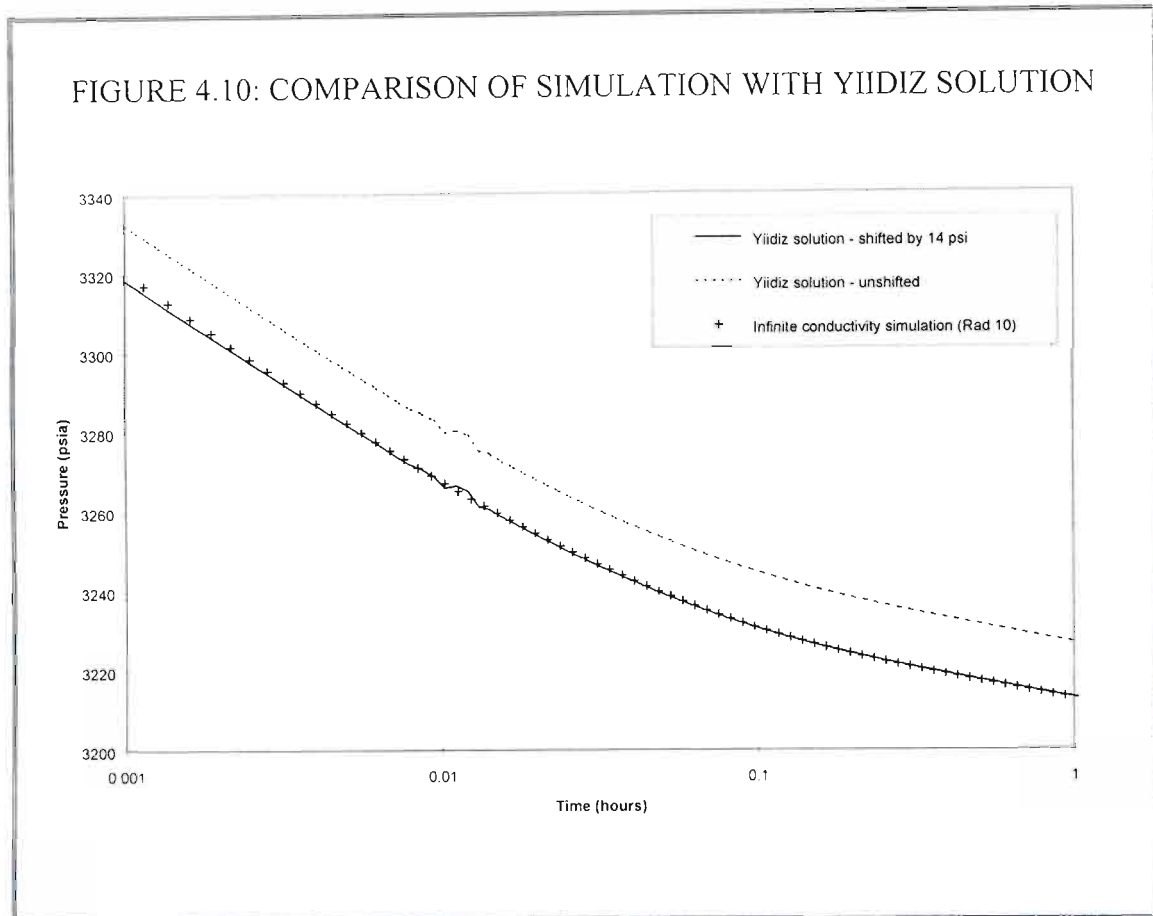
$$t_D = C_2 \frac{k_r t}{\phi \mu c_i r_w^2}, \quad (173)$$

where C_2 is 1 for absolute unit systems and 2.637×10^{-4} for field units.

The pressure solution for our idealised problem was obtained by numerically inverting the Laplace space solution using the Stehfest⁴¹ algorithm. The computer program implementing the solution and the numerical inversion is listed in Appendix 2.

Comparison of the Yiidiz solution with the infinite conductivity simulation showed very good agreement between the rate of change of pressure with time. The analytical solution did however show a substantial and constant offset in pressure (14 psi). Figure 4.10 shows the level of agreement once this offset was removed. The slight oscillation in pressure for the Yiidiz solution at a time of 0.01 hr is believed to be an artefact related to the use of the Stehfest algorithm for the numerical inversion. Better results could probably be obtained using a more robust technique such as Talbot's method⁴². Nevertheless, the level of agreement is sufficient to confirm that the infinite conductivity simulation is giving an accurate result.

FIGURE 4.10: COMPARISON OF SIMULATION WITH YIIDIZ SOLUTION

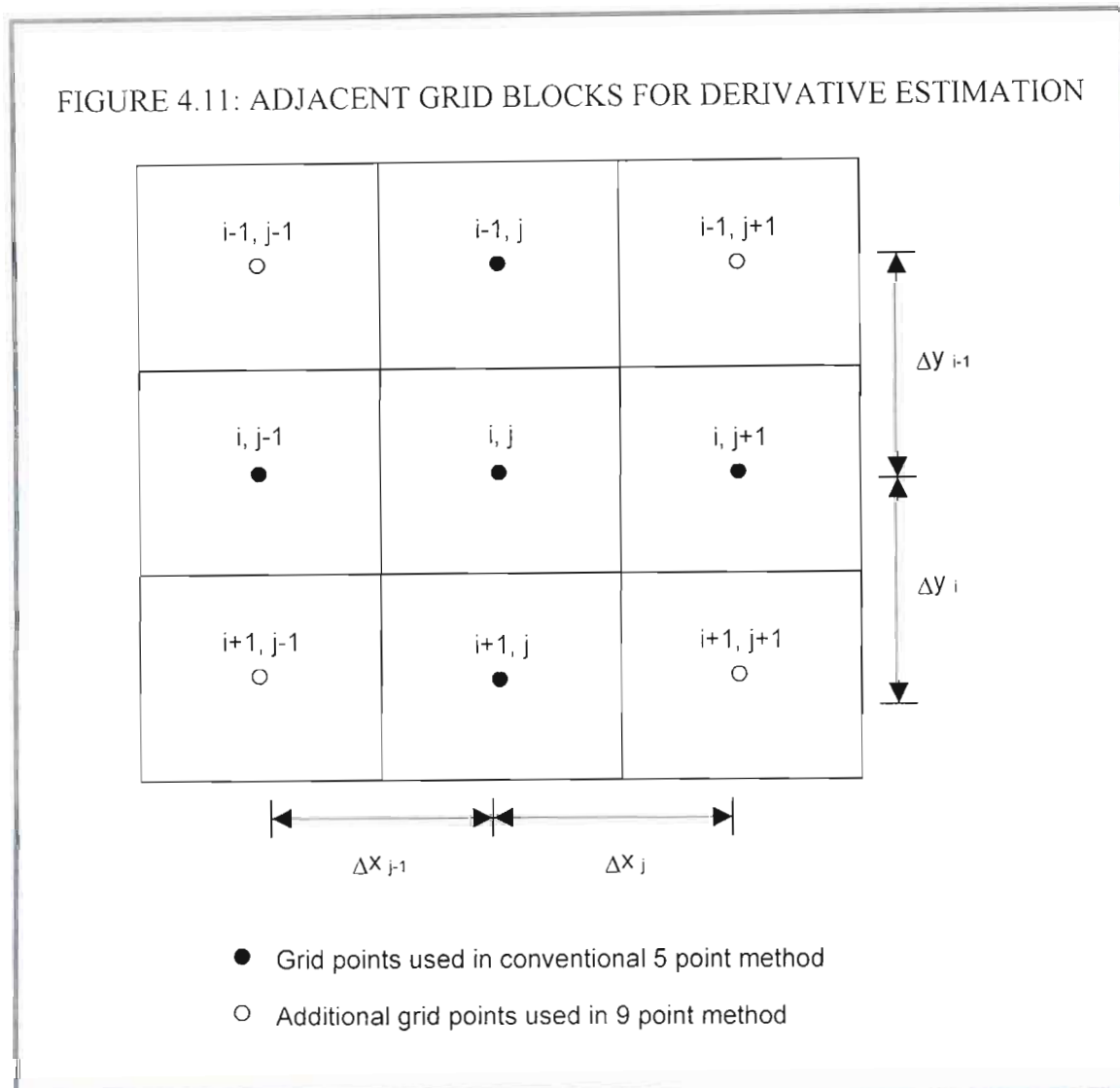


4.5 Use of a Nine-Point Scheme

A possible alternative to using a refined grid to improve accuracy is to use a higher order approximation for the spatial derivative in the discretisation process. Typically this would be achieved by increasing the number of points used in calculating the derivative. One such method is the nine-point scheme devised by Yanosik and McKracken⁴³. In this method transmissibilities are defined for diagonally adjacent grid points in addition to the grid points from immediately adjacent blocks (i.e. blocks that share a face with the block being considered). In two dimensions this implies an increase from a five point to a nine point discretisation scheme (Figure 4.11) whereas in three dimensions the increase is from seven to twenty-seven points. The nine-point method was originally intended to reduce grid orientation effects but may be useful for the current problem given the large diagonally orientated pressure gradients close to the tip of the well.

Several approaches can be used to derive a nine-point method. The Yanosik and McKracken approach is based on forming a linear combination of the five-point equations for parallel and diagonal grids. The ECL advanced simulation course⁴⁴

presents an alternative approach using Taylor series. A modified version of their approach as applied to deriving a nine-point method for a Cartesian grid is summarised below:



The aim is to find a linear combination of adjacent grid point pressures (or strictly speaking, pressure potentials) that approximates the flow divergence, $\nabla \cdot F = \nabla \cdot k\lambda \nabla \Psi$, as discussed in Chapter 3. For the purposes of the derivation the mobility, λ , is assumed to be 1 as we are only concerned with saturation and component independent properties. In other words we are trying to find the transmissibilities, T_i , that best satisfy the equation:

$$\nabla \cdot k \nabla \Psi \approx \sum_i T_i \Delta \Psi_i, \quad (174)$$

where the sum is over the adjacent grid-points and $\Delta\Psi_i$ represents the potential difference between a pair of grid-points.

To simplify the demonstration we assume that permeability is anisotropic and homogenous. At a particular grid-point i,j the problem becomes equivalent to solving for the coefficients a to l that best satisfy the equation:

$$\begin{aligned} (\nabla \cdot k \nabla \Psi)_{i,j} &= \left(k_x \frac{\partial^2 \Psi}{\partial x^2} + k_y \frac{\partial^2 \Psi}{\partial y^2} \right)_{i,j} \\ &\approx a\Psi_{i-1,j-1} + b\Psi_{i-1,j} + c\Psi_{i-1,j+1} + d\Psi_{i,j-1} + e\Psi_{i,j} + f\Psi_{i,j+1} \\ &\quad + g\Psi_{i+1,j-1} + h\Psi_{i+1,j} + l\Psi_{i+1,j+1} \end{aligned} \quad (175)$$

where $\Psi_{i+1,j-1}$ represents the potential at the grid point $i+1, j-1$. Expanding $\Psi_{i+1,j-1}$ as a Taylor series about the point i, j gives:

$$\begin{aligned} \Psi_{i+1,j-1} &= \Psi_{i,j} - \Delta x_{j-1} \left(\frac{\partial \Psi}{\partial x} \right)_{i,j} + \Delta y_i \left(\frac{\partial \Psi}{\partial y} \right)_{i,j} + \frac{\Delta x_{j-1}^2}{2} \left(\frac{\partial^2 \Psi}{\partial x^2} \right)_{i,j} \\ &\quad - \Delta x_{j-1} \Delta y_i \left(\frac{\partial^2 \Psi}{\partial x \partial y} \right) + \frac{\Delta y_i^2}{2} \left(\frac{\partial^2 \Psi}{\partial y^2} \right)_{i,j} + R_{i+1,j-1} \end{aligned} \quad (176)$$

where $R_{i+1,j-1}$ represents all terms of third or higher order.

Similar series can be derived for all the other grid points surrounding i,j . Substituting for the potential at all surrounding grid-points in Equation 175 we get an equation involving only derivatives of the potential evaluated at the central point and grid point distances on the right hand side of the equation. Grouping together terms involving $\partial^2 \Psi / \partial x^2$ on both sides of this equation gives:

$$k_x \frac{\partial^2 \Psi}{\partial x^2} = \frac{1}{2} \frac{\partial^2 \Psi}{\partial x^2} \left[(a+d+g)\Delta x_{j-1}^2 + (c+f+l)\Delta x_j^2 \right], \quad (177)$$

implying:

$$(a+d+g)\Delta x_{j-1}^2 + (c+f+l)\Delta x_j^2 = 2k_x. \quad (178)$$

Similarly, grouping together other derivatives of the same order:

$$(a+b+c)\Delta y_{i-1}^2 + (g+h+l)\Delta y_i^2 = 2k_y; \quad (179)$$

$$a\Delta x_{j-1}\Delta y_{i-1} - c\Delta x_j\Delta y_{i-1} - g\Delta x_{j-1}\Delta y_i + l\Delta x_j\Delta y_i = 0; \quad (180)$$

$$(c + f + l)\Delta x_i - (a + d + g)\Delta x_{i-1} = 0; \quad (181)$$

$$(g + h + l)\Delta y_i - (a + b + c)\Delta y_{i-1} = 0; \quad (182)$$

$$a + b + c + d + e + f + g + h + l = 0. \quad (183)$$

Equations 178 to 183 form a set of six simultaneous equations with nine unknowns. In the special case where the block dimensions are constant throughout the grid, symmetry requires that $a = c = g = l$, $b = h$ and $d = f$. Substituting for these variables eliminates Equations 180 to 182 and results in a system of three equations with four unknowns:

$$(2a + d)\Delta x^2 = k_x; \quad (184)$$

$$(2a + b)\Delta y^2 = k_y; \quad (185)$$

$$4a + 2b + 2d + e = 0. \quad (186)$$

In order to solve these equations we introduce a new variable, β , that represents the degree to which the diagonal grid-points are used in calculating the flow divergence. When $\beta = 1$ the result should revert to the standard 5-point method where $a = 0$ and

$$e = -2 \left(\frac{k_x}{\Delta x^2} + \frac{k_y}{\Delta y^2} \right). \quad (187)$$

We therefore define β in terms of the equation:

$$e = -2\beta \left(\frac{k_x}{\Delta x^2} + \frac{k_y}{\Delta y^2} \right). \quad (188)$$

The remaining variables then become:

$$a = \frac{(1 - \beta)}{2} \left[\frac{k_x}{\Delta x^2} + \frac{k_y}{\Delta y^2} \right]; \quad (189)$$

$$b = \beta \frac{k_y}{\Delta y^2} - (1 - \beta) \frac{k_x}{\Delta x^2}; \quad (190)$$

$$d = \beta \frac{k_x}{\Delta x^2} - (1 - \beta) \frac{k_y}{\Delta y^2}. \quad (191)$$

The coefficients can be converted into transmissibilities by multiplying by the cell volume, $V_{i,j}$:

- $aV_{i,j}$ is the diagonal transmissibility;
- $bV_{i,j}$ is the transmissibility in the y direction
- $dV_{i,j}$ is the transmissibility in the x direction.

Choosing $\beta = 5/6$ for square grid blocks gives an identical formulation to that of Yanosik and McKracken.

No derivation of a nine-point method for a two-dimensional (rz) cylindrical grid could be found in the literature. The Taylor series approach summarised above was therefore used to try to find the necessary weighting factors.

In a two-dimensional radial co-ordinate system the equation to be satisfied is:

$$\begin{aligned} (\nabla \cdot k \nabla \Psi)_{i,j} &= \left(\frac{k_k}{r} \frac{\partial \Psi}{\partial r} + k_r \frac{\partial^2 \Psi}{\partial r^2} + k_z \frac{\partial^2 \Psi}{\partial z^2} \right)_{i,j} \\ &\approx a\Psi_{i-1,j-1} + b\Psi_{i-1,j} + c\Psi_{i-1,j+1} + d\Psi_{i,j-1} + e\Psi_{i,j} + f\Psi_{i,j+1} \\ &\quad + g\Psi_{i+1,j-1} + h\Psi_{i+1,j} + l\Psi_{i+1,j+1} \end{aligned} \quad (192)$$

Substituting the Taylor expansions for potential at each of the adjoining grid points and collecting terms of similar order gives:

$$(a + d + g)\Delta r_{i-1}^2 + (c + f + l)\Delta r_j^2 = 2k_r; \quad (193)$$

$$(a + b + c)\Delta z_{i-1}^2 + (g + h + l)\Delta z_i^2 = 2k_z; \quad (194)$$

$$a\Delta r_{j-1}\Delta z_{i-1} - c\Delta r_j\Delta z_{i-1} - g\Delta r_{j-1}\Delta z_i + l\Delta r_j\Delta z_i = 0; \quad (195)$$

$$(c + f + l)\Delta r_j - (a + d + g)\Delta r_{j-1} = \frac{k_r}{r}; \quad (196)$$

$$(g + h + l)\Delta z_i - (a + b + c)\Delta z_{i-1} = 0; \quad (197)$$

$$a + b + c + d + e + f + g + h + l = 0. \quad (198)$$

In order to reduce the number of variables it is assumed that the spacing of the blocks in the z-direction is constant. Note that the radial spacing cannot be assumed to be constant as this would give a very unrealistic grid for single well problems. (In Chapter 3 it was shown that steady state flow in a radial grid with a well at the centre is best modelled using grid blocks where the radial width of adjacent blocks increases by a constant factor.) These assumptions require that $a = g$, $c = l$ and $b = h$. Substituting into Equations 193 to 198 gives:

$$(2a + d)\Delta r_{j-1}^2 + (2c + f)\Delta r_j^2 = 2k_r \quad (199)$$

$$(a + b + c)\Delta z^2 = k_z \quad (200)$$

$$(2c + f)\Delta r_j - (2a + d)\Delta r_{j-1} = \frac{k_r}{r} \quad (201)$$

$$2a + 2b + 2c + d + e + f = 0 \quad (202)$$

Thus we now have a system of 4 equations with 6 unknowns. Solving this system requires the introduction of two new equations. We cannot therefore use exactly the same approach as for the Cartesian case given above. One approach is to take the formulae that would result for the five-point method and then assume that the introduction of additional point points would act to scale down the contribution of the laterally adjacent grid points in constant proportion. In other words, both the variables d and f would be reduced by a constant factor in the nine-point method in comparison with their value in the five-point method.

Substituting $a = c = 0$ and solving the system of equations gives the five-point formulation where:

$$d = \frac{k_r(2 - \Delta r_j/r)}{\Delta r_{j-1}^2 + \Delta r_j \Delta r_{j-1}}; \quad (203)$$

$$f = \frac{k_r(2 + \Delta r_{j-1}/r)}{\Delta r_j^2 + \Delta r_{j-1} \Delta r_j}. \quad (204)$$

The two additional equations to be used in solving the nine-point method are therefore given by:

$$d = \frac{\beta k_r(2 - \Delta r_j/r)}{\Delta r_{j-1}^2 + \Delta r_j \Delta r_{j-1}}; \quad (205)$$

$$f = \frac{\beta k_r(2 + \Delta r_{j-1}/r)}{\Delta r_j^2 + \Delta r_{j-1} \Delta r_j}, \quad (206)$$

where β is a parameter to be optimised for the problem at hand. The resulting set of equations (Equations 199 to 202, 205, and 206) were solved by substituting for d and f in Equations 199 and 201, eliminating one of the remaining variables and then back substituting, giving:

$$a = \frac{(1 - \beta)k_r (2 - \Delta r_j / r)}{2\Delta r_{j-1} (\Delta r_{j-1} + \Delta r_j)}, \quad (207)$$

$$c = \frac{(1 - \beta)k_r (2 - \Delta r_{j-1} / r)}{2\Delta r_j (\Delta r_{j-1} + \Delta r_j)}, \quad (208)$$

$$b = \frac{2k_z}{\Delta z^2} - \frac{(1 - \beta)k_r [\Delta r_j (2 - \Delta r_j / r) + \Delta r_{j-1} (2 - \Delta r_{j-1} / r)]}{2\Delta r_{j-1} \Delta r_j (\Delta r_{j-1} + \Delta r_j)}, \quad (209)$$

$$e = -\frac{4k_z}{\Delta z^2} - \frac{\beta k_r [\Delta r_j (2 - \Delta r_j / r) + \Delta r_{j-1} (2 - \Delta r_{j-1} / r)]}{\Delta r_{j-1} \Delta r_j (\Delta r_{j-1} + \Delta r_j)}. \quad (209)$$

Comparison of analytically calculated derivatives with the nine-point approximation showed that the optimum value of β was 1 suggesting that the assumptions reflected by Equations 205 and 206 are not effective in producing an improvement over the standard five-point method.

The difficulties in applying the ECL approach to a nine-point method for a radial grid and the lack of any similar derivations in the literature prevented the application of the method to the current problem. It is therefore not clear whether other formulations of the method could have offered an improvement in accuracy. One possible alternative approach that could be grounds for future research is to use the Control Volume Finite Differencing (CVFD) technique suggested by Rozon⁴⁵.

In CVFD the grid block is sub-divided into smaller control volumes. Flow across each sub-face is calculated assuming that pressure is bi-linearly related to the values at the three closest grid points. When the flow is summed over all the sub-faces the result is a flow accumulation term that depends on the values of the nine adjacent points. Unlike the conventional nine-point method Rozon's method does not have diagonal transmissibilities and would therefore require modifications to the simulation program in order to implement the method. It therefore contradicts our aim of having a technique that can be universally applied by engineers using their existing software. Note that CVFD is currently being used successfully in implementing the flexible PEBI grid approach discussed in Chapter 3^{27,28}.

Given the success and the transparency of the grid refinement procedure demonstrated in Section 4.4, the failure of the nine-point method is not serious. Grid refinement was therefore chosen as the method to be used in solving the real life problem.

4.6 Chapter Summary

In this chapter finite-difference simulation was applied to modelling a hypothetical partially penetrating well. Results of the simulation were compared to an analytical solution for the same problem. Discrepancies between the two sets of results were noted and attempts were made to resolve these through use of selective grid refinement and use of small time steps. It was found that radial width of grid blocks close to the well needed to be approximately 0.1 feet in order to improve the early time match. A geometric increase of the block widths in the radial direction was found to give good results. Similarly, the thickness of layers at the base of the perforated interval needed to be reduced to approximately 0.1 feet. This is believed to be a consequence of the high pressure gradients and the flow convergence that takes place at the base of the perforated interval. Reducing time-step duration after rate changes to below 0.00005 days (~ 4 seconds) did not lead to any further improvement in the match.

Residual early-time differences between simulated and analytically derived results remained and proved to be related to the nature of the boundary conditions (uniform flux along the perforated interval) used in the analytical solution. Implementation of an infinite conductivity solution showed that the numerical simulation had reached a high level of accuracy. The use of a nine-point discretisation method for spatial derivatives was investigated as a means of obtaining a better pressure match without needing the same degree of grid block refinement. It was found that the assumptions that lead to a successful nine-point method for a Cartesian grid using a Taylor series method fail to do the same for a radial grid. The reason for this is that the underlying nature of the problem geometry and spatial derivatives leads to an underdetermined set of equations. Attempts were made to solve the system by providing additional equations that scale the transmissibilities used in the five-point method. These proved to offer no improvement in accuracy over the traditional five-point method.

In the next chapter the finite difference approach will be applied to the modelling and analysis of a real well test of a partially penetrating well. The same techniques of selective grid refinement and use of small time steps after rate changes that were perfected in this chapter will be applied to the real-life problem. The importance of first modelling the hypothetical problem is that one can proceed with confidence that all significant sources of numerical error have been eliminated. Any discrepancies between the measured pressures and modelled pressures that are noted must then be due to the mismatch of the properties and they can therefore be adjusted accordingly.

Chapter 5: Application to a Real Life Problem

This chapter applies the numerical model derived in Chapter 3 to modelling the pressure response of a real partially completed oil well to changes in oil rate. Techniques were derived in Chapter 4 that succeed in matching analytical solutions with the numerical model to a high level of accuracy. These are applied to the real life problem to ensure that the results obtained are not an artefact of the modelling process. Actual pressure results measured from the well are then used to constrain the simulation model. The properties of the model are altered in order to obtain a match to the recorded pressures. Implications of the matching properties are then discussed.

5.1 Background

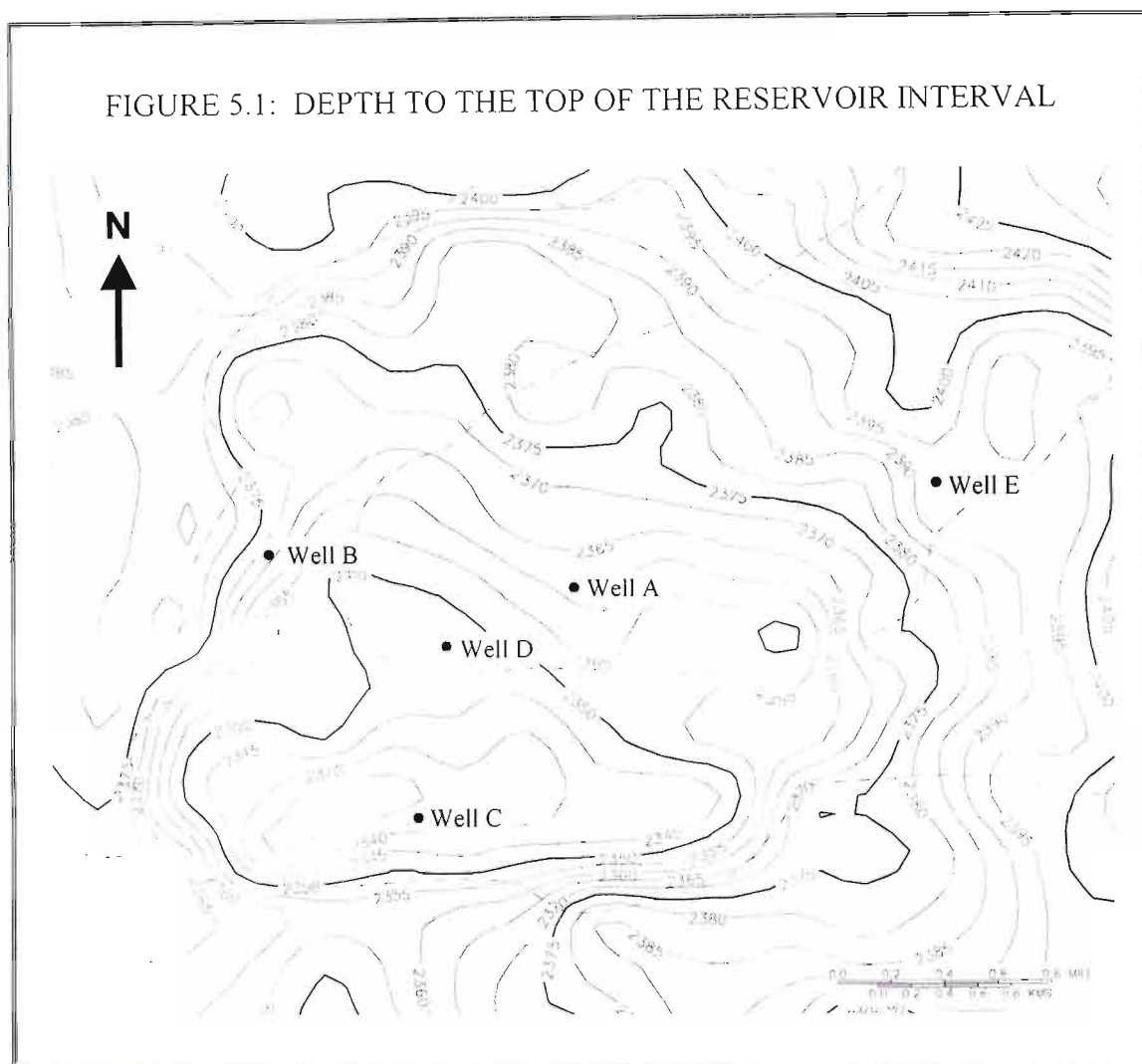
The well to be modelled is the discovery well for one of SOEKOR's most promising oil fields. For reasons of confidentiality the name of the field and well may not be revealed. A total of five wells have been drilled in the area. These wells have been labeled A to E in chronological order. Two of the wells (A and D) intersected an oil bearing reservoir; wells B and C were drilled beyond the edge of the reservoir; and well D was drilled into a water bearing interval to allow the injection of water during production.

In this particular field, as in all the oil and gas finds offshore South Africa, the reservoir lithology is sandstone. Overlying claystone and siltstone layers form impermeable barriers to the oil, trapping its upward movement. Oil therefore accumulates in the upper portion of the sandstone structure. Detailed descriptions of the field geology and geophysics have been given by Winters and Pfderkamfer⁴⁶. A layman's description covering the chief points of interest is given below.

5.2 Geology and Geophysics

The field has been mapped by interpreting a seismic data set comprising a series of seismic lines. Data from each line are processed to give a vertical slice of subsurface reflections along the length of the line. The vertical axis of the plot is based on the two-way travel time for the seismic pulses to travel from surface to a reflector and then back again. Such a plot is known as a seismic section. The reservoir interval is characterised by a change in seismic impedance in moving from the overlying shales into the reservoir sandstone, followed by a reversal at the base of the reservoir. This is visible on the seismic section as a peak that is related to the top of the reservoir interval followed by a trough related to the base of the reservoir, which occurs at a slightly later two-way travel time. Mapping out the peak and converting the travel

time to a depth gives a depth map of the top of the reservoir. This, and the various well locations, is depicted in Figure 5.1.



Geologically the reservoir is believed to be part of a turbidite system triggered by changes in sea-level during the Cretaceous era approximately 100 million years ago. Typically the turbidite system is initiated by a relative decrease in sea level that exposes much of the continental shelf. The sediment on the shelf is then subject to erosion. Accumulation of the eroded material at the shelf-edge can be unstable. A turbidity current forms when portions of this material break free and rush down the continental slope as a slurry of sediment and water, moving together. At the base of the continental slope the velocity of the current diminishes and thus its ability to carry solids decreases. Since the coarsest grained particles require the highest velocities to remain in suspension they are deposited first. Finer grained particles are deposited as the velocity of the current decreases. Sediment associated with a single turbidity

current is known as a turbidite. The sandstone reservoir is a stacked succession of many individual turbidites.

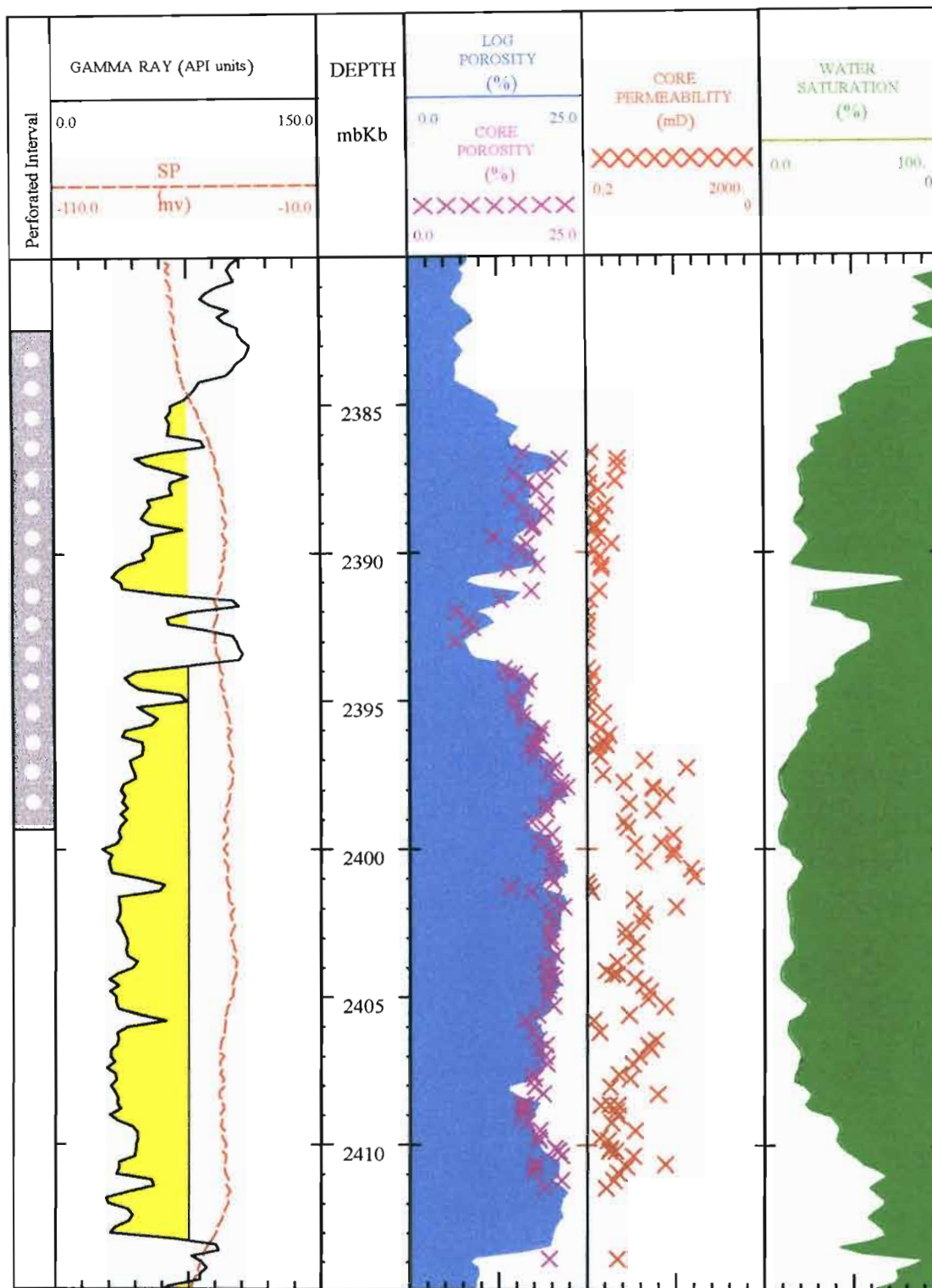
As the strength of each current diminishes it is possible for finer grained material to be deposited leaving an impermeable layer above the sandy sediment. The next turbidity current may erode all or part of this layer or may leave it intact forming a barrier to vertical flow. Frequently, remnants of the finer grained material may be found incorporated into the next sandy layer in the form of rip-up clasts even though no intervening layer remains. Vertical permeability within the overall package is therefore largely a function of the extent to which the impermeable (claystone or siltstone) layers have been preserved. Within each of the sandstone layers the vertical permeability is expected to be similar to the horizontal permeability. This has been confirmed by core experiments on wells A and D which compare measurements made using vertically cut plugs with those taken from horizontally cut plugs. Typically the ratio of vertical permeability to horizontal permeability was about 0.8.

Outcrop studies conducted on turbidites near Laingsburg and Tankqwa⁴⁷ in South Africa have shown that the lateral extent of claystone and siltstone layers within similar sandstone packages can vary enormously. In some cases the clay and siltstone layers are almost entirely absent or only extend for a few metres. The ratio of vertical to horizontal permeability for these cases would be close to unity. In other cases the claystone layers can be followed for several hundred metres and the ratio of vertical to horizontal permeability could be of the order of 0.01 or less.

Close examination of the core for well A has provided evidence that the energy of deposition was high for the lower portion of the reservoir interval. Although claystone layers are preserved in the core it is likely that these are not laterally extensive. Closer to the top of the interval the energy of deposition appears to be less and the claystone layers are believed to be more continuous. This upward fining sequence is typical of channelized turbidites. The overall geological model for the field is that of an amalgamated channel complex within a broad erosional valley. Towards the edges of the valley the sediment is mud rich, as in wells B and C for example, whereas the sediment in the centre of the valley is predominately sandstone as detected by wells A, D, and E.

The reservoir properties and lithologies for well A, the well to be modelled, are depicted in Figure 5.2.

FIGURE 5.2: PROPERTIES OF THE RESERVOIR INTERVAL, WELL A



Data used to create Figure 5.2 were gathered from a variety of sources. A portion of the reservoir was cored and the rock sample brought to the surface for examination by geologists. Rock plugs were subsequently cut from the core and subjected to laboratory measurements that included porosity, permeability, and electrical properties.

Special geophysical logging tools were run into the borehole to measure the natural gamma ray radiation, density, and resistivity of the rock in-situ. The gamma ray readings give an indication of the clay content. On the whole the intervals with a high gamma ray reading consist of claystones or silts whereas the intervals with low gamma ray values are sandstones. Density readings are used to derive a continuous porosity curve that is calibrated against core porosities. Resistivity readings, when used in conjunction with porosity, allow the hydrocarbon saturation to be determined.

Close examination of Figure 5.2 will reveal a prominent interval of high gamma ray readings between the depths of 2391 and 2394 mbKB corresponding to interbedded claystone and siltstone layers. Similar intervals have been noted in wells D and E. It is therefore believed that this feature could be present over a large portion of the reservoir and would represent a regional hiatus in sand deposition. As such, the feature could provide a widespread seal between the upper and lower portions of the reservoir. The three wells in question do, however, fall on a line that is almost parallel to the direction that the channels are believed to follow. A higher degree of continuity can be expected in a direction parallel to the channel axis than at right angles to it. It is therefore possible that the layer is discontinuous in a direction orthogonal to channel axis.

5.3 Reservoir Engineering

Numerous full field flow simulations of the reservoir have been conducted¹⁴. These have evaluated the sensitivity of production to the various geological uncertainties including the presence or absence of the previously mentioned claystone/shale layer. Whether the layer is continuous or not has a major impact on the forecasted oil recovery for the field. If the layer was very discontinuous and overall vertical permeability was high then recoveries of up to 52% of the oil in place could be expected. On the other hand if the shale extended over the entire field and vertical permeabilities were low throughout then the recovery could be as low as 38% of the oil in place. The difference in total value of the oil produced under the two scenarios is approximately \$132 million for an oil price of \$20/bbl and estimated oil in place of

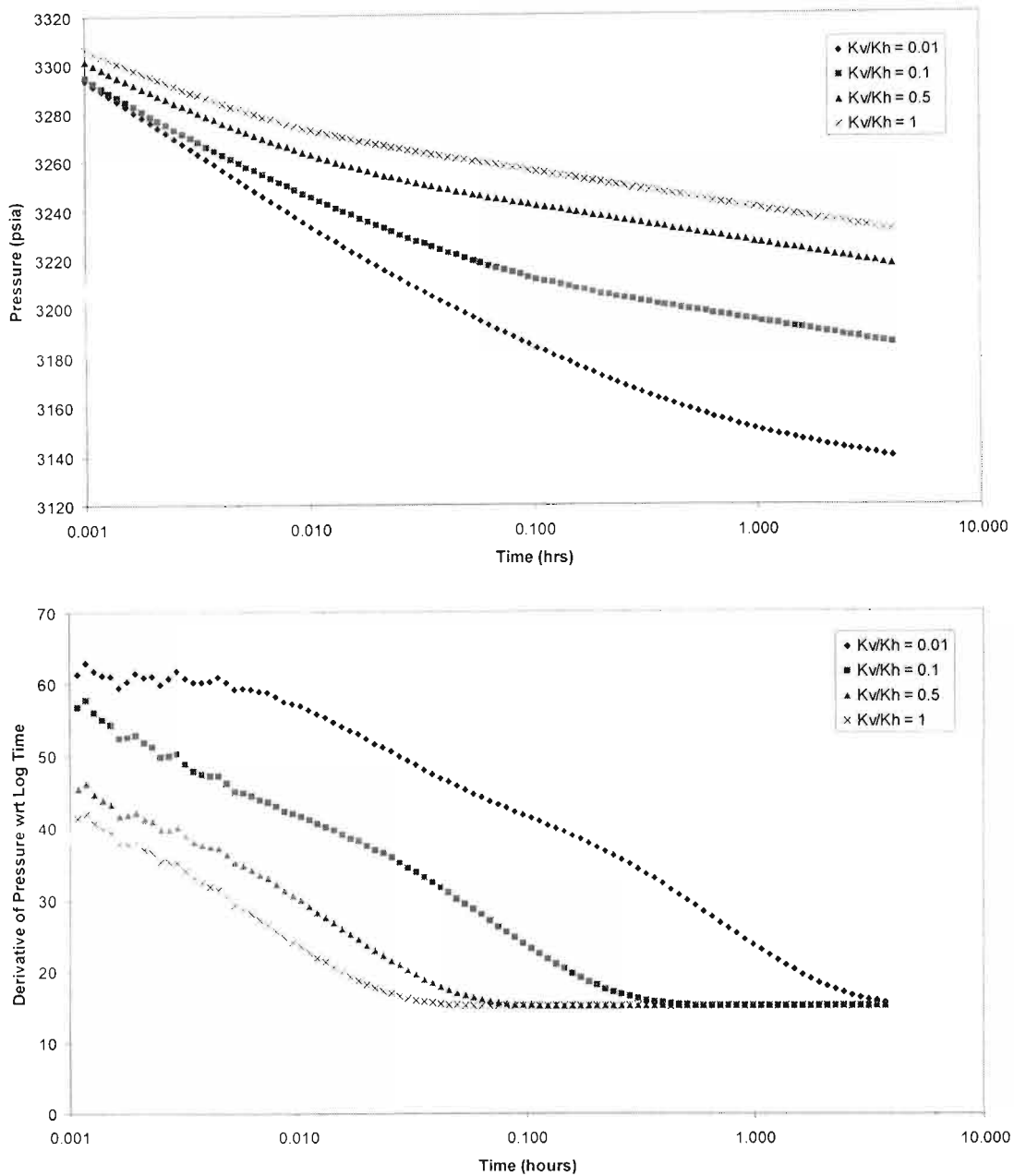
47 million stb. The impact on the economic value of the field could be even greater than this because the recovery is accelerated if vertical permeabilities are high. Clearly, prior knowledge of the likely magnitude of the vertical permeability is an important parameter in making a development decision for an oil field.

In principle, the pressure behaviour of partially penetrating wells can be used to place constraints on the vertical permeability. Analytical methods can be used to show how the vertical permeability affects the character of the build-up pressure curve for a hypothetical well. One such method is the solution of the Hantush equation that was discussed in Section 4.2. This was used to prepare a series of pressure responses for a hypothetical well with a penetration ratio of 25% and various ratios of vertical to horizontal permeability. The bottomhole pressure and associated derivative versus log of flowing time are displayed in Figure 5.3.

The derivative response can largely be broken into two periods, an initial decline of the derivative with time followed by a period where the derivative has constant value. In a physical sense this can be interpreted in terms of the propagation of the pressure disturbance caused by the change of rate at the well bore. Initially the pressure disturbance propagates both laterally and vertically. This is reflected by the decreasing derivative curve. Once the disturbance has propagated to the top and base boundaries and the pressure gradients near the well have stabilized then the further propagation of the pressure pulse is laterally away from well. This is essentially cylindrically radial flow over the entire reservoir interval. As a consequence the derivative stabilizes to a constant value whose magnitude is inversely related to the total permeability thickness product for the entire reservoir interval.

From Figure 5.3 it can be seen that the magnitude of the vertical permeability affects the length of time taken for the late time linear (in Log time space) pressure decline (or constant derivative) to be reached. In the case of a vertical to horizontal permeability ratio of 1/100 the entire interval is only beginning to contribute to flow some four hours after the start of production whereas in the case of equal horizontal and vertical permeability the pressures are linear after as little as 0.06 hours of flow. The magnitude of the early time derivative is a function of both horizontal and vertical permeability. If the horizontal permeability is kept constant then as the vertical permeability increases the early time derivative decreases. Thus, in principle, it is possible to estimate the magnitude of vertical permeability by measuring the time taken to reach the late time linear portion of the pressure plot or by matching the initial decline in the pressure derivative.

FIGURE 5.3: SENSITIVITY OF PRESSURE RESPONSE OF A PARTIALLY PENETRATING WELL TO VERTICAL PERMEABILITY



Although the rate of change of pressure at the end of the flow period is identical from case to case, the final flowing pressures are displaced from each other with the lowest flowing pressure corresponding to the lowest vertical permeability. If the pressure response for a well that fully penetrates the reservoir interval were to be compared with the other curves then we would find that this would have the highest flowing

pressures. These pressure differences are a manifestation of what the literature has often called flow convergence skin⁷ (the concept of skin was discussed in Section 1.3). An additional pressure loss is incurred in comparison to a fully penetrating well because the total fluid volume is forced to flow through a smaller interval and to travel a greater hydraulic distance. Vertical permeability plays a role in that a vertical component is introduced into the fluid movement. The lower the vertical permeability the greater the loss of pressure in converging on the perforated interval.

Reservoir engineers are typically interested in using analysis of pressure response to make long-term forecasts of well performance. In the case of a partially penetrating well the long term behaviour is indistinguishable from true radial flow with high skin damage. Analysis of these wells therefore often focuses on determining permeability thickness product and apparent skin for the total interval from the late time portion of the pressure response.

It would seem that a measurement of apparent skin would be sufficient to determine vertical permeability. This is not the case as the apparent skin is a composite value comprising the flow convergence skin in addition to a mechanical skin owing to near well formation damage (or stimulation) that is largely unknown. For many years there has been a debate on how these two factors combine. Some authors maintain that the two skins are purely additive while others suggest that the contribution of the mechanical skin is amplified by dividing by the penetration ratio (the ratio of flowing interval to total reservoir interval), that is:

$$S = \frac{S_m}{b_p} + S_p, \quad (210)$$

where S_m is the mechanical skin, b_p is the penetration ratio, and S_p is the flow convergence skin. If we define mechanical skin in terms of the degree of permeability impairment (i.e. the mechanical skin used is that which we would see on a fully penetrating well with the same degree of permeability impairment) then Equation 210 is the correct formula to use. This is relatively easy to prove for conditions of steady state flow.

The perforated interval, 2382.4 to 2399.4 mbKB, is displayed in Figure 5.2 where it can be seen that there is a dramatic increase in permeability immediately below the base of the perforations. This will act to increase the partial completion effects on the pressure behaviour.

Al Khalifa and Odeh²³ have suggested that the penetration ratio should be regarded as the ratio of kh/μ for perforated interval to the composite kh/μ for the entire interval (which may include a gas cap or aquifer), i.e.:

$$b_p = \frac{k_p h_w / \mu_p}{\sum_i k_i h_i / \mu_i}, \quad (211)$$

where the subscript p refers to properties measured over the perforated interval and the subscript i refers to sub-intervals throughout the total interval of permeable formation that is in direct pressure communication with the well. Note that use of Equation 211 will reduce the calculated penetration ratio for cases where the permeability of the perforated interval is much smaller than the rest of the interval.

The relationship between the flow convergence skin and the penetration ratio can either be determined using a late time approximation to the Hantush solution (Section 4.2) or through use of a relationship given by Saidikowski¹²:

$$S_p = \frac{1-b_p}{b_p} \left[\ln \left(\frac{h}{r_w} \right) \sqrt{\frac{k_h}{k_v}} - 2.0 \right]. \quad (212)$$

Note that a small penetration ratio implies a large flow convergence skin.

5.4 Review of Well Test Using Analytical Techniques

It is useful to apply classical analysis techniques to the pressure response of the well prior to applying reservoir simulation for matching purposes.

Properties to be used in the analysis are given in Table 5.1. Fluid properties are derived from laboratory tests conducted on oil sampled from an adjacent well. Porosity and water saturations are averages based on the log-derived porosity as shown in Figure 5.2. Rock compressibility is an average value based on tests conducted on core plugs that were obtained from the same formation in a nearby well.

The pressure record for drill stem test (DST) that was conducted on the well is shown in Figure 5.4. The test comprised several flow periods at different rates (Table 5.2) followed by periods of no flow (build-ups) where the well was closed off using a downhole valve. Detailed analysis is normally restricted to the build-up periods because the flow periods are often subject to changes in the rate that mask the pressure response.

Table 5.1: Fluid and Rock Properties for Well A

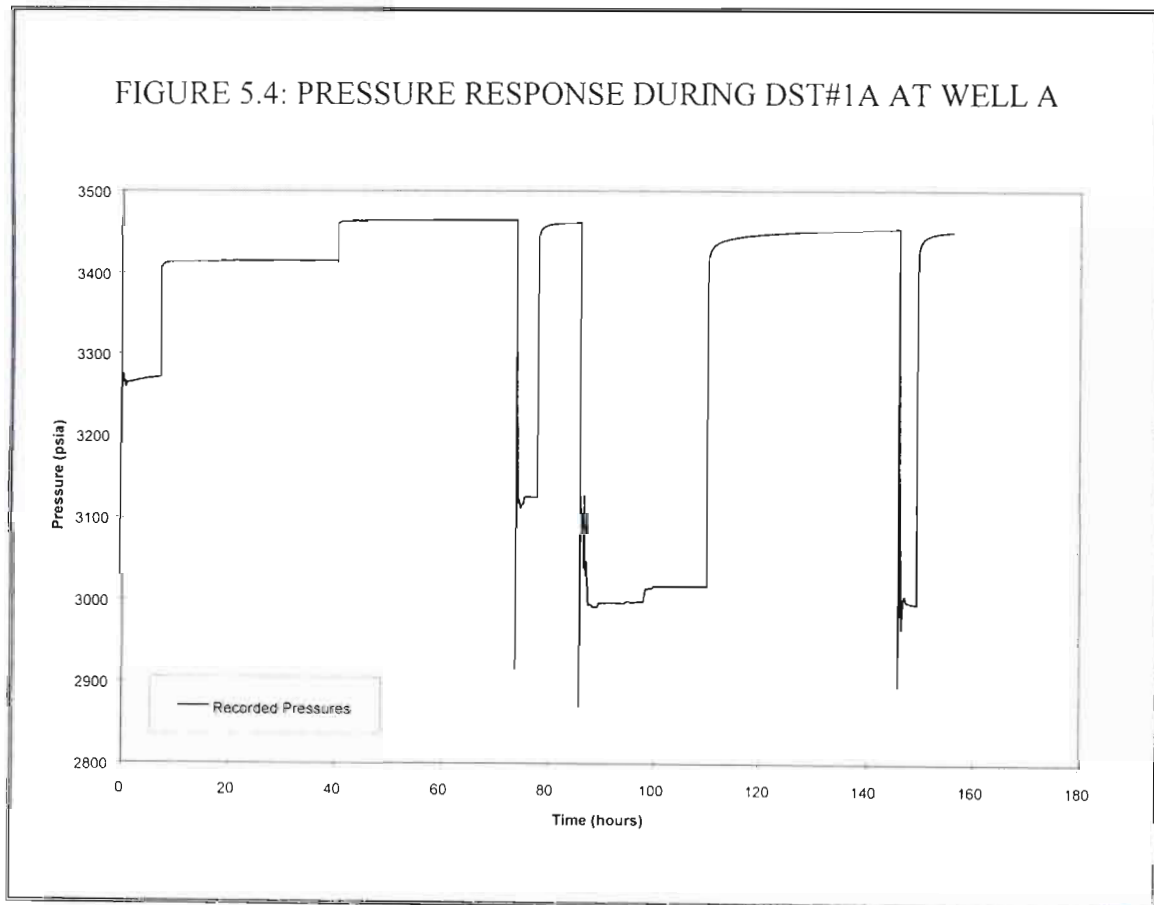
Rock Properties		
Porosity	ϕ	0.175
Rock Compressibility	c_r	3.1×10^{-6} psi
Fluid Properties		
Oil Viscosity	μ_o	0.43 cP
Oil Formation Volume Factor	B_o	1.436 rb/stb
Oil Compressibility	c_o	16×10^{-6} psi
Water Compressibility	c_w	3.0×10^{-6} psi
Water Saturation	s_w	0.2
Initial Fluid Pressure	p_i	3465 psia
Reservoir Geometry		
Reservoir Thickness	h	94.8 feet
Perforated Interval	h_w	54.7 feet
Distance to the Top Perforation	h_1	0.0 feet
Distance to the Bottom Perforation	h_2	40.1 feet
Wellbore Radius	r_w	0.3615 feet

Table 5.2: Rates and Times for Flow Periods During DST#1A at Well A

Flow Rate (stb/d)	Duration (hours)	Comments
6000	0.2528	Perforation and initial flow
0	3.0083	Initial Build-up
2870	6.9861	Clean-up Flow
790	33.5778	Sampling Flow
0	33.7528	Sampling Build-up
5200	3.9944	Reservoir Evaluation Flow
0	8.0167	Reservoir Evaluation Build-up
7735	23.9778	Extended Flow
0	36.0333	Extended Build-up
8730	3.4639	Maximum flow
0	6.5417	Final Build-up

The method of Horner⁴ (see Section 1.3) can be used to establish the portions of the pressure response that correspond to transience (unbounded cylindrically radial flow). This method assumes that the pressure during the build-up is the superposition of the

solutions for the rate change at the beginning of the previous flow and at the beginning of the build-up. The influence of earlier changes in rate is assumed to be negligible. For a single rate change the pressure drop at the well is linear with respect to the logarithm of time since the rate change took place. By transforming the time variable when analysing a build-up, we can preserve linearity when transient flow is taking place.



As shown in Section 1.3, under conditions of transience the pressure drop during a build-up is given by

$$\Delta p = -\frac{q\mu B_o}{4\pi kh} \ln\left(\frac{t + \delta t}{\delta t}\right), \quad (213)$$

where t is the length of the flow period, and δt is the time since the build-up started. Thus the transformed time variable is $\tau = (t + \delta t)/\delta t$ and plotting Δp against $\log \tau$ (typically known as a Horner plot) will give a straight line for transient flow. The permeability thickness product of the interval corresponding to flow can be determined from the slope, m , of the line from the equation

$$m = \frac{q\mu_o B_o}{4\pi kh} \quad (214)$$

Calculating and plotting the derivative of pressure with respect to the logarithm of transformed time (i.e. $\partial p/\partial \ln \tau$) will allow the transient period to be identified and highlight subtle changes in the slope that are related to changes in properties as one moves away from the well bore.

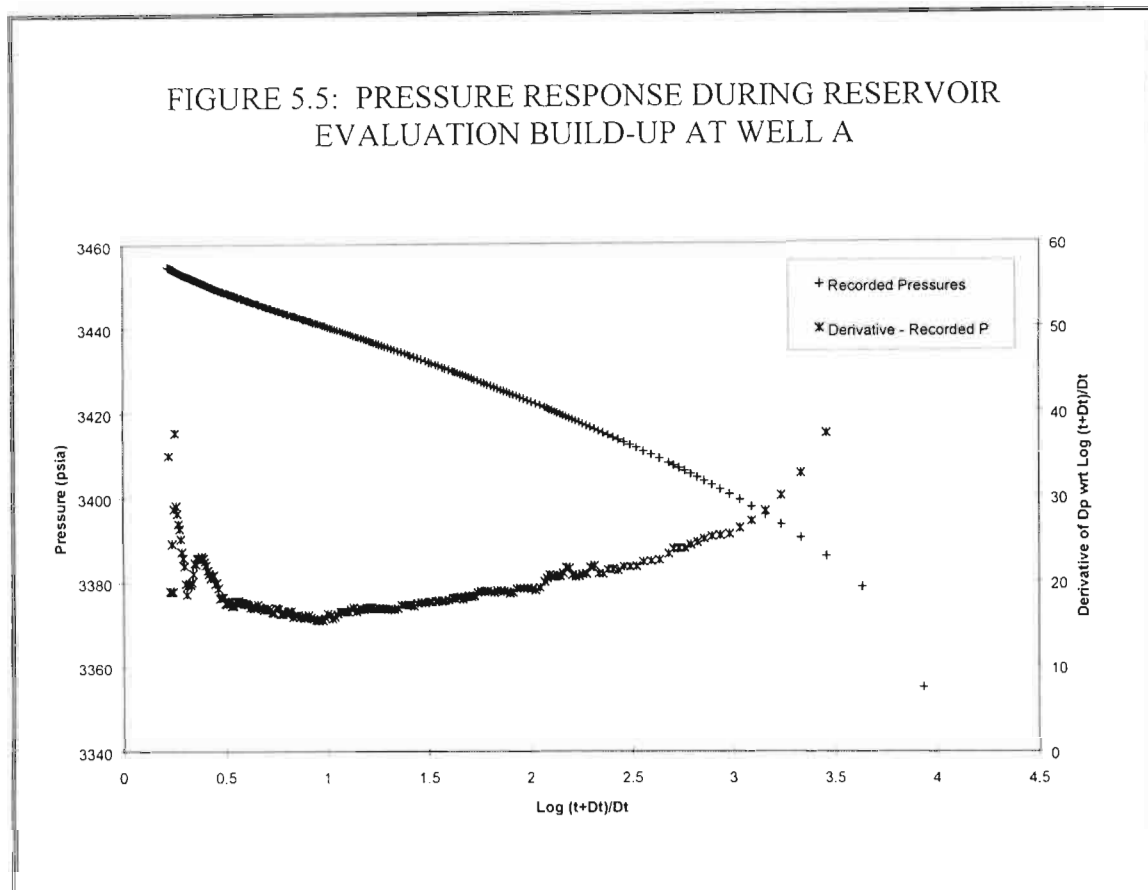
The skin can only be evaluated from flowing data. During the build-up the flow is negligible and the skin therefore drops out of the equation. In order to evaluate the skin the flowing pressure at the end of the previous flow period is used in conjunction with parameters determined from the build-up (Equation 214). The skin can be shown²⁵ to be given by

$$S = \frac{1}{2} \left[\frac{Z^* - p_{wf}}{m} - \ln \frac{4kt}{\xi \phi \mu_o c_i r_w^2} \right], \quad (215)$$

where Z^* is the extrapolated pressure (intercept) on the Horner plot and ξ is the exponent of Euler's constant (i.e. $\xi = \exp(0.5772...) \approx 1.781$). Both formulae (Equations 214 and 215) assume the use of an absolute unit system such as the SI.

A Horner plot and associated derivative for the longest build-up in the testing sequence is shown in Figure 5.5. Before calculating the parameters for each build-up it is useful to make a qualitative assessment of what the pressure history plot and Horner plot can tell us about the properties of the reservoir. What is noteworthy about the pressure is the very stable and at times increasing pressure during the flow periods (Figure 5.4). An increase in flowing pressure can only take place through a reduction of rate (which the surface records show has not taken place) or a reduction in skin. The nature of skin in a partially penetrating well is such that any changes in the skin over the perforated interval are amplified by the penetration ratio (Equation 210). Thus relatively small reductions in the mechanical skin throughout the test could explain the very stable flowing pressure. This reduction could take place through ongoing removal of fine debris from the perforation interval by the flowing fluid. In this particular well the drilling mud was inadvertently allowed to fall back on the perforated interval and it is quite likely that this would have had a partially plugging effect on the perforations.

FIGURE 5.5: PRESSURE RESPONSE DURING RESERVOIR EVALUATION BUILD-UP AT WELL A



The Horner plot shows a rapid decrease in slope/derivative initially (at large transformed time τ) followed by a more gradual decline. Towards the end of the build-up (at small τ) the overall slope/derivative increases once again. The oscillations in the derivative towards the end of the build-up have a twelve-hour period and are likely to be tidal in nature and not related to any variation in reservoir properties. Note that there is no clearly defined portion of the build-up where the slope is constant indicating transient flow and as a consequence no clear indication of when the vertical growth of the pressure disturbance comes to an end.

Comparison of the magnitude of the derivative with what would be expected given the core permeabilities suggests that the total thickness must be contributing to the flow from very early on in the build-up implying a high vertical permeability. The bulk of the build-up shows a slope that is too small given the core permeability. This implies that the quantity kh/μ must increase away from the well bore. One possible reason for this is that the reservoir dips to the North North West (Figure 5.1). At the well location the water contact falls near the base of the sandstone interval. As one moves to the North North West the reservoir dips into the water and the proportion of the sandstone that is water-bearing increases. As the viscosity of the water is less than that of the oil (0.27 as opposed to 0.43) this implies that the total kh/μ must also

increase even if the permeabilities remain constant. Thus the slope on the Horner plot will decrease progressively as the thickness of the water bearing interval increases.

The late time upturn in the derivative is consistent with the presence of a distant no-flow boundary such as would be provided by the presence of a sealing geological fault or the edge of sandstone deposition. Exactly such a feature has been interpreted from the seismic at a distance of roughly 500 metres to the South of the well. This distance is largely consistent with the time at which the derivative starts to increase.

The effective permeability-thickness product, kh , and the apparent skin were determined for each of the pressure build-ups using Horner analysis^{4,25}. In each case the Horner slope was calculated using the pressures from between 0.1 and 0.2 hours after the start of the build-up. The results are given in Table 5.3. Note the steadily decreasing skin through the test. The overall skin values are higher than one would normally expect from this sort of well. The permeability thickness product varies from 35100 to 38500 mD.ft, which is somewhat higher than the core derived value of 29700 mD.ft.

Table 5.3: Results of Horner Analysis for DST#1A at Well A

Period	Permeability Thickness (mD.ft)	Skin
Sampling Build-up	38 500	20.2
Reservoir Evaluation Build-up	35 300	19.1
Extended Build-up	36 800	16.1
Final Build-up	35 100	13.9

The penetration ratio calculated using the ratio of perforation length to total thickness is 0.55. Using Equation 212 in conjunction with a vertical to horizontal permeability ratio of 0.5 gives a partial penetration pseudo skin (S_p) of 4.9. Any mechanical skin over the perforations would be further amplified by the inverse of the perforation ratio as per Equation 210. In order to achieve a total skin of 13.9 the mechanical skin would need to be 5.0. Similarly, to achieve a total skin of 20.2 the mechanical skin would need to be 8.8. These mechanical skins are still unusually high. Typically, if these skins were encountered in a fully penetrating well they would suggest that some remedial action would need to be taken to remove the near well damage and improve the productivity of the well. The factors to be considered are the potential cost of

intervening to remove the well damage as compared with the potential loss of revenue from the well producing at a lower rate than would otherwise be the case.

If the calculations are repeated using core permeabilities and taking the ratio of perforated to total permeability thickness as shown in Equation 211 then the penetration ratio drops to 0.34 and the pseudo skin becomes 11.6. The mechanical skin will then be amplified by a factor of 3.0. A mechanical skin of 2.9 at the beginning of the test dropping to 0.77 by the end of the test would be sufficient to match the observed total skin. This suggests that the residual damage at the end of the test is negligible and that there is little reason to intervene to remove it.

The simulation study will be used to confirm the small values of mechanical skin needed to match the test.

5.5 Simulation Modelling of the Well Test

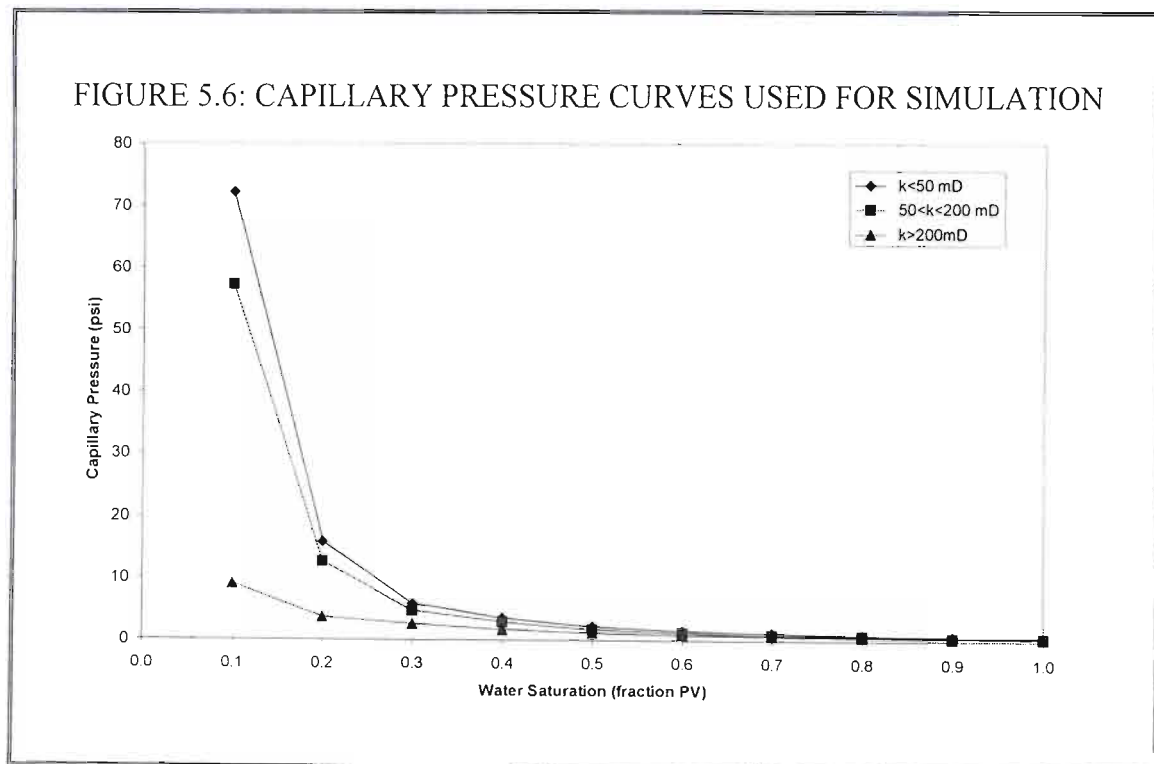
In addition to the properties already discussed in Sections 5.2 to 5.4, the simulation model requires saturation dependent properties such as capillary pressure and relative permeability. The time scale (well test duration) on which the simulation will be conducted is such that large changes in the grid block saturations are not expected. Thus the role of the saturation dependent properties is mainly to define the initial state of the system. Capillary pressure curves define the initial water saturation as a function of height. The hydrostatic pressure differences between the phases are calculated using the live fluid densities and the height above the fluid contact. The saturation is then adjusted so that the capillary pressure is equal to the hydrostatic pressure difference. Relative permeability values define the extent to which the effective permeability differs from absolute permeability given the initial fluid saturation.

Relative permeability and capillary curves are a function of the saturation history of the rock not just the present state. Drainage curves are those that result from an increase of the non-wetting phase, in this case oil, whereas imbibition curves result from the opposite process. Typically imbibition curves are used in modelling production from a water-wet reservoir on the basis that the reduction of pressure in the reservoir often leads to the influx of water from a neighbouring aquifer. Thus the water saturation can be expected to increase. For the current problem, however, drainage curves should be used as the water saturations in the reservoir are unlikely to change significantly as a result of water influx during the short flow test. The process that occurred as the oil migrated into the reservoir would have led to a steady reduction of water saturation; hence the choice of drainage curves.

Capillary pressure curves have been derived from numerous experiments performed on core plugs. The full procedure followed is beyond the scope of this thesis but is described in the SOEKOR development planning document for this field⁴⁸. In summary, a correlating function known as the Leveritt J function was used to define a characteristic curve for the formation that averages the capillary pressure results. This curve is then used to generate capillary pressure curves for several rock classes based on the core plug permeability and porosity. Finally a comparison is made between water saturations derived from the capillary pressure curves and those calculated from the geophysical logging tools. Parameters that control the shape of the curve are varied to obtain an optimum agreement between the two methods. For the purposes of this simulation capillary pressure curves have been defined for three rock classes:

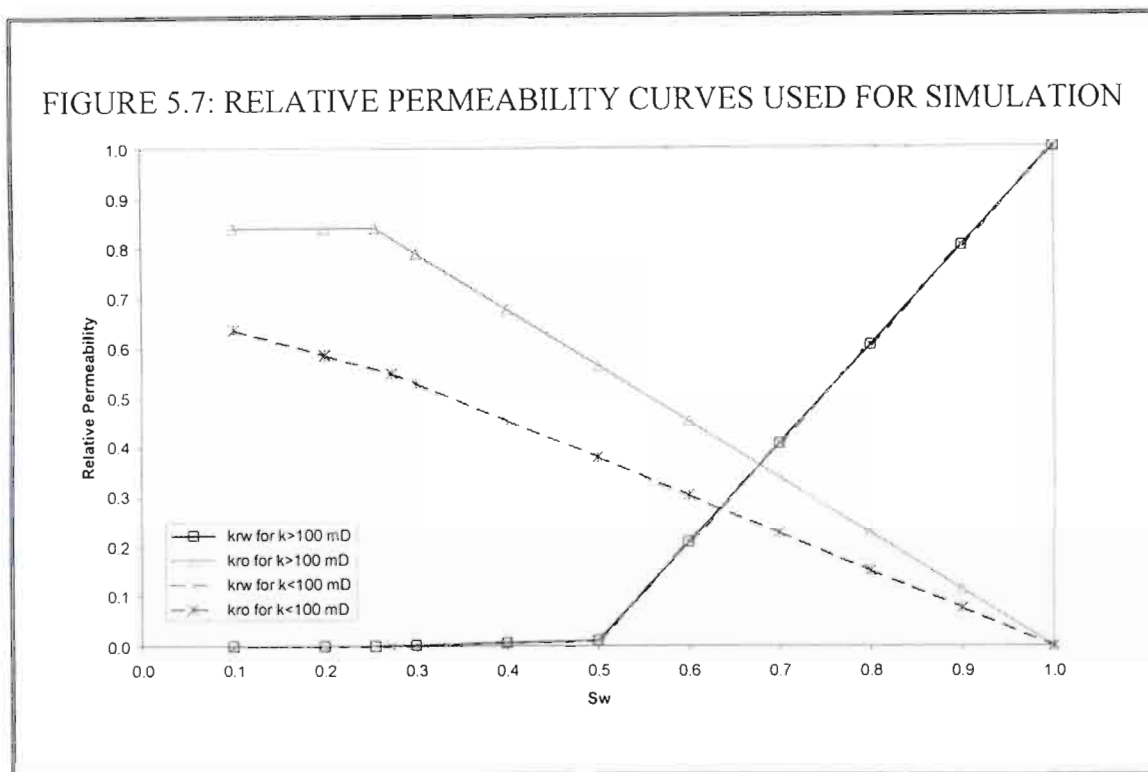
1. Permeability less than 50 mD
2. Permeability greater than 50 mD but less than 200 mD
3. Permeability greater than 200 mD

The capillary pressure curves are displayed in Figure 5.6



Laboratory measurements of relative permeability for this field were acquired under conditions of increasing water saturation and are therefore not appropriate for use in this study. The endpoint relative permeability to oil at irreducible water saturation will, however, be the same for both drainage and imbibition curves. Two rock classes were defined on the basis of the endpoints. When permeability is less than 100 mD

the endpoint is 0.636 otherwise the endpoint value is 0.840. At 100% water saturation the relative permeability must be unity by definition. As the bulk of the model will be at conditions of either close to irreducible water saturation or close to being fully water saturated, the model should not be particularly sensitive to the shape of the relative permeability curves between these points. Simplified curves using straight-line sections were defined for both rock classes (Figure 5.7).



Porosity and permeability for use in the model were derived from core and logging measurements. The reservoir was split into a series of zones that showed similar characteristics. Zone boundaries were placed at positions where the properties changed or at positions of potential barriers or baffles to flow such as significant claystone layers. The zone definition and properties are shown in Table 5.4.

A radial grid with 22, 8, and 44 cells in the radial, transverse, and vertical direction respectively, was defined taking into account the lessons learned from modelling the abstract problem. In the radial direction the cell widths increase in a geometric progression starting from a width of 0.1 feet. In the vertical direction the layers are defined to honour the zone boundaries with additional layers within some zones to give the required level of detail at critical positions (such as at the base of the perforated interval for example, where the layer thickness reduces to 0.1 feet).

Table 5.4: Zonation and Rock Properties for Well A

Zone	Zone Thickness (feet)	Net-to-gross (fraction)	Porosity (fraction)	Horizontal Permeability (mD)	Number of Layers	Description
1.1	8.39	0.83	0.134	60	2	Interbedded sandstone and shale layers
1.2	8.39	0.93	0.179	160	2	Massive sandstone interval
1.3	8.39	0.63	0.155	160	2	Occasional claystone layers within sandstone
2.1	7.57	0.20	0.120	30	2	Major interbedded silt/claystone interval
3.1	10.11	0.89	0.162	90	3	Occasional claystone layers within sandstone
3.2	13.80	0.97	0.200	770	22 ¹	High energy sandstone (erosive contacts) with minor claystone layers, rip-up clasts
3.3	14.81	0.99	0.194	500	5 ²	As above
3.4	11.61	0.98	0.181	480	3	As above
3.5	11.70	0.95	0.194	290	3	Occasional claystone layers within sandstone

1. Zone subdivided in layers with layer thickness in feet as follows:

2.27, 1.73, 1.29, 0.97, 0.73, 0.54, 0.41, 0.31, 0.23, 0.17, 0.13, 0.10, 0.10, 0.13, 0.17, 0.23, 0.31, 0.41, 0.54, 0.73, 0.97, 1.33

2. Zone subdivided in layers with layer thickness in feet as follows:

1.78, 2.37, 3.16, 3.75, 3.75

Breaking the grid into 8 segments allowed the elevation of the top of the reservoir to be modelled so that the tilt of the reservoir into the aquifer could be accommodated and so that a crude approximation of the field boundaries could be defined.

A rate schedule was defined based on the full test sequence as shown in Table 5.2. The solver options were adjusted to give a highly accurate pressure solution with a small initial time step after any rate change (0.001 days for flow period and 0.0001 days for a build-up). The well model used by the simulator is the strongly coupled well model described in Section 3.10 with a constant pressure boundary condition along the well bore.

Simulated well pressures were compared with measured pressures on a linear pressure versus time plot and on a Horner plot for the extended build-up. It was observed from the initial run that allowing the formation to dip into the water reproduced the decreasing derivative during the latter portion of the build-up. The overall permeability in the model would, however, need to be significantly increased to match the overall magnitude of the derivative. There is therefore evidence that permeability increases away from the well bore in addition to the increasing mobility as one dips into the water. The high vertical permeabilities used in the initial model gave a good early time match to the derivative. Flowing pressures were mismatched implying a need to adjust the mechanical skin but did confirm that only a small mechanical skin would be needed to match the test and that this skin needed to change through the test.

Additional runs were conducted with adjusted properties until an acceptable match was obtained. The pressure match from the final model is shown in Figures 5.8 and 5.9 and the simulator command file is reproduced in Appendix 3. In order to achieve a match, the horizontal permeability was increased by a factor of 1.6 from a distance of 6 feet away from the well. This is justified on the basis that the core permeabilities represent the permeability at the well itself. As permeability is a highly variable property it is possible that the larger scale average is higher than that measured at a single location. Vertical permeabilities equal to half of the horizontal permeabilities are used in the matching model. Reducing the vertical permeability beyond this point degrades the quality of the early time match to the derivative. The model is particularly sensitive to the magnitude of vertical permeability below the perforations. The mechanical skin was reduced in stages through the run. During the initial flow periods a mechanical skin of 2.2 was used, reducing to 1.0 for the extended and maximum rate flows. This confirms that the degree of near well damage is not significant and has already been largely eliminated by progressive cleaning of the perforations as the well flows.

Some residual mismatches are evident from Figures 5.8 and 5.9. The flowing pressures only match at the end of the flow period. This is a consequence of the fact that the skin is continuously decreasing through the flow period and simulator file has discrete changes in skin. The match at the end of the flow period shows that the skin at this point in time is correct.

FIGURE 5.8: PRESSURE MATCH ON LINEAR TIME PLOT

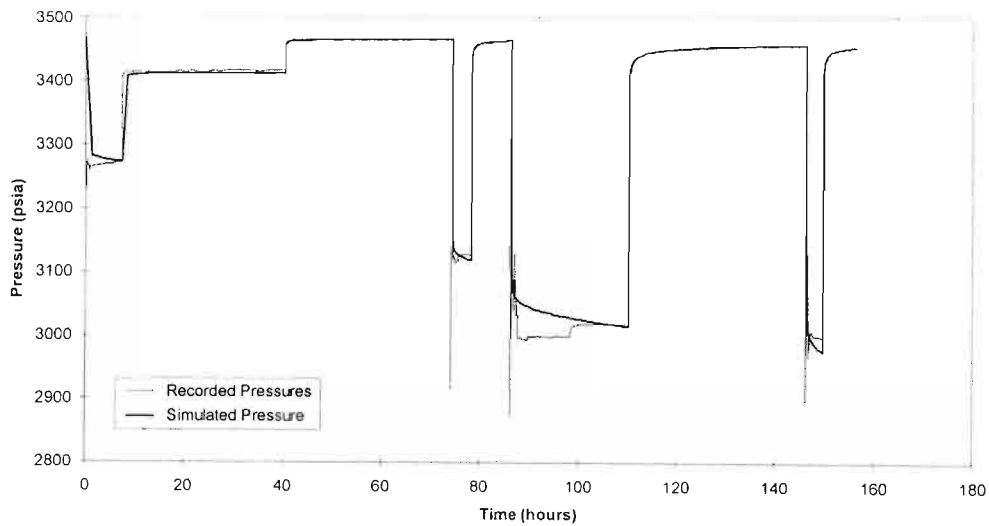
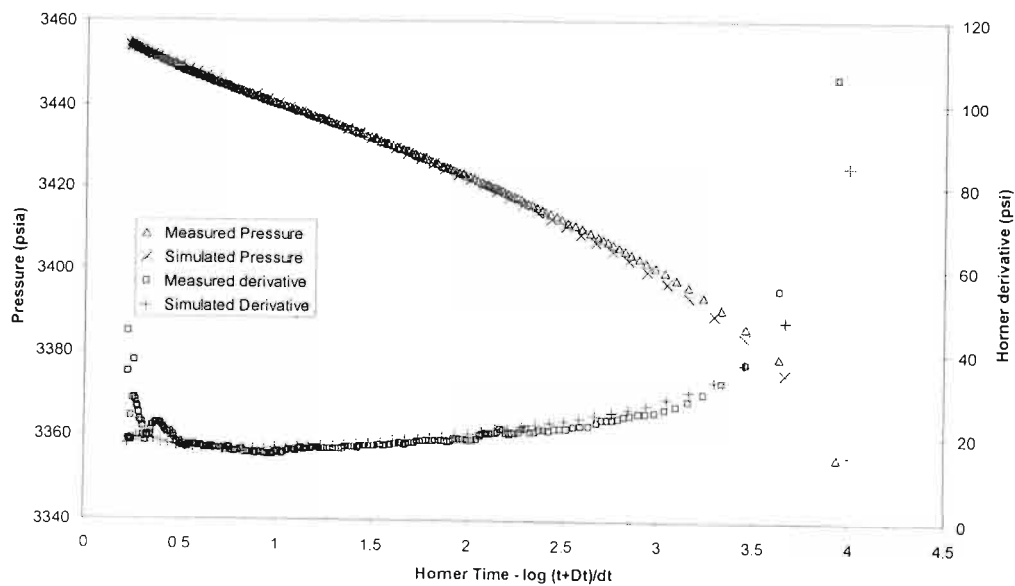


FIGURE 5.9: PRESSURE MATCH ON HORNER PLOT



Horner derivatives from measured pressures are higher than simulated derivatives for the first two points. This could be a consequence of what is known as well bore storage or afterflow where the finite compressibility of the fluid in the well bore implies that once the flow has been shut off by closing a valve the well continues to flow for while in order to compress the fluid volume trapped between the valve and the formation. In this well the valve is located down hole, close to the perforations, to minimise the volume that needs to be compressed and hence the degree to which afterflow takes place. Any afterflow should be eliminated in the first few seconds of the build-up. Nevertheless, the first few points may still be affected by this phenomenon.

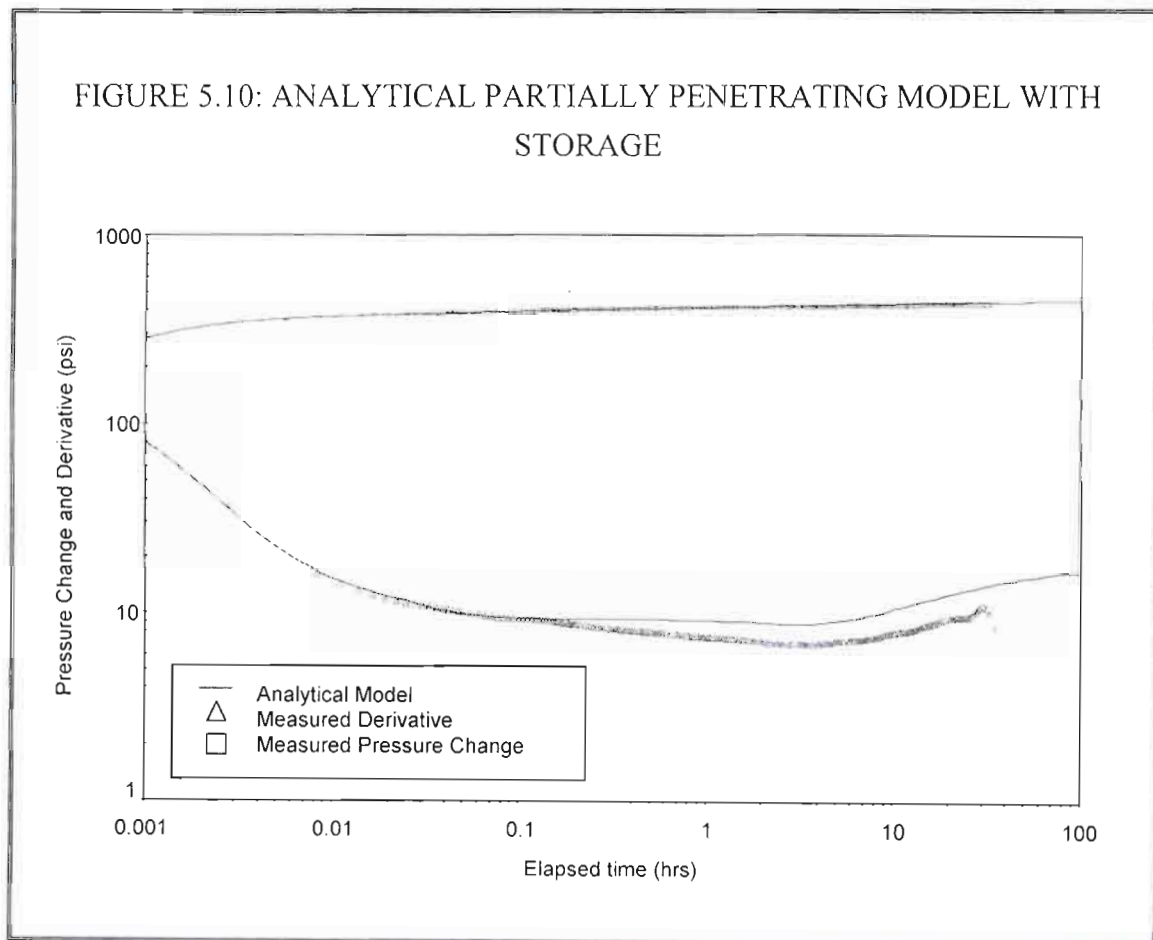
The late time simulated derivative fails to match the increase observed on the measured data. This is an indication that mapped distance to this boundary is probably too great. Attempts were made to match this by moving the boundary closer but these were of limited success partly because of the difficulty in defining a linear boundary using a radial grid.

The residual mismatch in the derivative was investigated using a commercial well test analysis package (Interpret 2001) with an analytical partially penetrating model. The model was set up to have an adjusted penetration ratio of 0.34 thus crudely taking into account the difference in permeability between the perforated and unperforated intervals. A vertical to horizontal permeability ratio of 0.5 was used. Results are shown in Figure 5.10 using what is known as a log-log plot. In this format two quantities, the pressure change since the end of the previous flow period and an associated pressure derivative, are plotted against the logarithm of time since the start of the build-up. The derivative is the derivative of pressure with respect to the logarithm of superposition time. This is very similar to the Horner derivative used earlier in this chapter, the only difference being that superposition of the full rate history of the test is used in forming the time variable instead of just using the last two changes in rate.

A good match to the very early time derivative was obtained by adjusting the degree of storage ultimately giving a compressibility volume product of 0.0006 bbls/psi. Using the live oil compressibility of 16×10^{-6} /psi implies a storage volume of 37.5 bbl, which seems too large given the position of the testing valve. This early-time difference between the measured data and simulation model may therefore be related to other effects such as the time it takes the valve to completely seal or even to transient gauge errors. More importantly, having a storage volume of considerably

less than 37.5 bbl implies that storage effects should have been completely eliminated even at very early times in the build-up and that the analysis for vertical permeability will not be affected this phenomenon.

The shape and timing of the late time increase in derivative could be matched by moving the no-flow boundary associated with the fault to a distance of 1000 ft (~300m), somewhat closer than mapped. Note the mismatch on the magnitude of the derivative at late time, a manifestation of the fact that the analytical solution does not take the topography and consequent lateral changes in mobility into account.



5.5 Chapter Summary

In this chapter the real life problem of matching pressures recorded on a test of a partially penetrating well was discussed. A successful match was obtained by using a simulation model that accounted for vertical variation in rock properties, vertical and lateral changes in fluid saturation, lateral boundaries to flow, near well geometry, and reservoir topography. The accurate modelling of many of these effects is beyond the capability of purely analytical methods. In the case of this well test significant errors

would have been introduced by ignoring these factors. For example the dipping of the reservoir into the aquifer introduced an uncertainty into the calculation of permeability and could have led to unrealistic expectations for very high permeabilities away from the well location. However, using analytical techniques in conjunction with numerical simulation modelling proved to be a powerful way of evaluating the possible impact of proposed changes and then testing them.

Specifically the modelling work conducted here indicates that:

- Average permeability at the well location is 60% higher than suggested by the core values
- Vertical permeability is relatively high (greater than 50% of the horizontal value)
- The distance to the edge of the field is approximately 300 metres (considerably closer than mapped)
- A low mechanical skin can successfully match the flowing pressures implying that there is little need for remedial action to remove near well damage
- Use of the permeability thickness products to calculate the penetration ratio is an appropriate technique that leads to more realistic estimates of mechanical skin for partially penetrating wells.

Using a simulation grid definition with small grid blocks (dimensions of as little as 0.1 feet) close to the well bore and at the base of the perforated interval has resolved much of the early time mismatch that originally motivated this work. The results of matching the analytical model were helpful in defining the level of detail that would be required in terms of both spatial and temporal discretisation.

Implications of the high vertical permeability are that the vertical sweep efficiency can be expected to be high and therefore the expected recovery should be towards the upper end of the forecasted range of values. Since this work was conducted, the field in question has been brought on production and the volumes of recovered oil have been larger than expected. The work matching the well test provided early evidence suggesting that the recovery would be high and helped to justify the upside forecasts. This in turn increased the expectation value for net-present-value (NPV) for the field providing an additional incentive to take the decision to develop the field, a decision that has proved to be highly successful. Results from this work should be useful in terms of understanding the high recoveries in this field and using this insight to optimise future production.

Chapter 6: Conclusions

This study has achieved its main aims of:

1. Assessing and minimizing the errors inherent in simulating the pressure response of partial penetrating wells;
2. Gaining an understanding of the reservoir characteristics of the specific well being studied and the consequent implications for future production.

The required level of accuracy in modelling pressure behaviour in partially penetrating wells using finite-difference simulation can be achieved through minimizing the discretisation error by:

1. Selectively refining grid block sizes in areas with high pressure gradients;
2. Using sufficiently small time steps after any major change in rate.

In the case of a partially penetrating well this implies using grid blocks with small radial width (~ 0.1 feet) close to the well bore and thin layers (~ 0.1 feet) at the base of the perforations. In order to reduce the overall size of the grid the dimensions of the blocks should be allowed to progressively increase when moving away from the problem areas. In many respects horizontal wells represent a similar geometry to partially penetrating wells and one could expect that accurate simulation of pressure in this case would require using a higher degree of refinement at tips of the well (toe and heel).

It is not necessary to use specialized software to achieve the required results for partially penetrating wells; a conventional finite-difference reservoir simulation package using an orthogonal radial grid is quite adequate. Such software is available to the majority of practising reservoir engineers implying that the approach demonstrated here is widely applicable. It would be useful to investigate whether more geometrically flexible, though less widely available, techniques such as perpendicular bisection (PEBI) grids may offer an advantage in terms of being able to achieve the required accuracy with fewer grid blocks. The shape of the grid blocks required could, however, become very complex for partially penetrating wells with permeability anisotropy.

Another area that is worth researching further is the use of multi-point flux approximations where diagonally adjacent grid blocks are used in addition to immediately adjacent blocks in calculating the flux across the face of a grid block. Attempts to derive such a scheme while preserving the use of a conventional simulator proved to be unsuccessful for a radial grid. The approach that has been used successfully to derive such a scheme for Cartesian grids cannot easily be extended to

radial grids given the difference in the structure of the underlying differential equations.

In comparing analytical solutions to the results of finite-difference simulation some discrepancies were noted. These could be traced to the use of a constant flux boundary condition at the well bore in some analytical solutions as opposed to the more appropriate constant pressure boundary condition used by the simulation. Analytical solutions that used a constant pressure boundary condition proved to be in good agreement with the simulation results. The importance of this finding is two-fold:

1. It demonstrates convergence between the analytical and simulation models as the degree of spatial and temporal discretization is increased, which shows that this approach is sufficient to model the problem
2. It highlights the fact that engineers need to be careful when trying to match early-time data using the analytical methods available in many of the commercial well test analysis packages

In some cases the phenomenon of well bore storage would mask the early time data but in cases using downhole shut-in valves these data would be preserved. Although the differences are small, conclusions regarding the degree of permeability anisotropy based on matching the early time data with inappropriate analytical methods could be invalid. This would have consequences for the estimated recovery factor from an oil field and might influence the decision to develop a field or optimum choice of development scenario for a field. Many of the analytical techniques used for analysing horizontal well tests are also based on constant flux assumptions and can be expected to suffer from the same problems at early time.

Application of the simulation approach to a real well test of a partially penetrating well showed the power of the technique in being able to model lateral and vertical property changes (absolute permeability, saturation and hence effective fluid mobility, reservoir topography, no-flow boundaries). These variations in properties could not be modelled in combination using purely analytical methods and proved to be important in understanding the pressure response at the well in question. Ignoring factors that cannot be modelled analytically could easily result in erroneous interpretations. For example:

- Tilting of the reservoir into the aquifer resulted in a steadily decreasing derivative that could easily be mistaken for an increase in permeability at a distance from the well

- The contrast in permeability over the perforated and unperforated intervals magnified the apparent skin implying that only a small mechanical skin was necessary to match the test

While both these influences on the pressure behaviour were suspected prior to running the simulations, it was only through the simulation that these could be confirmed. Thus, the simulation provided a basis for testing hypotheses regarding the nature of the pressure behaviour.

In the case of the well being studied, it was possible to demonstrate that the vertical permeability must be high in order to match the early time pressure behaviour. This implies that the vertical sweep efficiency (ability to uniformly replace oil by water) of this reservoir is also likely to be high. Oil recovery can therefore be expected to be towards the upper side of the range of previously forecasted values with delayed water breakthrough at the wells. Both of these factors (i.e. higher total oil recovery and faster oil recovery) considerably enhance the value of the field in net-present-value (NPV) terms. Recent production data from the field have confirmed that recoveries are beyond expectation.

The use of numerical simulation to model well test behaviour is a powerful technique that should be applied more often. It is of particular relevance to the high cost offshore environment where development decisions can involve hundreds of millions, or in extreme cases billions, of dollars. These decisions often need to be taken on the basis of very limited data. Although numerical simulation of well test pressure behaviour is extremely time consuming in comparison to the use of purely analytical techniques it has the potential to extract additional information regarding reservoir properties from the limited data available. This in turn should lead to a better understanding of the risks involved in developing the field concerned and a more accurate expectation value for the field concerned.

References

1. Matthews, C.S., and Russell, D.G., "Pressure Buildup and Flow Tests in Wells", SPE of AIME Monograph Series (1967) **I**.
2. Muskat, M., "Use of Data on the Build-up of Bottomhole Pressures", Trans. AIME (1937) **123**, 44-48.
3. Miller, C.C., Dyes, A.B., and Hutchinson, C.A., "The Estimation of Permeability and Reservoir Pressure from Bottom Hole Pressure Build-up Characteristics", Trans. AIME (1950) **189**,91-104.
4. Horner, D.R., "Pressure Build-Up in Wells", Proc. Third World Pet. Cong., E.J.Brill, Leiden (1951) **II**, 503.
5. Muskat, M., "Physical Principles of Oil Production", McGraw-Hill Book Co., Inc., New York (1949).
6. Nisle, E.G., "The Effect of Partial Penetration on Pressure Build-up in Oil Wells", Trans. AIME (1958) **213**, 83-90.
7. Brons, F., and Marting, V.E., "The Effect of Restricted Fluid Entry on Well Productivity", J. Pet. Tech. (February. 1961), 172-174.
8. Hantush, M., "Advances in Hydroscience", Ven Te Chow (Ed.), Academic Press, New York and London (1964) **I**, 307.
9. Odeh, A.S., "Steady-State Flow Capacity of Wells with Limited Entry to Flow", Soc. Pet. Eng. J. (March 1968), 43-51.
10. Gringarten, A. C., and Ramey, H. J., "An Approximate Infinite Conductivity Solution for a Partially Penetrating Line Source Well", SPEJ, (April 1975), 140.
11. Bilhartz, H. L., and Ramey, H. J., "The Combined Effects of Storage, Skin, and Partial Penetration on Well Test Analysis", SPE paper 6753, presented at the SPE 52nd Annual Technical Conference and Exhibition, Denver, (October 1977)
12. Saidikowski, R. M., "Numerical Simulations of the Combined Effects of Wellbore Damage and Partial Penetration", SPE paper 8204, presented at the

- SPE 54th Annual Technical Conference and Exhibition, Las Vegas, (September 1979).
13. Barnum, R. S., and Frederick, K. A., "Vertical Permeability Determination from Pressure Buildup Tests in Partially Perforated Wells", SPE paper 20114, presented at the 1990 Permian Basin Oil and Gas Recovery Conference, Midland, (March 1990).
 14. Strauss, J. P., "Simulation Studies of the ___ Area*", SOEKOR internal report SOE-PEN-RPT-049 (April 1992).
 15. Darcy, H., "Les Fontaines Publiques de la Ville de Dijon", Victor Dalmont, Paris (1856).
 16. King Hubbert, M., "Darcy's Law and the Field Equations of the Flow of Underground Fluids", Trans. AIME (1956), **207**, 222-239.
 17. van Everdingen, A.F., "The Skin Effect and its Impediment to Fluid Flow into a Wellbore", Trans. AIME (1953), **198**, 171-176.
 18. Odeh, A. S., and Babu, B. K., "Transient Flow Behaviour of Horizontal Wells, Pressure Drawdown and Build-up Analysis", SPE paper 18802 (1989).
 19. Ozkan, E., and Raghavan, R., "New Solutions for Well-Test-Analysis Problems: Part 1- Analytical Considerations; Part 2 - Computational Considerations and Applications", SPEFE. (September 1991), 359-378.
 20. Ding, W., and Reynolds, A. C., "Computation of the Pseudoskin Factor for a Restricted-Entry Well", SPEFE, (March 1994), 9-14.
 21. Strelstova-Adams, T. D., "Pressure Drawdown in a Well with Limited Flow Entry", JPT, (November 1979), 1469-1476.
 22. Strelstova-Adams, T. D., "Pressure Transient Analysis for Afterflow-Dominated Wells Producing from a Reservoir with Gas Cap", JPT, (April 1981), 172-174.
 23. Al-Khalifa, A. J., and Odeh, A. S., "Well Test Analysis in Oil Reservoirs with Gas Caps and/or Water Aquifers", SPE paper 19842, presented at the SPE 64th Annual Technical Conference and Exhibition, San Antonio, (October 1989).

24. Earlougher, R. C., Jr., "Advances in Well Test Analysis", SPE of AIME Monograph Series (1977) 5.
25. Dake, L. P., "Fundamentals of Reservoir Engineering", Elsevier Scientific Publishing Company (1978).
26. Abdou, M. K., Pham, H. D., and Al-Aqueeli, A. S., "Use of Orthogonal and Nonorthogonal Grids for the Simulation of a Faulted Reservoir", SPE paper 21391, presented at the 1991 SPE Middle East Oil Show, Bahrain, (November 1991)
27. Heinemann, Z. E., and Deimbacher, F. X., "Advances in Reservoir Simulation Gridding", Proc. Fourth Intl. Forum on Reservoir Simulation (September 1992)
28. Amando, L. C. N., Ganzer, L., and Heinemann, Z. E., "Finite Volume Discretization of the Fluid Flow Equations on General Perpendicular Bisection Grids", Proc. Fifth Intl. Forum on Reservoir Simulation (December 1994)
29. Aziz, K., and Settari, A., "Petroleum Reservoir Simulation", Elsevier Applied Science Publishers (1979)
30. Aziz, K., "Fundamentals of Reservoir Simulation", Course notes prepared for Stanford University, California (1993)
31. Intera, "Eclipse 100 - Technical Appendices (Release 94A)", Intera Information Technologies Ltd, Oxfordshire (1993)
32. Vinsome, P.L.W., "Orthomin, an Iterative Method for Sparse Banded Sets of Simultaneous Equations", SPE paper 5729, presented at the SPE-AIME Fourth Symposium on Reservoir Simulation, Los Angeles, (1976)
33. Appleyard, J. R., and Cheshire, I. M., "Nested Factorization", SPE paper 12264, presented at the Seventh SPE Symposium on Reservoir Simulation, San Francisco, (1983)
34. Cheshire, I. M., "The Solution of Linear Equations in Implicit Simulators", Proc. Fourth Intl. Forum on Reservoir Simulation (September 1992)
35. Holmes, J. A., "Enhancements to the Strongly Coupled, Fully Implicit Well Model: Wellbore Crossflow Modeling and Collective Well Control", SPE

- paper 12259, presented at the Seventh SPE Symposium on Reservoir Simulation, San Francisco, (1983)
36. Muskat, M., "The Flow of Homogeneous Fluids through Porous Media", J. W. Edwards Inc., (1946)
 37. Kuchuk, F. J., Goode, P. A., Wilkinson, D. J., and Thambynayagam, R. K. M., "Pressure Transient Behaviour of Horizontal Wells With and Without Gas Cap or Aquifer", SPE paper 17413, presented at the SPE California Regional Meeting in Long Beach, California, (1988)
 38. Ozkan, E., Sarica, C., Hacıislamoglu, M., and Raghavan, R., "Supplement to SPE 24683. Effect of Conductivity on Horizontal-Well Pressure Behaviour", SPE paper 30230, (1995)
 39. Ozkan, E., Sarica, C., Hacıislamoglu, M., and Raghavan, R., "Effect of Conductivity on Horizontal-Well Pressure Behaviour", SPE paper 24683, SPE Adv. Tech. Series, Vol. 3, No. 1, (1995)
 40. Yiidiz, T., and Bassiouni, Z., "Transient Pressure Analysis in Partially Penetrating Wells", SPE Paper 21551 presented at Joint CIM/SPE International Technical Meeting, Calgary, (June 1990)
 41. Stehfest, H., "Algorithm 368 - Numerical Inversion of Laplace Transforms", Comm. ACM, Vol. 13, No. 1, (January 1970)
 42. Talbot, "The Accurate Numerical Inversion of Laplace Transforms", J. Inst. Math. Appl., Vol. 23, (1979)
 43. Yanosik, J. L., and McKraken, T. A., "A Nine-Point, Finite-Difference Reservoir Simulator for Realistic Prediction of Adverse Mobility Ratio Displacements", SPEJ, (August 1979)
 44. ECL, "Advanced Reservoir Simulation using ECLIPSE", course notes, ECL Petroleum Technologies, 1990
 45. Rozon, B. J., "A Generalized Finite Volume Discretization Method for Reservoir Simulation", SPE paper 18414, presented at the SPE Reservoir Simulation Symposium, Houston, (February 1989)
 46. Winters, S. and Pfderkamfer, H., "Geological and Geophysical Appraisal of the ___ Field*", SOEKOR Internal Report, 1994

- 47 Winters, S., "Architectural Geometries of Fan 5 in the Skoorsteenbergr Region, Tanqua Sub-basin, Permian Ecca, South Africa", SOEKOR Internal Report SOE-EXP-RPT-0327, 1995
- 48 Burger, C. A. J., Van Niekerk, A. B., Ridley, T. P., and Strauss, J. P., "____ Development Study*", SOEKOR Internal Report SOE-PET-RPT-152, 1994
- 49 Burger, C. A. J., Personal Communication, 2002

** Name of well or field withheld for reasons of confidentiality.*

Nomenclature

Roman Letters:

A	The Jacobian matrix for solution on the finite difference equations (Sections 3.6 to 3.10 only).
A_m	Surface area of the m-th face of the grid-block being considered.
b	Represents the residual in the Newton iterations used in solving the finite difference equations (Sections 3.6 to 3.10 only).
b_p	Penetration ratio in formulae for partial penetration skin.
B	An easily inverted approximation to the Jacobian matrix used in solved the finite difference equations (Sections 3.6 to 3.10 only).
B_o, B_w, B_g	Formation volume factors for oil, water, and gas respectively.
c	Total isothermal compressibility.
c_o, c_w, c_g	Isothermal compressibilities for oil, water, and gas respectively.
c_r	Compressibility associated with the reduction of pore space as pressure increases.
d	Diagonal in the tri-diagonal Jacobian matrix (Sections 3.6 to 3.10 only).
D	Depth.
F	Vector representing the flow terms in the black-oil fluid flow equations (Section 3.2, Equation 51).
g	Acceleration due to gravity.
k	Permeability.
k_h, k_v	Component of permeability in the horizontal and vertical directions respectively.
k_p	Horizontal permeability over the perforated interval.

k_{ro}, k_{rw}, k_{rg}	Relative permeability to oil, water, and gas respectively.
K_0, K_1	Modified Bessel functions of the second kind of order 0 and 1 respectively.
h	Formation thickness.
h_w	Length of well interval that is open to flow.
h_w, h_1, h_2	Lengths defining the completion geometry (Figure 1.4).
H_j	Hydrostatic head correction for calculating well flow (Section 3.2, Equation 84).
I	The identity matrix.
l_1, l_2, l_3	Lower side bands in the Jacobian matrix (Sections 3.6 to 3.10 only).
m	Slope from a Horner plot.
M	Mass accumulation vector in black-oil fluid flow formula (Section 3.2, Equation 50).
p	Pressure.
p_i	Initial pressure, i.e. pressure before any flow has taken place to disturb initial equilibrium.
p_{bh}	Well bottom hole pressure, finite difference model (Section 3.4).
p_c	Capillary pressure.
p_{wf}	Well flowing pressure.
\tilde{p}	Laplace transform of pressure.
P	Matrix used in the nested factorisation process in solving a set of linear equations (Section 3.9).
q	Fluid flow rate.
Q	Mass sink vector associated with a well in the finite difference equations (Section 3.4).

r	Radius or radial distance from centre of well to a given position.
r_0, r_1, r_n	Residual vectors in solution of a set of linear equations (Sections 3.8 to 3.10 only).
$\bar{r}_0, \bar{r}_1, \bar{r}_n$	Saturation normalised residual vectors in solution of a set of linear equations (Sections 3.8 to 3.10 only).
r_{inv}	Radius of investigation.
r_w	Wellbore radius.
$\Delta r_0, \Delta r_1, \Delta r_n$	Residual search directions in solution of a set of linear equations (Sections 3.8 to 3.10 only).
$\Delta r_i, \Delta r_n$	Radial distance to face of adjacent grid cell (Section 4.3, Figure 4.4).
$\Delta r_{j-1}, \Delta r_j$	Radial distance between adjacent grid points (Section 4.5).
R	Residual vector for the solution of the non-linear finite difference equations (Section 3.2).
R_1, R_2, R_3	Radii used in calculation of transmissibilities (Section 3.3).
s	The transformed equivalent to time in the Laplace transform for pressure.
S	The skin factor.
S_o, S_w, S_g	The fluid saturations for oil, water, and gas respectively.
S_p	Flow convergence or partial penetration skin.
S_m	Mechanical skin (skin due to near well damage).
t	Time.
T	Temperature when discussing PVT properties or transmissibility when discussing flow from grid-block to grid-block.
T	Matrix used in nested factorisation procedure when solving a set of linear equations (Section 3.9 only).
u	Flow velocity as a scalar property.

u_1, u_2, u_3	Upper side bands in the Jacobian matrix (Sections 3.6 to 3.10 only).
\underline{u}	Flow velocity as a vector property.
V	Volume.
w	Represents the well state, i.e. flowing pressure and produced fluid fractions for water and gas (Section 3.4).
x, y	Horizontal position in a Cartesian reference system.
x	The change in the state vector at each non-linear iteration when solving the finite difference equations, note that this is equivalent to the solution of the linear equations (Sections 3.6 to 3.10 only).
x_0, x_1, x_n	Estimates of required solution for set of linear equations (Sections 3.8 to 3.10 only).
$\Delta x_0, \Delta x_1, \Delta x_n$	Solution search directions for solution of a set of linear equations (Sections 3.8 to 3.10 only).
X	State vector for finite difference model, i.e. contains the value of oil pressure, water saturation, and gas saturation for every grid block (Section 3.2).
z	Vertical position (Cartesian or cylindrical reference system).
$\Delta z_i, \Delta z_{i-1}$	Vertical distance between adjacent grid points (Section 4.5).
Z^*	Intercept on a Horner plot, i.e. extrapolation of best-fit line to infinite time.

Greek Letters:

$\alpha_0, \alpha_1, \alpha_n$	Weighting factors used in solution of finite difference equations to minimise residual when moving along a particular search direction.
β	Weighting factor, used in nine point method to determine optimum contribution of diagonal grid points (Section 4.5 only).

β_{10}, β_{nm}	Weighting factors, used in solution of finite difference equations to ensure each search direction is orthogonal to the last direction (Section 3.8 only).
Δ	Implies a change or difference.
ε_t	Time discretisation error.
ρ	Density.
μ	Fluid viscosity.
μ_p	Fluid viscosity across the perforated interval.
Φ	Fluid potential.
λ	Fluid mobility (Section 3.2).
ϕ	Porosity.
γ	Hydrostatic pressure gradient for a fluid, i.e. product of fluid density and acceleration due to gravity.
γ_e	Euler's constant, i.e. $\gamma_e = 0.5772\dots$
σ	Diagonal matrix used in solution of set of linear equations with tri-diagonal structure (Sections 3.7 to 3.10 only).
τ	Horner or superposition/transformed time.
Ψ	Pressure potential.
ξ	The exponent of Euler's constant, i.e. $\xi = \exp(0.5772\dots)$.
θ	Tangential component in a cylindrical co-ordinate system.

Subscripts:

D	Implies a dimensionless property.
i, j, k	Typically used as indices, when used in combination in a grid system they represent the grid block index according to the three co-ordinate axes.

o, w, g	Oil, water, or gas phase respectively.
x, y, z	Directions/components in a Cartesian reference system.
v, h	Vertical and horizontal direction/component respectively.
p	Either phase (oil, water, or gas) or partial depending on context.

Glossary

Anisotropic – Implies properties that differ in value depending on the direction they are measured in.

Absolute Permeability – The permeability associated with a porous medium when the pore space is completely filled by a single fluid phase. (See also *permeability*, *effective permeability*, and *relative permeability*)

Build-up – A period, following a flow period, when the well is closed to prevent further flow to surface. During this time the pressure in the well will steadily increase (build-up).

Capillary Pressure – The pressure difference between immiscible fluid phases that share the pore space. This pressure difference is a consequence of the interfacial tension between the phases.

Claystone – A rock that contains a large proportion of clay minerals and other very fine grained material.

Compressibility – A measure of the degree to which the volume of a substance can be changed by the application of pressure, i.e. the ratio of volume change to pressure change per unit volume.

Coning – The formation of a cone of fluid from an overlying or underlying zone to the well in response to the pressure drop at the well with the typical consequence that unwanted fluid (water or gas) is produced.

Darcy Units – A hybrid system of units that avoids the use of unnecessary conversion factors in flow equations and has units of more convenient size than the S.I. (Table 1.1: Comparison of Different Unit Systems)

Drainage – A dynamic process where the saturation of the wetting phase (i.e. the phase that preferentially wets the surfaces of the grains) decreases with time.

Drill stem test (DST) – A well test that is conducted using drill pipe to convey the fluid from the reservoir to surface or vice versa. (See also *Well Test*)

Effective Permeability – The permeability associated with a particular fluid phase when the pore space is filled by more than one fluid phase. (See also *permeability*, and *relative permeability*)

Field Units – A system of imperial units that is commonplace in the oil industry (Table 1.1)

Formation Volume Factor – The ratio of reservoir volume to surface volume for a given fluid.

Heterogeneous – Implies properties that change from one position to another.

History Matching – The process of adjusting the properties in the simulation model so that it is able to closely reproduce the observed production history.

Homogenous – Implies properties that are the same everywhere throughout the system (note that a body may have homogenous but anisotropic properties).

Horner Plot – A specialized plot for analysing pressure behaviour during a build-up. The x-axis is based on a transformed time function that is designed to give a straight line on the plot when transient flow (i.e. infinitely acting radial flow) is taking place. The slope of the line is inversely proportional to the permeability thickness of the interval contributing to flow (Sections 1.3 and 5.4).

Imbibition – A dynamic process where the saturation of the wetting phase (i.e. the phase that preferentially wets the surfaces of the grains) increases with time.

Interbedded – Alternating layers of different rock types.

Isotropic – Implies properties that are identical in all directions.

Lithology – Rock type, typically referring to the general characteristics of the rock such as bulk composition and texture, for example.

Massive – As applied to describing rocks, it implies a single continuous body without significant internal structure.

Net Present Value (NPV) – A measure of the total value of a future cash flow that takes the time value of money (i.e. money now is better than money tomorrow) into account. This is achieved by discounting cash flows by progressively larger amounts the further in the future they occur. NPV can therefore be described as a cumulative discounted cash flow.

Partially penetrating well – A well that does not completely penetrate the reservoir interval (Figure 1.2a).

Partially completed well – A well where only part of the reservoir interval is open to flow (Figure 1.2b).

PEBI Grid – A perpendicular bisection grid, also known as a Voronoi grid. This is a flexible gridding technique where the faces of the grid blocks perpendicularly bisect the lines joining adjacent grid blocks (Section 3.1).

Permeability – The fluid conductivity of a porous medium, i.e. a measure of the ease with which fluid can move through the medium. Permeability is a directional property and is therefore normally described by a diagonal property tensor. It is defined through Darcy's Law (Section 1.2, Equations 1 to 4).

Pore space – Space between the solid particles (grains) that make up the rock.

Porosity – The fraction of the bulk volume of rock that is not solid (pore space) and is therefore available for occupation by gas or liquids.

PVT – Refers to measurements taken under changing conditions of pressure, volume, and temperature (Section 2.6).

Relative Permeability – A factor that is applied to absolute permeability in order to account for the reduction of the effective permeability when part of the pore space is filled by another fluid (Section 2.2, Equation 21).

Sandstone – A rock that comprises mainly relatively coarse grains (1/16 to 2 mm in size), typically made up predominantly of quartz.

Saturation – The volume fraction of the pore space that is filled by a particular fluid.

Siltstone – A fine-grained rock with a grain size less than sandstone and coarser than shale/claystone.

Seismic – Refers to the elastic waves that are used in order to assess sub-surface geometry and properties. The waves are generated by a source and the resulting reflections recorded. Changes in the elastic properties will cause the waves to reflect and/or refract and thus interpretation of the recordings allow reconstruction of what lies below the surface.

Skin – A factor that is introduced to account for an additional (or reduced) pressure drop over and above that expected from homogenous transient flow (Section 1.3). It is a manifestation of the difference between near-well and larger scale properties. In

the case where there is a zone of damaged rock (reduced permeability) immediately around the well bore, one would expect a high skin.

Solution Gas Oil Ratio – The volume of dissolved gas associated with a unit volume of oil, both being measured at surface conditions. This gas would originally be dissolved in the oil at reservoir conditions and is released by bringing the oil to surface conditions.

Specific gravity – The density of a fluid relative to water, i.e. density divided by the density of pure water, normally measured at a standard temperature and pressure.

Turbidite – The sediment deposited by, or associated with, a turbidity current (Section 5.2). A turbidity current is essentially a slurry of water and sediment moving together underwater. These currents form when sediment that is deposited on the edge of the continental slope breaks free and rushes down the slope.

Viscosity – A fluid property that is a measure of the resistance of fluids to flow.

Well test – Typically describes the process of producing fluid from or injecting fluid into a well under controlled conditions in order to assess the properties of the reservoir.

Appendix 1:

Eclipse Command File for Hypothetical Problem

Appendix 1: Eclipse Command File for Hypothetical Problem

This is the command file listing for the Eclipse reservoir simulation package that was used to model the hypothetical problem, that of a well test conducted on a partially penetrating well in an homogeneous but anisotropic formation.

```

RUNSPEC
  RAD8: PART. PEN. WELL, Kv/Kh = 0.1, half cell at base and top
= NDIVR NDIVTHETA NDIVIZ QRDIAL NUMRES QNNCON MXNAQN MXNAQC QDPORO
QDPERM
  33      1      34      T      1      f      0      0      F
F /
= OIL  WATER  GAS  DISGAS  VAPOIL
  T      T      f      f      F      / LIVE OIL ABOVE BUBBLE POINT
= UNIT CONVENTION
  'FIELD ' /
= NRPVT  NPPVT  NTPVT  NTROCC  QROCKC  QRCREV
  1      3      1      1      F      T      /
= NSSFUN  NTSFUN  QDIRKR  QREVKR  QVEOPT  QHYSTR
  3      1      f      T      F      F      /
= NDRXVD  NTEQUL  NDPRVD  QUIESC  QTHPRS  QREVTH
  1      1      100     F      F      T      /
= NTFIP  QGRAID  QPAIR
  1      F      F      /
= NWMAXZ  NCWMAX  NGMAXZ  NWGMAX  MAXLGR  MAXCLS  NCOARS
  1      160     1      1      0      0      0      /
= QEXGOP  NWFRIC  NUPCOL
  F      0      3      /
= MXMFLO  MXMTHP  MXMWFR  MXMGFR  MXMALQ  NMMVFT
  1      1      1      1      1      0      /
= MXSFLO  MXSTHP  NMSVFT  MXCFLO  MXCWOC  MXCGOC  NCRTAB
  1      1      0      0      0      0      0 /
= NAQFET  NCAMAX
  0      0      /
= DAY  MONTH  YEAR
  11   'APR'  1993 /
= QSOLVE  NSTACK  QFMTOU  QFMTIN  QUNOUT  QUNINP
  T      24     F      F      f      F      /

```

```
-- END OF RUNSPEC SECTION=====
```

GRID

```

=====
----- IN THIS SECTION , THE GEOMETRY OF THE SIMULATION GRID AND
THE
----- ROCK PERMEABILITIES, POROSITIES AND NET-TO-GROSS RATIOS ARE
DEFINED.
--
=====

```

ACTNUM

```
1122*1 /
```

INRAD

```
0.3615 /
```

DRV

```
0.1 0.1 0.2 0.2 0.3 0.3 0.4 0.5 0.6 0.7 0.9 1.1 1.4 1.7 2.3 2.9
4.0
```



```

5.5 8.2 13.0 20 32 51 80 126 200 315 499 788 1246 1968 3109
4913 /

DTHETAV
  360 /

BOX
  1 33 1 1 1 1 /
TOPS
  33*7000 /
ENDBOX

EQUALS

'PERMR' 500      1 33 1 1 1 34 /
'NTG'   1.0     /
'PORO'  .20     /
'DZ'   12.26    1 33 1 1 1 1 /
'DZ'   4.25     1 33 1 1 2 2 /
'DZ'   2.97     1 33 1 1 3 3 /
'DZ'   2.08     1 33 1 1 4 4 /
'DZ'   1.46     1 33 1 1 5 5 /
'DZ'   1.02     1 33 1 1 6 6 /
'DZ'   0.71     1 33 1 1 7 7 /
'DZ'   0.50     1 33 1 1 8 8 /
'DZ'   0.35     1 33 1 1 9 9 /
'DZ'   0.22     1 33 1 1 10 10 /
'DZ'   0.11     1 33 1 1 11 11 /
'DZ'   0.10     1 33 1 1 12 12 /
'DZ'   0.10     1 33 1 1 13 13 /
'DZ'   0.1      1 33 1 1 14 14 /
'DZ'   0.1      1 33 1 1 15 15 /
'DZ'   0.1      1 33 1 1 16 16 /
'DZ'   0.1      1 33 1 1 17 17 /
'DZ'   0.1      1 33 1 1 18 18 /
'DZ'   0.1      1 33 1 1 19 19 /
'DZ'   0.1      1 33 1 1 20 20 /
'DZ'   0.11     1 33 1 1 21 21 /
'DZ'   0.22     1 33 1 1 22 22 /
'DZ'   0.30     1 33 1 1 23 23 /
'DZ'   0.43     1 33 1 1 24 24 /
'DZ'   0.52     1 33 1 1 25 25 /
'DZ'   0.87     1 33 1 1 26 26 /
'DZ'   1.30     1 33 1 1 27 27 /
'DZ'   1.83     1 33 1 1 28 28 /
'DZ'   3.09     1 33 1 1 29 29 /
'DZ'   4.43     1 33 1 1 30 30 /
'DZ'   8.33     1 33 1 1 31 31 /
'DZ'   12.62    1 33 1 1 32 32 /
'DZ'   12.62    1 33 1 1 33 33 /
'DZ'   25.26    1 33 1 1 34 34 /

/

COPY
  'PERMR' 'PERMTHT' /
  'PERMR' 'PERMZ'   /

/

MULTIPLY
-- Define Kv/Kh

```

```

'PERMZ' 0.1 /
/

-- TURN THE BLOCKS AT THE TOP AND BASE OF RESERVOIR INTO HALF BLOCKS
BOX
  1 33 1 1 1 1 /
MULTR
  33*0.5 /
MULTPV
  33*0.5 /
BOX
  1 33 1 1 34 34 /
MULTR
  33*0.5 /
MULTPV
  33*0.5 /
ENDBOX

RPTGRID
  1 0 1 1 1 1 0 0 0 1 1 1 1 / FOR DEBUGGING
-- 35*0 / AFTER DEBUGGING

GRIDFILE
2 /

NEWTRAN

-- END OF GRID
SECTION=====

PROPS
=====

-- RELATIVE PERMS AND PC'S
SWOF
--      SW      KRW      kro      PC
      0.10     0.0      1.000     1.0
      0.5      0.0      1.000     0.5
      1.0      1.0      0.000     0.0 /

--      REF. PRES. REF. FVF  COMPRESSIBILITY  REF VISCOSITY
VISCOSIBILITY
PVTW
      3500      1.036      3.0E-6      0.272      5.03E-6
/

-- ROCK COMPRESSIBILITY
--      REF. PRES  COMPRESSIBILITY
ROCK
      3500      2.0E-6 /

DENSITY
-- SURFACE DENSITIES OF RESERVOIR FLUIDS

-- FROM E-BT1 DST#1; &O = 0.810; &G = 0.9430 (PVT REPORT FULL
FLASHING)
-- &W = 1.01 FROM WATER ANALYSIS OF E-AD1 SAMPLE
--      OIL    WATER    GAS
      50.6    63.05    0.0888 /

```

```

PVDO
-- OIL PVT FOR E-BT FROM DST#1 AT E-BT1
--           Peq      BO          UO
--           (psia) (rb/stb) (cP)
--           3000    1.515    0.5
--           3500    1.500    0.5
--           4000    1.485    0.5 /

/

RSCONSTT
  .750 2000 /

RPTPROPS
19*0 /

-- END OF PROPS
SECTION.=====

REGIONS

RPTREGS
4*0 /

SOLUTION
=====
----- THE SOLUTION SECTION DEFINES THE INITIAL STATE OF THE
SOLUTION
----- VARIABLES (PHASE PRESSURES, SATURATIONS AND GAS-OIL RATIOS)
-----
---
-- DATA FOR INITIALISING FLUIDS TO POTENTIAL EQUILIBRIUM
--
--   DATUM  DATUM  MFWL  MFWL  GOC  GOC  RSVD  RVVD  SOLN
--   DEPTH  PRESS  DEPTH  PCOW  DEPTH  PCOG  TABLE  TABLE  METH
EQUIL
  7000    3500    8500    0.0   6000    0     0     0     0 /
EBT1

-- SWITCH ON OUTPUT OF INITIAL SOLUTION
RPTSOL
  0 0 1 0 0 0 4 2 1 /

SUMMARY
=====

FOPR      - oil production rate
FOPT      - oil production total
FWPR      - water production rate
FWPT      - water production total
FWCT      - water cut
WBHP      - well bottom hole pressures
'W1' /

-- REQUEST A SEPARATE RUN SUMMARY FILE
RUNSUM
SEPARATE

```

RPTSMRY
1 /

SCHEDULE

RPTSCHED
6*0 4 2 2 0 2 2 0 0 2 /

WELSPPCS
'W1' 'RAD' 1 1 1* 'OIL' /
/

COMPDAT
--WELL CONNECT FLAG SAT TRANS DIA KH S
'W1' 1 1 1 13 'OPEN' 1* 1* .723 1* 0.0 /
/

-- FLOW PERIOD 1

WCONPROD
'W1' 'OPEN' 'ORAT' 5000 1* 1* 1* 1* 1000 /
/

TUNING
.000002 10 .000005 .015 1.09 /
/
/

TSTEP
0.166666667
/

END

Appendix 2:

Listing of Computer Programs

Appendix 2: Computer Program Listings

Listing of the program Hantush.cpp

Used to calculate pressures from the Hantush analytical solution.

```
// Hantush: Program to calculate pressures for a partially penetrating well
// using the Hantush analytical solution.

#include <iostream.h>
#include <math.h>
#include <stdio.h>

double pd( double td, double b, double hd, double h1d, double h2d, double zd);
double improper( double x, double beta);
double adapt(double lower, double upper, double beta);
double f( double x, double beta);
int enter_val(double *tmax, int *num_points ,double *td_mult, double *pd_mult,
             double *b, double *hd, double *h1d, double *h2d, double *zd,
             double *p_init);
void display_values( double tmax, int num_points, double td_mult,
                   double pd_mult, double b, double hd, double h1d,
                   double h2d, double zd);

const double gamma = 0.577215664901532;
const double pi = 3.14159265358979;
const double limit = 1e-5;

int main()
{
    double pressure[100], time[100], t, t_space, tmax, td_mult, p_init,
        pd_mult, b, hd, h1d, h2d, zd;
    int n,num_points;
    char trash;
    FILE *outfile;

    while (enter_val( &tmax, &num_points, &td_mult, &pd_mult,
                    &b, &hd, &h1d, &h2d, &zd, &p_init))
        cout << "\n\nERROR IN ONE OF THE ENTERED VALUES. TRY AGAIN\n";
    display_values( tmax, num_points, td_mult, pd_mult, b, hd, h1d, h2d, zd);
    t_space = exp( (log(tmax)-log(0.001))/num_points);
    if ( (outfile=fopen("PRESS.LIS","w")) == NULL )
        cout << "\nUnable to open output file";
    else
    {
        for (zd=0.05; zd<=0.25; zd+=0.05)
        {
            for (t=0.001, n=0; n<(num_points+1); t*=t_space, n++)
            {
                time[n] = t;
                pressure[n] = p_init - pd_mult * pd( td_mult*t, b, hd, h1d, h2d, zd);
            }
            fprintf( outfile, "\n zd = %f",zd);
            fprintf( outfile, "\n Time Pressure");
            for (n=0; n<(num_points+1); n++)
                fprintf( outfile, "\n %f %f", time[n], pressure[n]);
        }
        fclose( outfile);
    }
    return 0;
}

void display_values( double tmax, int num_points, double td_mult,
                   double pd_mult, double b, double hd, double h1d,
                   double h2d, double zd)
{
    char trash;
```

```

cout << "\n\nTHESE ARE THE VALUES TO BE USED IN CALCULATING PD\n";
cout << "\n tmax is " << tmax;
cout << "\n numpoints is " << num_points;
cout << "\n td_mult is " << td_mult;
cout << "\n pd_mult is " << pd_mult;
cout << "\n b is " << b;
cout << "\n hd is " << hd;
cout << "\n h1d is " << h1d;
cout << "\n h2d is " << h2d;
cout << "\n zd is " << zd;
cout << "\nEnter a character value to continue ";
cin >> trash;
}

int enter_val(double *tmax, int *num_points ,double *td_mult, double *pd_mult,
             double *b, double *hd, double *h1d, double *h2d, double *zd,
             double *p_init)
{
double h,k,kv,poro,cr,sw,bo,co,uo,cw,rw,h1,h2,q,ct;
int error;

cout << "\nENTER THE FORMATION PROPERTIES:";
cout << "\nFormation thickness, h (feet) , ";
cin >> h;
cout << "Horizontal permeabilty, k (mD), ";
cin >> k;
cout << "Vertical permeability, kv, ";
cin >> kv;
cout << "Porosity as a fraction, ";
cin >> poro;
cout << "Rock (pore volume) compressibility, Cr (per psi), ";
cin >> cr;
cout << "Water saturation as a fraction, ";
cin >> sw;
cout << "\nENTER THE FLUID PROPERTIES:";
cout << "\nOil formation volume factor";
cin >> bo;
cout << "Oil compressibility, Co (per psi), ";
cin >> co;
cout << "Oil viscosity, uo (cP), ";
cin >> uo;
cout << "Water compressibility, Cw (per psi), ";
cin >> cw;
cout << "Initial pressure, Pi (psia)";
cin >> *p_init;
cout << "\nENTER THE WELL PROPERTIES";
cout << "\nRadius of the wellbore, rw (feet), ";
cin >> rw;
cout << "Distance from the top of the formation to the top of the perforations,";
cout << "\nh1 (feet), ";
cin >> h1;
cout << "Distance from the top of the formation to the bottom of the ";
cout << "\nperforations, h2 (feet), ";
cin >> h2;
cout << "\nENTER THE PRODUCTION DETAILS";
cout << "\nRate of flow, q (stb/d), ";
cin >> q;
cout << "Duration of flow in hours, ";
cin >> *tmax;
cout << "Number of pressure points to simulate, ";
cin >> *num_points;
error = 0;
if ((sw<0.0) || (sw>1.0)) error=1;
ct = co*(1.0-sw) + cw*sw + cr;
*td_mult = 0.0002637*k/(poro*uo*ct*rw*rw);
*pd_mult = 141.2*q*uo*bo/(k*h);
*b = (h2-h1)/h;
if ((*b<0.0) || (*b>1.0)) error=1;
if ((h1<0.0) || (h1>h)) error=1;
if ((h2<0.0) || (h2>h)) error=1;
*h1d = h1/h;
*h2d = h2/h;
*hd = h*sqrt(k/kv)/rw;
*zd = (h1+h2)/2/h;

```

```

    return(error);
}

double f( double u, double beta)
// function to be integrated numerically
{ return( exp( -1.0*u - beta*beta/(4.0*u)) / u ); }

double pd( double td, double b, double hd, double h1d, double h2d, double zd)
// Calculate the dimensionless pressure for a given dimensionless time
// for a partially penetrating well using the Hantush solution.
{
    double bn,check,delta,n,rn,total;

    n = 1.0;
    total = pi*b*improper(1.0/(4.0*td), 0.0)/2.0;
    rn = 1.0;
    do
    {
        bn = n*pi;
        rn = 1.0/n * ( sin(bn*h2d) - sin(bn*h1d) ) * cos(bn*zd);
        check = improper( 1.0/(4.0*td), bn/hd);
        total += rn * check;
        n += 1.0;
        cout << "\nTOTAL=" << total << " N=" << n << " TD=" << td;
        cout << "\nZD=" << zd;
    }
    while (0.001<fabs(1.0/n*check));
    return(total/(pi*b));
}

double adapt(double lower, double upper, double beta)
// adapts the number of intervals used by simpsons rule until the required
// accuracy is reached
{
    double f_start, f_end, twos, fours, h, integ, last_int, x;
    int intervals, m;

    h=(upper-lower)/2.0;
    f_start=f(lower,beta);
    fours=4.0*f(lower+h,beta);
    twos=0.0;
    f_end=f(upper,beta);
    integ = (f_start+twos+fours+f_end)*h/3.0;
    intervals=2;
    do {
        intervals*=2;
        last_int=integ;
        twos = twos + fours/2.0;
        for (
            m=1, h=(upper-lower)/double(intervals), fours=0.0, x=lower+h;
            m<(intervals/2+1);
            fours+=4.0*f(x,beta), x+=h+h, m++ );
        integ = (f_start+twos+fours+f_end)*h/3.0;
    }
    while (fabs(last_int-integ)>limit);
    cout << "\nIntervals " << intervals << " lower " << lower << " upper " << upper;
    return(integ);
}

double improper( double x, double beta)
// Calculates the improper integral of the function f from x to infinity
// by calculating the integral to larger and larger limits
{
    double h,integ,last_int,lower,upper;
    int count;

    count=1;
    lower=x;
    upper=50.0*x;

```



```
integ=adapt(lower, upper, beta);
while ((fabs(integ/limit)<100.0) && (upper<1000.0))
  { upper=10.0*upper; integ = adapt(lower, upper, beta); }
do {
  lower=upper; upper=10.0*lower;
  last_int=integ;
  integ+=adapt(lower,upper,beta);
  count++;
}
while ((fabs(integ-last_int)>limit) && (count<10));
if (count == 10)
  cout << "\nWARNING!! LIMIT EXCEEDED IN IMPROPER INTEGRATION"
        << "\n RESIDUAL ERROR IS > " << fabs(integ-last_int);
cout << "\nResult of integration is " << integ;
cout << "\nUpper limit is " << upper;
return(integ);
}
```

Listing of the program Stehfest.cpp

Used to calculate pressures from the Yiidiz and Bassiouni analytical solution using the Stehfest algorithm for inverse Laplace transformation

```
// Stehfest: Program to calculate pressures for a partially penetrating well
// using the Yiidiz and Bassiouni analytical solution in Laplace space
// in conjunction with the Stehfest algorithm for Laplace transform
// inversion. (J.P.Strauss, April 1997)

#include <iostream.h>
#include <stdio.h>
#include <math.h>
#include <alloc.h>
#include <process.h>

double pd( double td, double rD);
double pd_inv( double s, double rD);
int enter_val(double *tmax, int *num_points ,double *td_mult, double *pd_mult,
             double *hDp, double *hD, double *hDb, double *pi);
void display_values( double tmax, int num_points, double td_mult,
                   double pd_mult, double hDp, double hD, double hDb);
void steh_weights(double *v, int n);

double K0(double x);
double Ei(double x);
double K0_div_K1(double x);

const double gamma = 0.577215664901532;
const double pi = 3.14159265358979;
const double limit = 1e-5;

/* Stehfest weighting factors for n=12 */
double v[12]={ -0.0166666666666666, 16.0166666666666, -1247.0000000002,
              27554.33333318, -263280.8333323, 1324138.699994,
              -3891705.533308, 7053286.333279, -8005336.499933,
              5552830.499949, -2155507.19998, 359251.199968 };

double v2[50];
FILE *s; /* Output file for calculated pressures */

int main()
{
    double pressure, press1, pi, rD, t, t_space, tmax, td_mult, pd_mult,
          hDp, hD, hDb;
    int i,n,num_points, n_weights;
    char trash;

    /* Open output file */
    if ((s=fopen("stehfest.txt", "wt"))==NULL)
        cout << "\nUnable to open output file. Program terminating.\n";
    else
    {
        fprintf(s, "\nIMPLEMENTATION OF THE GENERAL LINE-SOURCE, INFINITE-ACTING
SOLUTION");
        fprintf(s, "\nUses the Stehfest algorithm with 12 weighting factors to numerically
");
        fprintf(s, "\ninvert the solution in Laplace space and compares this to the
solution");
        fprintf(s, "\nin real space (i.e. the exponential integral.\n");
        while (enter_val( &tmax, &num_points, &td_mult, &pd_mult,
                        &hDp, &hD, &hDb, &pi))
            cout << "\n\nERROR IN ONE OF THE ENTERED VALUES. TRY AGAIN\n";
        display_values( tmax, num_points, td_mult, pd_mult, hDp, hD, hDb);

        /* Define weighting factors */
        do
        {
            cout << "\nEnter the number of weighting factors to use \n";
            cin >> n_weights;
            if (n_weights>50) cout << "\nRestricted to less than 50. Try again!\n";
        }
        while (n_weights>50);
        steh_weights(v2, n_weights); // Calculate weighting factors
    }
}
```

```

/* Compare weighting factors */
if (n_weights==12)
{
    fprintf(s, "\n\nComparison of weighting factors\n");
    fprintf(s, "\nOriginal      Calculated      Fractional error\n");
    for (i=0; i<n_weights; i++)
        fprintf(s, "%15.5f %15.5f %15.5f\n", v[i], v2[i], (v[i]-v2[i])/v2[i] );
}

/* Calculate time spacing for pressures */
t_space = exp( (log(tmax)-log(0.001))/num_points);
rD=1.0;
fprintf(s, "\n\nCALCULATED SOLUTION\n");
fprintf(s, "\n
INTEGRAL")
LAPLACE INVERSION      EXPONENTIAL
          tD          time          pD          deltaP          pD
deltaP");
          (hours)          (psi)
(psi)");

fprintf(s, "\n=====");
;
    cout << "\ntD      Pressure      Press1 \n";
    for (t=0.001, n=0; n<(num_points+1); t*=t_space, n++)
    {
        /* Calculate pressure drop for each time value */
        cout << "td_mult*t << " ";
        pressure = pd_mult * pd( td_mult*t, rD);
        cout << "pressure << " ";
        press1 = pd_mult * 0.5*Ei(rD*rD/(4.0*td_mult*t));
        cout << "press1 << "\n";
        fprintf(s, "\n %10.2f %10.5f %10.5f %10.5f %10.5f %10.5f",
            td_mult*t, t, pressure/pd_mult, pressure, press1/pd_mult, press1);
    }
    fclose(s);
}
return 0;
}

void display_values( double tmax, int num_points, double td_mult,
                    double pd_mult, double hDp, double hD, double hDb)
{
    fprintf(s, "\n\nDERIVED PARAMETERS USED IN SOLUTION");
    fprintf(s, "\n td_mult      %7.7f", td_mult);
    fprintf(s, "\n pd_mult      %7.7f", pd_mult);
    fprintf(s, "\n hDp         %7.7f", hDp);
    fprintf(s, "\n hD          %7.7f", hD);
    fprintf(s, "\n hDb         %7.7f", hDb);
}

int enter_val(double *tmax, int *num_points, double *td_mult, double *pd_mult,
             double *hDp, double *hD, double *hDb, double *pi)
{
    double h, k, kv, poro, cr, sw, bo, co, uo, cw, rw, h1, h2, q, ct;
    int error;
    cout << "\n\nENTER THE FORMATION PROPERTIES:";
    cout << "\nFormation thickness, h (feet) , ";
    cin >> h;
    cout << "Horizontal permeability, k (mD), ";
    cin >> k;
    cout << "Vertical permeability, kv, ";
    cin >> kv;
    cout << "Porosity as a fraction, ";
    cin >> poro;
    cout << "Rock (pore volume) compressibility, Cr (per psi), ";
    cin >> cr;
    cout << "Water saturation as a fraction, ";
    cin >> sw;
    cout << "\n\nENTER THE FLUID PROPERTIES:";
    cout << "\nOil formation volume factor";
    cin >> bo;
    cout << "Oil compressibility, Co (per psi), ";
    cin >> co;
    cout << "Oil viscosity, uo (cP), ";
    cin >> uo;
    cout << "Water compressibility, Cw (per psi), ";
}

```

```

cin >> cw;
cout << "Initial pressure, Pi (psia)";
cin >> *pi;
cout << "\nENTER THE WELL PROPERTIES";
cout << "\nRadius of the wellbore, rw (feet), ";
cin >> rw;
cout << "Distance from the top of the formation to the top of the perforations,";
cout << "\nh1 (feet), ";
cin >> h1;
cout << "Distance from the top of the formation to the bottom of the ";
cout << "\nperforations, h2 (feet), ";
cin >> h2;
cout << "\nENTER THE PRODUCTION DETAILS";
cout << "\nRate of flow, q (stb/d), ";
cin >> q;
cout << "Duration of flow in hours, ";
cin >> *tmax;
cout << "Number of pressure points to simulate, ";
cin >> *num_points;
error = 0;
if ((sw<0.0)|| (sw>1.0)) error=1;
ct = co*(1.0-sw) + cw*sw + cr;
*td_mult = 0.0002637*k/(poro*uo*ct*rw*rw);
*pd_mult = 141.2*q*uo*bo/(k*h);
*hDp = (h2-h1)/h;
if ((*hDp<0.0)||(*hDp>1.0)) error=1;
if ((h1<0.0)|| (h1>h)) error=1;
if ((h2<0.0)|| (h2>h)) error=1;
*hDb = h1/h;
*hD = h*sqrt(k/kv)/rw;
if (!error)
{
    fprintf(s, "\nPROBLEM PARAMETERS WERE AS FOLLOWS:\n\nFORMATION PROPERTIES\n");
    fprintf(s, "\nFormation thickness, h (feet), %5.5f", h);
    fprintf(s, "\nHorizontal permeabilty, k (mD), %5.5f", k);
    fprintf(s, "\nVertical permeability, kv, %5.5f", kv);
    fprintf(s, "\nPorosity as a fraction, %4.4f", poro);
    fprintf(s, "\nRock (pore volume) compressibility, Cr (per psi), %5.5e", cr);
    fprintf(s, "\nWater saturation as a fraction, %5.5f", sw);
    fprintf(s, "\n\nFLUID PROPERTIES");
    fprintf(s, "\nOil formation volume factor, %5.5f", bo);
    fprintf(s, "\nOil compressibility, Co (per psi), %5.5e", co);
    fprintf(s, "\nOil viscosity, uo (cP), %5.5f", uo);
    fprintf(s, "\nWater compressibility, Cw (per psi), %5.5e", cw);
    fprintf(s, "\nInitial pressure, Pi (psia), %5.5f", *pi);
    fprintf(s, "\n\nWELL PROPERTIES");
    fprintf(s, "\nRadius of the wellbore, rw (feet), %5.5f", rw);
    fprintf(s, "\nDistance from the top of the formation to the top of the
perforations,");
    fprintf(s, "\nh1 (feet), %5.5f", h1);
    fprintf(s, "\nDistance from the top of the formation to the bottom of the ");
    fprintf(s, "\nperforations, h2 (feet), %5.5f", h2);
    fprintf(s, "\n\nPRODUCTION DETAILS");
    fprintf(s, "\nRate of flow, q (stb/d), %5.5f", q);
    fprintf(s, "\nDuration of flow in hours, %5.5f", *tmax);
    fprintf(s, "\nNumber of pressure points to simulate, %5u", *num_points);
}
return(error);
}

void steh_weights(double *v, int n)
/* Calculates the Stehfest weighting factors */
{
double fact[50];
int i,j,k,l_lim, u_lim;

cout << "\nCalculating Stehfest weighting factors for " << n << " weights\n";

/* Calculate the required factorials */
for(j=1, fact[0]=1.0; j<n+1; j++)
{
    fact[j] = fact[j-1]*(double)j;
    cout << j << "! is " << fact[j] << "\n"; }

/* Calculate weighting factors */

```

```

for (i=1; i<n+1; i++)
{
  if (i>(n/2)) u_lim=n/2; else u_lim=i;
  l_lim=(i+1)/2;
  v[i-1]=0.0;
  for (k=l_lim; k<u_lim+1; k++)
    v[i-1]+=( pow(k,n/2)*fact[2*k] )/
      ( fact[n/2-k]*fact[k]*fact[k-1]*fact[i-k]*fact[2*k-i] );
  if ( ((n/2+i)%2)==1 ) v[i-1]*=-1.0;
}
}

double pd( double td, double rD)
/* Uses the Stehfest Algorithm and the Laplace inverse of pd in
   order to calculate pd */
{
  double total,s;
  int i;
  for (i=1, total=0.0; i<13; i++)
    total+=v2[i-1]*pd_inv( log(2.0)/td*(double)i, rD );
  return(log(2.0)/td*total);
}

double pd_inv( double s, double rD)
/* The laplace inverse of the pd function */
{
  double x;
  x=sqrt(s);
  if (x>15) cout << "\nWarning! argument to K0_div_K1 is outside range of validity ";
  return(K0_div_K1(x)/s/x);
}

double K0(double x)
//The modified zero order Bessel function of the second kind
{
  double K0,r,invr,x_sq,pow_x,phi,
    lnx2,delta,loc_limit;
  char trash;

  delta =1.0;
  lnx2 = log(x/2.0);
  K0 = -lnx2-gamma;
  phi = 0.0;
  r =1.0;
  x_sq=x*x/4.0;
  pow_x=1.0;
  loc_limit=limit*fabs(K0);
  do
  {
    invr = 1.0/r;
    phi += invr;
    pow_x*=x_sq*invr*invr;
    delta = pow_x*(phi-lnx2-gamma);
    K0 += delta;
    r += 1.0;
    loc_limit=limit*fabs(K0);
  }
  while (loc_limit<fabs(delta));
  return(K0);
}

double Ei(double x)
{
  double total,r,rfact,delta,loc_limit;
  char trash;

  delta =1.0;
  total = log(x)+gamma;
  rfact = 1.0;
  r =1.0;
  do
  {
    rfact *= r;
    delta = pow((-1.0*x),r)/(r*rfact);
  }
}

```

```

    total += delta;
    r += 1.0;
    loc_limit=limit*fabs(total);
  }
  while (loc_limit<fabs(delta));
  return(-1.0*total);
}

double K0_div_K1(double x)
//Returns K0(x)/K1(x)
{
  double K0,K1,r,invr,invr1,x_sq,pow_x,pow_x1,phi,phi1,
    ln2,delta,delta1,lim_K1,lim_K0;

  delta =1.0;
  delta1=1.0;
  ln2 = log(x/2.0);
  K0 = -ln2-gamma;
  lim_K0=limit*K0;
  K1 = 1.0/x+(ln2+gamma-0.5)*x/2.0;
  lim_K1=limit*K1;
  phi = 1.0;
  phi1=1.0;
  r =1.0;
  x_sq=x*x/4.0;
  pow_x=1.0;
  pow_x1=x/2.0;
  invr1=1.0;
  do
  {
    invr=invr1;
    invr1=1.0/(r+1.0);
    phi1 += invr1;
    if (lim_K0<fabs(delta))
    {
      pow_x*=x_sq*invr*invr;
      delta = pow_x*(phi-ln2-gamma);
      K0 += delta;
      lim_K0=limit*K0;
    }
    if (lim_K1<fabs(delta1))
    {
      pow_x1*=x_sq*invr*invr1;
      delta1 = pow_x1*(ln2+gamma-0.5*(phi+phi1));
      K1 += delta1;
      lim_K1=limit*K1;
    }
    phi = phi1;
    r += 1.0;
  }
  while ( (lim_K0<fabs(delta)) && (lim_K1<fabs(delta1)) );
  return(K0/K1);
}

```

Appendix 3:

Eclipse Command File for Real-Life Problem

Appendix 3: Eclipse Command File for Real-Life Problem

This is the command file listing for the Eclipse reservoir simulation package for the model that was used to match the pressure response for a real-life well test

```
-- Relative Permeability modified to immobilise water
-- Vertical perm everywhere made equal to 0.5 kh
-- Closest boundary moved in by 400 ft

RUNSPEC
  WELLARAD2: simulation of the Well A well test with a radial grid.
= NDIVIX NDIVIY NDIVIZ QRDIAL NUMRES QNNCON MXNAQN MXNAQC QDPORO
QDPERM
  22      8      44      t      1      T      16      14      F
F /
= OIL    WATER  GAS    DISGAS  VAPOIL
  T      T      f      f      F      / LIVE OIL ABOVE BUBBLE POINT
= UNIT CONVENTION
  'FIELD ' /
= NRPVT  NPPVT  NTPVT  NTROCC  QROCKC  QRCREV
  10     10     1      1      F      T      /
= NSSFUN NTSFUN QDIRKR QREVKR  QVEOPT  QHYSTR
  25     8      T      F      F      F      /
= NDRXVD NTEQUL NDPRVD QUIESC  QTHPRS  QREVTH  QMOBIL
  20     1      100     F      F      T      T /
= NTFIP  QGRAID QPAIR
  4      F      F      /
= NWMAXZ NCWMAX NGMAXZ  NWGMAX  MAXLGR  MAXCLS  NCOARS
  3      328    2      4      0      4000  1550 /
= QIMCOL  NWCOLC  NUPCOL
  F      0      4      /
= MXMFLO  MXMTHP  MXMWFR  MXMGFR  MXMALQ  NMMVFT
  7      3      7      4      0      2      /
= MXSFLO  MXSTHP  NMSVFT  MXCFLO  MXCWOC  MXCGOC  NCRTAB
  8      3      1      0      0      0      0 /
= NAQFET  NCAMAX
  0      0      /
= DAY    MONTH  YEAR
  14     'APR'  1991 /
= QSOLVE NSTACK QFMTOU QFMTIN QUNOUT QUNINP
  T      50     F      F      f      F      /

-- END OF RUNSPEC SECTION=====

GRID
=====
----- IN THIS SECTION , THE GEOMETRY OF THE SIMULATION GRID AND
THE
----- ROCK PERMEABILITIES, POROSITIES AND NET-TO-GROSS RATIOS ARE
DEFINED.
--
=====

INRAD
-- inner radius for the radial grid, in this case the same as the
well bore
  0.3617 /
```


DRV

```
-- 1 2 3 4 5 6 7 8 9 10
    0.1 0.2 0.4 0.8 1.6 3.2 6.0 9.7 15.8 25.5
    41.3 66.9 108 176 284 461 480 963 1276 1530
    2130 2840 /
```

DTHETAV

8*45 /

BOX

1 10 1 8 1 1 /

TOPS

80*7749.7 /

BOX

10 22 1 8 1 1 /

TOPS

```
7749.927 7750.063 7750.281 7750.635 7751.209
7752.139 7753.644 7756.313 7760 7792
7809 7842 7874
```

```
7749.511 7749.372 7749.146 7748.782 7748.191
7747.235 7745.685 7741.986 7727 7743
7743 7743 7743
```

```
7749.147 7748.769 7748.156 7747.164 7745.558
7743.16 7743.16 7740.459 7741 7741
```

7741 7741 7741

```
7747.804 7746.544 7744.503 7742.571 7740.964
7738.362 7734.146 7726.675 7727 7727
7727 7727 7727
```

```
7749.147 7748.769 7748.156 7747.164 7745.558
7742.733 7733.95 7715.595 7700 7700
7700 7700 7700
```

```
7749.46 7749.289 7749.01 7748.559 7747.829
7746.646 7744.73 7735.986 7730 7727
7727 7727 7727
```

```
7750.441 7750.914 7751.679 7752.919 7754.928
7758.181 7762.155 7768.381 7776 7809
7809 7809 7809
```

```
7751.262 7752.274 7753.914 7756.569 7759.9
7761.687 7764.583 7769.715 7779 7809
7809 7809 7809 /
```

ENDBOX

-- DEFINE RESERVOIR SHAPE USING ACTIVE/INACTIVE BLOCKS

ACTNUM

7744*1 /

BOX

21 22 2 8 1 44 /

ACTNUM

616*0 /

```

BOX
  20 20 2 7 1 44 /
ACTNUM
  264*0 /

```

```

BOX
  18 19 3 4 1 44 /
ACTNUM
  176*0 /

```

```
ENDBOX
```

```
COORDSYS
```

```
-- Make sure that the 1st and last block in the theta direction are
linked
```

```
-- theta1 theta2
   1      8      'COMP' /
```

```
-- DEFINE RESERVOIR PROPERTIES AND LAYER THICKNESSES
EQUALS
```

```
-- ZONE 1.1
```

```

'PERMR' 60      1 22 1 8 1 2 /
'PERMTHT' 60      /
'PERMZ' 60      /
'NTG' .83      /
'PORO' .134     /
'DZ' 4.195     /

```

```
-- ZONE 1.2
```

```

'PERMR' 160     1 22 1 8 3 4 /
'PERMTHT' 160     /
'PERMZ' 160     /
'NTG' .93      /
'PORO' .179     /
'DZ' 4.195     /

```

```
-- ZONE 1.3
```

```

'PERMR' 160     1 22 1 8 5 6 /
'PERMTHT' 160     /
'PERMZ' 160     /
'NTG' .63      /
'PORO' .155     /
'DZ' 4.195     /

```

```
-- ZONE 2 - SHALE LAYER, AS FOR THE REST OF THE GRID
```

```

'PERMR' 30      1 22 1 8 7 8 /
'PERMTHT' 30      /
'PERMZ' 30      /
'NTG' .20      /
'PORO' .120     /
'DZ' 3.785     /

```

```
-- ZONE 3.1
```

'PERMR'	90	1	22	1	8	9	11	/
'PERMTHT'	90	/						
'PERMZ'	90	/						
'NTG'	0.89	/						
'PORO'	.162	/						
'DZ'	3.37	/						

-- ZONE 3.2

'PERMR'	770	1	22	1	8	12	33	/
'PERMTHT'	770	/						
'PERMZ'	770	/						
'NTG'	.97	/						
'PORO'	.200	/						

-- THICKNESSES FOR ZONE 3.2

'DZ'	2.27	1	22	1	8	12	12	/
'DZ'	1.73	1	22	1	8	13	13	/
'DZ'	1.29	1	22	1	8	14	14	/
'DZ'	0.97	1	22	1	8	15	15	/
'DZ'	0.73	1	22	1	8	16	16	/
'DZ'	0.54	1	22	1	8	17	17	/
'DZ'	0.41	1	22	1	8	18	18	/
'DZ'	0.31	1	22	1	8	19	19	/
'DZ'	0.23	1	22	1	8	20	20	/
'DZ'	0.17	1	22	1	8	21	21	/
'DZ'	0.13	1	22	1	8	22	22	/
'DZ'	0.10	1	22	1	8	23	23	/
'DZ'	0.10	1	22	1	8	24	24	/
'DZ'	0.13	1	22	1	8	25	25	/
'DZ'	0.17	1	22	1	8	26	26	/
'DZ'	0.23	1	22	1	8	27	27	/
'DZ'	0.31	1	22	1	8	28	28	/
'DZ'	0.41	1	22	1	8	29	29	/
'DZ'	0.54	1	22	1	8	30	30	/
'DZ'	0.73	1	22	1	8	31	31	/
'DZ'	0.97	1	22	1	8	32	32	/
'DZ'	1.33	1	22	1	8	33	33	/

-- ZONE 3.3

'PERMR'	500	1	22	1	8	34	38	/
'PERMTHT'	500	/						
'PERMZ'	500	/						
'NTG'	.99	/						
'PORO'	.194	/						

-- THICKNESSES FOR ZONE 3.3

'DZ'	1.78	1	22	1	8	34	34	/
'DZ'	2.37	1	22	1	8	35	35	/
'DZ'	3.16	1	22	1	8	36	36	/
'DZ'	3.75	1	22	1	8	37	37	/
'DZ'	3.75	1	22	1	8	38	38	/

-- ZONE 3.4

'PERMR'	480	1	22	1	8	39	41	/
'PERMTHT'	480	/						
'PERMZ'	480	/						
'NTG'	.98	/						

```

      'PORO'      .181  /
      'DZ'       3.87  /

-- ZONE 3.5

      'PERMR'    290      1  22  1   8  42  44  /
      'PERMTHT' 290      /
      'PERMZ'    290      /
      'NTG'      .95     /
      'PORO'     .194    /
      'DZ'       3.90    /

/

-----
--EQUALS
-- VERTICAL PERMS FOR LAYERS ABOVE THE SHALE
--   'PERMZ' 0.6 1 22 1 8 1 6 /
-- VERTICAL PERMS FOR THE SHALE LAYER
--   'PERMZ' 0.0 1 22 1 8 7 8 /
--/

-- VERTICAL PERMS FOR LAYERS BELOW THE SHALE LAYER
MULTIPLY
-- INCREASE THE HORIZONTAL PERMS BY 60%
      'PERMR' 1.6 6 22 1 8 1 44 /
      'PERMTHT' 1.6 /
-- REDUCE VERTICAL PERMS TO HALF OF THE HORIZONTAL
      'PERMZ' 0.5 1 22 1 8 1 44 /
/

-----

RPTGRID
  0 0 1 1 1 1 1 0 0 1 1 1 1 1 /  FOR DEBUGGING
--  35*0 /  AFTER DEBUGGING

GRIDFILE
2 /

NEWTRAN

-- END OF GRID
SECTION=====

PROPS
=====

-- READ SATURATION TABLES
INCLUDE
  'swof1.dat' /

-- REF. PRES. REF. FVF COMPRESSIBILITY REF VISCOSITY
VISCOSIBILITY
PVTW
      3540      1.036      3.09E-6      0.272      5.03E-
6 /

-- ROCK COMPRESSIBILITY

```

```
--
-- REF. PRES COMPRESSIBILITY
ROCK          3540          1.72E-6 /
```

```
DENSITY
-- SURFACE DENSITIES OF RESERVOIR FLUIDS
```

```
-- FROM E-BT1 DST#1; &O = 0.810; &G = 0.9430 (PVT REPORT FULL
FLASHING)
-- &W = 1.01 FROM WATER ANALYSIS OF E-AD1 SAMPLE
-- OIL WATER GAS
-- 50.6 63.05 0.0888 /
```

```
PVDO
-- OIL PVT FOR E-BT FROM DST#1 AT E-BT1
-- Peq BO UO
-- (psia) (rb/stb) (cP)
-- 2043 1.472 0.40
2120 1.470 0.41
2460 1.461 0.41
2988 1.448 0.42
3465 1.436 0.43
4055 1.423 0.44 /
```

```
RSCONSTT
.654 2043 /
```

```
RPTPROPS
19*0 /
```

```
-- END OF PROPS
```

```
SECTION.=====
```

```
REGIONS
```

```
-- READ REGIONS FOR FLUID IN PLACE AND SATURATIONS
```

```
-----
-- SPECIFY REGIONS FOR FLUID IN PLACE, AND SATURATION TABLES --
-- FOR THE E-BT SENSITIVITIES (100x100) --
-----
```

```
-- ONE EQUILIBRATION REGION FOR ENTIRE GRID
BOX
```

```
1 22 1 8 1 44 /
```

```
EQLNUM
```

```
7744*1 /
```

```
-----
-- E-BT REGION - LAYERS ABOVE THE SHALE -
-----
```

```
BOX
```

```
1 22 1 8 1 6 /
```

```
FIPNUM
```

```
1056*1 /
```

```
-----
-- E-BT REGION - LAYERS BELOW THE SHALE -
-----
```

BOX
 1 22 1 8 9 44 /
 FIPNUM
 6336*3 /

 -- E-BT REGION - SHALE LAYER --

BOX
 1 22 1 8 7 8 /
 FIPNUM
 352*2 /

 -- SATURATION TABLES FOR THE EBT REGION --

-- TABLES FOR THE X AND Y DIRECTIONS

BOX
 1 22 1 8 1 2 /
 SATNUM
 352*4 /

BOX
 1 22 1 8 3 6 /
 SATNUM
 704*2 /

BOX
 1 22 1 8 7 8 /
 SATNUM
 352*6 /

BOX
 1 22 1 8 9 44 /
 SATNUM
 6336*8 /

-- TABLES FOR THE Z+ DIRECTION

BOX
 1 22 1 8 1 2 /
 KRNUMZ
 352*3 /

BOX
 1 22 1 8 3 6 /
 KRNUMZ
 704*1 /

BOX
 1 22 1 8 7 8 /
 KRNUMZ
 352*5 /

BOX
 1 22 1 8 9 44 /

KRNUMZ
6336*7 /

ENDBOX

RPTREGS
4*0 /

SOLUTION

=====

-- DATA FOR INITIALISING FLUIDS TO POTENTIAL EQUILIBRIUM

--

	DATUM	DATUM	MFWL	MFWL	GOC	GOC	RSVD	RVVD	SOLN
	DEPTH	PRESS	DEPTH	PCOW	DEPTH	PCOG	TABLE	TABLE	METH
EQUIL	8038.5	3576.6	7841.6	0.0	6000	0	0	0	-5 /
EBT1									

-- SWITCH ON OUTPUT OF INITIAL SOLUTION

RPTSOL

1 1 1 0 1 0 4 2 /

SUMMARY

=====

FOPR	- oil production rate
FOPT	- oil production total
FWPR	- water production rate
FWPT	- water production total
FGPR	- field gas production rate
FGPT	- field gas production total
FWCT	- water cut
FGOR	- field gor
WBHP	- well bottom hole pressures
/	
WTHP	- well tubing head pressures
/	
FOIP	- field oil in place
FVPT	- field production volume total
FPR	- AVERAGE FIELD PRESSURE
rpr	
/	

-- REQUEST A SEPARATE RUN SUMMARY FILE

RUNSUM

SEPARATE

RPTSMRY

1 /

SCHEDULE

RPTSCHED

6*0 1 2 2 0 3 3 0 0 3 /

WELSPECS

'EBT1' 'EBT' 1 1 1* 'OIL' /

COMPDAT

```
'EBT1' 1 1 1 23 'OPEN' 1* 1* .723 1* 2.2 /
'EBT1' 1 2 1 23 'OPEN' 1* 1* .723 1* 2.2 /
'EBT1' 1 3 1 23 'OPEN' 1* 1* .723 1* 2.2 /
'EBT1' 1 4 1 23 'OPEN' 1* 1* .723 1* 2.2 /
'EBT1' 1 5 1 23 'OPEN' 1* 1* .723 1* 2.2 /
'EBT1' 1 6 1 23 'OPEN' 1* 1* .723 1* 2.2 /
'EBT1' 1 7 1 23 'OPEN' 1* 1* .723 1* 2.2 /
'EBT1' 1 8 1 23 'OPEN' 1* 1* .723 1* 2.2 /
```

/

-- SCHEDULE FOR FLOWS AND SHUTINS

-- FLOW PERIOD 1

WCONPROD

'EBT1' 'OPEN' 'ORAT' 2870 1* 1* 1* 1* 1000 /

/

TUNING

.05 2.0 .01 .015 /

/

12 1 75 /

TUNINGL

.05 2.0 .01 .015 /

/

12 1 75 /

TSTEP

0.3046296

/

-- FLOW PERIOD 2

WCONPROD

'EBT1' 'OPEN' 'ORAT' 790 1* 1* 1* 1* 1000 /

/

TUNING

.05 2.0 .01 .015 /

/

12 1 75 /

TUNINGL

.05 2.0 .01 .015 /

/

12 1 75 /

TSTEP

1.3855325

/

-- SHUT-IN 1

WCONPROD

'EBT1' 'STOP' '' 1* 1* 1* 1* 1* 1000 /

/

TUNING


```
.0001 0.10 .0001 .015 1.16 /
/
12 1 75 /
```

```
TUNINGL
.0001 0.10 .0001 .015 1.16 /
/
12 1 75 /
```

```
TSTEP
1.4063658
/
```

```
-----
-- FLOW PERIOD 3
```

```
WCONPROD
'EBT1' 'OPEN' 'ORAT' 5200 1* 1* 1* 1* 1000 /
/
```

```
TUNING
.001 0.02 .01 .015 /
/
12 1 75 /
```

```
TUNINGL
.001 0.02 .01 .015 /
/
12 1 75 /
```

```
TSTEP
0.1664350
/
```

```
-----
-- SHUT-IN 2
```

```
WCONPROD
'EBT1' 'STOP' '' 1* 1* 1* 1* 1* 1000 /
/
```

```
TUNING
.0001 0.10 .0001 .015 1.16 /
/
12 1 75 /
```

```
TUNINGL
.0001 0.10 .0001 .015 1.16 /
/
12 1 75 /
```

```
TSTEP
0.3340288
/
```

```
-----
-- FLOW PERIOD 4
```

```
-- adjust the well skin factor ie. cleaning up.
COMPDAT
```

```
'EBT1' 1 1 1 23 'OPEN' 1* 1* .723 1* 1.0 /
```

```

'EBT1' 1 2 1 23 'OPEN' 1* 1* .723 1* 1.0 /
'EBT1' 1 3 1 23 'OPEN' 1* 1* .723 1* 1.0 /
'EBT1' 1 4 1 23 'OPEN' 1* 1* .723 1* 1.0 /
'EBT1' 1 5 1 23 'OPEN' 1* 1* .723 1* 1.0 /
'EBT1' 1 6 1 23 'OPEN' 1* 1* .723 1* 1.0 /
'EBT1' 1 7 1 23 'OPEN' 1* 1* .723 1* 1.0 /
'EBT1' 1 8 1 23 'OPEN' 1* 1* .723 1* 1.0 /
/

```

WCONPROD

```

'EBT1' 'OPEN' 'ORAT' 7735 1* 1* 1* 1* 1000 /
/

```

TUNING

```

.001 0.02 .01 .015 /
/
12 1 75 /

```

TUNINGL

```

.001 0.02 .01 .015 /
/
12 1 75 /

```

TSTEP

```

0.9990750
/

```

-- SHUT-IN 3

WCONPROD

```

'EBT1' 'STOP' '' 1* 1* 1* 1* 1* 1000 /
/

```

TUNING

```

.0001 0.10 .0001 .015 1.16 /
/
12 1 75 /

```

TUNINGL

```

.0001 0.10 .0001 .015 1.16 /
/
12 1 75 /

```

TSTEP

```

1.5013875
/

```

-- FLOW PERIOD 5

WCONPROD

```

'EBT1' 'OPEN' 'ORAT' 8730 1* 1* 1* 1* 1000 /
/

```

TUNING

```

.001 0.02 .01 .015 /
/
12 1 75 /

```

TUNINGL

```

.001 0.02 .01 .015 /
/

```

12 1 75 /

TSTEP
0.1443292
/

-- SHUT-IN 4
WCONPROD
'EBT1' 'STOP' '' 1* 1* 1* 1* 1* 1000 /
/

TUNING
.0001 0.10 .0001 .015 1.16 /
/
12 1 75 /

TUNINGL
.0001 0.10 .0001 .015 1.16 /
/
12 1 75 /

TSTEP
0.2725667
/

END